# PROBLEMY EKSPLOATACJI

# MAINTENANCE PROBLEMS

no 1/2015

INSTITUTE FOR SUSTAINABLE TECHNOLOGIES
NATIONAL RESEARCH INSTITUTE

**Problemy Eksploatacji – Maintenance Problems**

**Scientific quarterly of the Institute for Sustainable Technologies – National Research Institute (ITeE – PIB)**

Information about articles printed in the Journal can be fund in the following three renowned databases:

- Index Copernicus – the international specialized platform promoting scientific achievements, and supporting national and international collaboration between scientists, publishers of scientific journals and R&D units;
- BazTech – bibliographic and abstract database about Polish technical journals, in which articles from selected Polish journals in the field of technical sciences and environmental protection are stored;
- TEMA (Technology and Menagement) WTI-Frankfurt eG, Frankfurt am Main.

Articles are reviewed by reviewers constantly cooperating with the Journal. The list of them is presented on the website of the Journal:
http://www.problemyeksploatacji.itee.radom.pl/index.php/wskazówki/lista-recenzentów.html



Adress:
ul. K. Pułaskiego 6/10, 26-600 Radom
tel. (0-48) 364-42-41 w. 298, fax (0-48) 364-47-60
e-mail: beata.belina@itee.radom.pl

Journal co-funded by the Ministry of Science and Higher Education

ISSN 1232-9312



Editing: Bożena Mazur, Joanna Iwanowska

Edition: 200 copies.

*2541. publication of the Institute for Sustainable Technologies – National Research Institute (ITeE – PIB)*
ITeE – PIB Press
K. Pułaskiego 6/10, 26-600 Radom, tel. (0048) 48 364-42-41, fax (048) 364-47-65
e-mail: instytut@itee.radom.pl http://www.itee.radom.pl

PROBLEMY
EKSPLOATACJI
**MAINTENANCE
PROBLEMS**

1/2015 (96)

## Contents

**Marcin CHODŹKO**
Institute of Manufacturing Technology,
West Pomeranian University of Technology, Szczecin
marcin.chodzko@zut.edu.pl

# THE SEARCH FOR WEAK ELEMENTS AFFECTING THE VIBROSTABILITY OF THE SYSTEM CONSISTING OF THE MACHINE TOOL AND THE CUTTING PROCESS, BASED ON SYMPTOMS OBSERVED DURING OPERATION

**Key words**

Machine tool, modal analysis, chatter, stability.

**Summary**

The paper presents a methodology for the search of the "weak element" in a dynamic system, consisting of the machine tool and the cutting process, using the methods of experimental modal analysis. The subject matter of this research was inspired by specific machining problems that occurred in the industrial operation of machine tools. It became necessary to identify the reasons of the loss of stability, establish the self-excited vibrations mechanism, indicate the "weak element" in the mass-spring-damping system, then specify the required changes in design, and verify them in practice. The paper also presents examples showing the practical effectiveness of the proposed research method.

## Introduction

Modern machine tools are designed according to the strictly regulated operational criteria. This applies to both universal machine tools, as well those designed to perform specific tasks. The variety of cutting variants achieved by universal machine tools is significant. This translates into a significant number of specific configurations of body elements of the machine tool. It also makes it necessary to use a large number of various cutting tools and technological parameters of cutting. These factors, in particular their variability, significantly affect the dynamic properties of the system, consisting of the machine tool and the cutting process (MT-CP), whose block diagram is shown in Fig. 1.

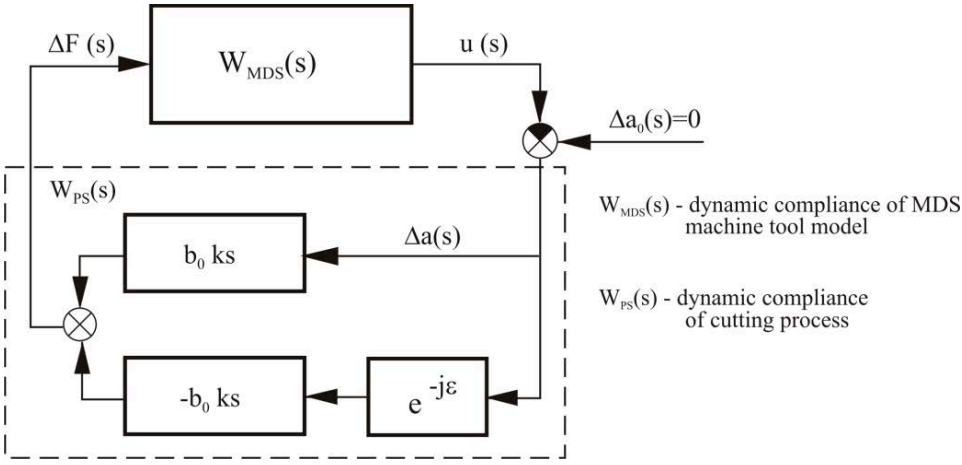


Fig. 1. Block diagram of the dynamic system consisting of the machine tool and the cutting process, including the regeneration effect [14]

Vibrostability is one of the basic operational criteria of the machine tool. The occurrence of self-excited vibrations, regardless of its source, disqualifies the machine tool and makes it impossible to perform cutting. There are several mechanisms behind this type of vibrations. Regenerative self-excited vibrations, due to the variability of geometric parameters of the cut, particularly the depth of cut, caused by the wave created on the cutting surface in the previous rotation of the tool or workpiece (regeneration effect) [1, 9, 12, 14]. The variability of these parameters results in the variation in cutting force, which under specified conditions, outcomes in the formation and development of the relative vibration of the tool and the workpiece. The maximum depth of cut, taking into account the regeneration effect, can be determined based on the following relationship [14]:

$$b_0 \, k_s \, W_{MDS}(j\omega) - b_0 \, k_s \, W_{MDS}(j\omega) e^{-j\varepsilon} = -1$$

where

$$b_{0lim} = -\frac{1}{2 \, k_s \, Re_{MDS\,min}}$$

where

$b_0$ – limit width of cut,
$k_s$ – cutting stiffness,
$W_{MDS}$ – dynamic compliance of machine tool MDS (mass--damping-spring) model,
$Re_{MDS\,min}$ – minimum of the real part of the dynamic compliance for a machine tool MDS model.

Parametric self-excited vibrations are very difficult to predict; it results from undesired configuration of the dynamic properties of the machine tool MDS system, reduced to the point of contact between the tool and the workpiece. The direction of the resultant cutting force can correspond with the main axis of stiffness ellipsoid, thereby resulting in high amplitude vibration [9, 12, 14].

The aforementioned mechanisms of self-excited vibrations are shown in Fig. 2. They can occur independently but also at the same time [14]. In the scientific literature, one can also find information about the frictional and thermo-mechanical self-excited vibrations, although they are much less frequent [14, 15].

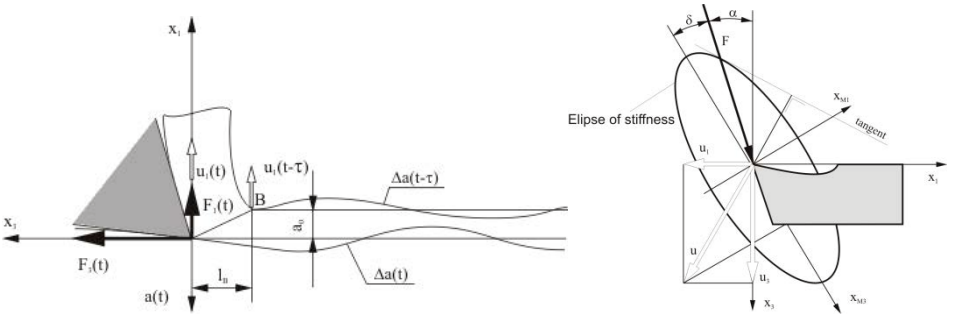


Fig. 2. The mechanism of self-oscillation: (a) due to the regenerative effect; (b) due to mode coupling effect, based on the example of turning [14]

The activation self-excited vibrations in the MT-CP system may result from the presence of a "weak element" caused by:

- Design or construction error,
- Assembling error,
- Improper mounting of the workpiece in a chuck,

- The use of interchangeable parts with incorrectly selected dynamic properties,
- The use of tools with significant overhang (high compliance),
- The high compliance of the workpiece (thin walled work-piece),
- Changes in the dynamic properties of the machine tool due to the wear of its elements during normal operation, and
- Deliberate changes to the MDS system of the machine tool, not supported by relevant model studies.

A common feature of mentioned reasons is that they cannot be identified before the production of the machine and its use in industrial conditions. One solution to this problem could be the performance of large-scale approval testing after the production of the machine tool. However, it seems economically unreliable, given the variability of factors affecting the stability of machining. As a result, in the case of the aforementioned negative factors, the user is forced to perform a number of actions designed to achieve stable machining conditions. There are many options here. First of all, it is possible to select appropriate parameters of cutting which would ensure the stability of the machining. The effective use of this method, however, requires the knowledge of the position of the stability lobes [13], enabling the selection of the optimal rotational speed of the tool or workpiece and the depth of cut. This, in turn, requires the implementation of appropriate procedures related to the modelling of the cutting process and the dynamics of the MDS model of the machine tool [3, 4, 15], which is usually not possible for machine tool users. Another method is to optimize the tool path, which would minimize the cutting force generated during machining. This is now made possible by advanced computer-aided manufacturing systems. One can also use tools with built-in dampers or various "smart" solutions, for example, active chuck systems [11]. However, they are usually very expensive and do not solve the problem completely. Besides the previously mentioned methods, it is very important to detect a "weak element" in the MT-CP system revealed during the operation of the machine and then to remove its negative influence. Therefore, it is reasonable to develop effective research methodology, enabling the discovery and localization of the "weak element" in the MT-CP system. It should be followed by the indication of the actions aimed at restoring the vibrostability of the machine tool.

## 1. Methodology of a „weak element" determination in the MT-CP system in operating conditions

A modern machine tool is a complex mechatronic system. Numerous interactions between its components and functional units influence its performance and determine its range of use. If the stages of design and construction involve computer modelling and a comprehensive simulation analysis, then there is a good chance of obtaining satisfactory characteristics of

the designed MT-CP system. If this is also accompanied by the identification research in prototypes, it is possible to make appropriate changes in the design of the machine tool, improving its dynamic properties and thus its stability.

There is a considerable volume of research on the mathematical modelling of the MT-CP system [4, 9, 10], experimental research in the field of static [2, 6] and dynamic properties [5], and predicting the vibrostability [7, 8], and other aspects of machine tool use. Despite this, very often the stages of design and construction of machine tools are carried out intuitively, based on the engineering experience of the designer. This approach to design does not always lead to optimal solutions, and if changes in design are necessary, it is not possible to predict their effect. Therefore, modelling and computer simulations play an important role in shaping the dynamic properties of the MT-CP system at the design stage.

However, in practice, information on the dynamic properties of the machine tool in operation are not known to the user, and the cause in the problems in machining, including self-excited vibrations, needs to be identified fast. This situation occurs mainly when the machine loses its desired properties in operation, due to the occurrence of certain factors. In this case, the user needs to take specific actions focused on removing the causes of the instability of MT-CP system, in the shortest time and lowest cost possible. When assuming that the physical and mathematical model of the machine tool in question is not available, it is proposed to use experimental modal analysis to identify the "weak element" in the MDS system as the cause of the formation and development of self-excited vibrations in the MT-CP system.

The algorithm for identifying a "weak element" in the MT-CP system in operational conditions with the use of the experimental modal analysis is proposed as follows:

1. Analysis of factors associated with the machining technology:
   a. Verification of the selection of technological parameters of machining,
   b. Determination of machining cases at which vibrostability is lost,
   c. Validation of the clamping of the workpiece, cutting tool, its overhang,
   d. Verification of the correctness of the machining program.
2. Analysis of the MDS system in the machine tool:
   a. Analysis of the MDS system structure and the evaluation of its technical condition,
   b. The determination of design changes and modifications made prior to the difficulty of machining,
   c. Identification of possible failures and their sources that may have occurred during operation,
3. Identification of the self-excited vibration mechanism:
   a. Visual assessment of unstable machining marks on the surface of the workpiece,

   b. Determination of the frequency at which the machine tool vibrostability is lost,
   c. The determination of spatial configuration of the machine tool body components at which instability occurs
4. Plan of experiment:
   a. Analysis of the machine tool in terms of the selection of excitation type (impact test, use of exciters, operational modal analysis);
   b. The analysis of the machine tool body in order to perform a proper selection of the locations of measurement points;
   c. The choice of reference point, excitation points, and directions;
   d. The selection of proper transducers respect to response level and frequency range;
   e. Establishing the parameters of signal processing, availability of the algorithms of modal model estimation.
5. Experiment:
   a. Machining tests - estimating of self-oscillation frequency and amplitude of vibration levels on the selected elements of the MDS system;
   b. Comprehensive modal tests for all measuring points distributed on an object in order to determine the vibration modes and animation of the motion for each of the natural frequencies;
   c. Complementary tests, detailing the unambiguity of the identification of the "weak element" of the MDS system in the machine tool.
6. Conclusion:
   a. Comparative analysis of vibration amplitude levels on the selected elements of the machine tool body,
   b. Spatial interpretation of vibration including the significance of vibration amplitude levels,
   c. The creative interpretation of information acquired in the course of the entire test - the indication of the "weak element" and to proposing changes to the MDS system in the machine tool that will remove the cause of the loss of vibrostability.

The presented methodology seems to be complete but may be modified in certain cases. For example, there may be a problem of the insufficient length of cables in the case of large machine tools, or the problem of isolating the machine tool from ambient influences when surrounded by other machinery and equipment. However, the main conclusion is that the modal research carried out in consultation with the manufacturer and the user allows for the unambiguous identification of the causes of self-excited vibrations, an indication of "weak element" of the MDS system, and the determination of required specific structural modifications or changes in manufacturing technology. Examples of the effective application of the presented methodology are shown in Section 2.

## 2. Examples of applications

First of all, the search for the "weak elements" in the system consisting of the machine and the cutting process, based on the symptoms during operation, requires the existence of a critical situation in which machining loses stability. The aforementioned actions of the user, often carried out in consultation with the manufacturer of the machine tool or tools, can bring desirable results. However, it often happens that the introduction of intuitive changes can have undesirable effects. In points 2.1 - 2.3 the real problems of machining were described, and demonstrated the effectiveness of the methodology proposed in Section 1 and the conclusion based on the results of experimental modal analysis.

### 2.1. Regenerative self-excited vibrations in turning process

The practical effectiveness of the methodology proposed in Section 1 for the search of "weak elements" in the MT-CP system has been demonstrated in examples, which resulted from the need to solve specific operational problems. The first example relates to the research whose aim was to identify a "weak element" of the MDS system of lathe, responsible for the formation of self-excited vibrations during intense turning – Fig. 3. These vibrations appeared for a very short overhang of the workpiece and short overhang of the tool.

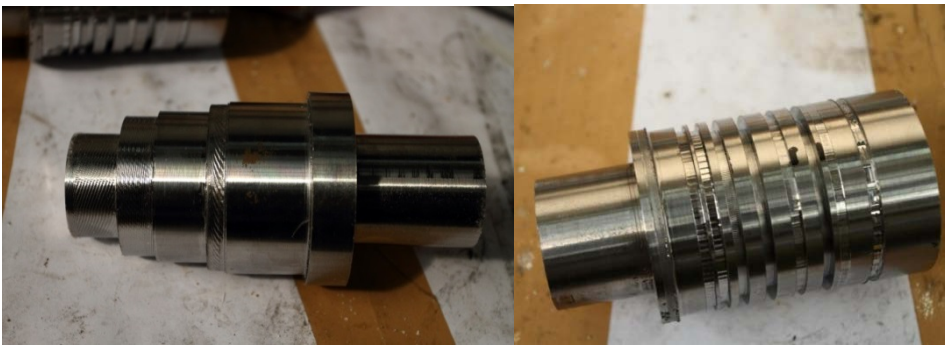

Fig. 3. Marks of unstable machining: (a) in longitudinal turning b) in cutting

The machine tool worked properly in its original structural set-up. Then, it was modernized: Slidings were replaced by rolling-element guideways in the connection between the main body of the lathe and a tool turret. The spindle and several components of the power transmission system were replaced as well. These actions caused by an unspecified change in the dynamic properties of the MDS system of the lathe. It should be emphasized that these changes were made intuitively based on the assumption that they would improve the dynamic properties and hence vibrostability. In fact, it turned out that the changes were

unfavourable from the point of view of stability. In order to determine the reasons, the research methodology presented in Section 1 was used.

The nature of self-excited vibrations was identified as regenerative vibrations (chatter), and based on the multiple implementation of the unstable cutting process at different speeds, its frequency was determined to be 300 Hz. Then the location of the measurement points and excitation points were chosen based on lathe structure study. Accelerations and forces signals were measured at the certain points of the MDS system of the machine tool – Fig. 4.

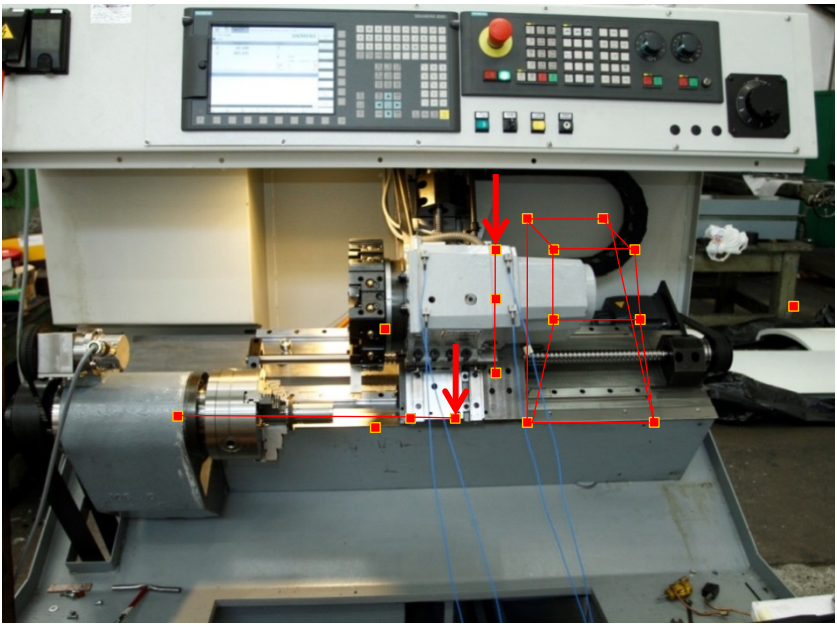

Fig. 4. A view of the studied lathe with the schematic indication of selected measurement points and the points of force application

The research was performed using a test set consisting of a PCB 356A32 acceleration transducers with a sensitivity of approximately 10 mV/(m/s$^2$) and a measuring range of about 500 m/s$^2$, with the weight of 6 grams. Excitation of vibration was performed with the use of the Kistler 9726A20000 modal hammer with the sensitivity 0.23 mV/N. Signal acquisition and processing were performed using the Difa SCADAS III, with 24-bit analog to digital transducer cards and anti-aliasing filters. During the tests, the individual machine axes were positioned and held in an equilibrium position by a drive (not brakes) in order to match the dynamic behaviour of the machine during machining as closely as possible.

Then, a comparative analysis of frequency transfer functions was performed based on signals of the exciting force and accelerations, in order to indicate the elements with the dominant levels of the amplitudes at the selected frequencies. This was necessary because the animation of vibrations does not allow the assessment of the significance of movement but only of its form. The workpiece was the element that had the dominant amplitude compared to other elements of the MDS system of the machine tool. However, it was not possible to definitely conclude that the workpiece was a "weak element," because self-excited vibrations were observed for machining carried out with the minimum overhang, which meant that the stiffness of the workpiece was very high compared to the stiffness of other components of the MDS system. Therefore, it was necessary to perform modal testing. A test was carried out, consisting in excitation of vibrations with a modal hammer on the workpiece and tool sides of the branch, respectively. This procedure allowed obtaining satisfactory coherence function. Then, using the Polymax algorithm of modal parameter estimation, and after the rejection of non-orthogonal modes of vibration, the modal model of the lathe was established – Tab. 1.

Table 1. Modal model of lathe

| Pole | Frequency [Hz] | Modal damping [%] |
|---|---|---|
| 1 | 129.669 | 2.87 |
| 2 | 168.015 | 1.92 |
| **3** | **200.255** | **1.70** |
| **4** | **256.319** | **1.64** |
| 5 | 274.777 | 2.08 |
| **6** | **370.611** | **1.46** |
| 7 | 390.630 | 2.83 |
| 8 | 432.158 | 2.03 |
| 9 | 487.611 | 3.84 |
| 10 | 584.230 | 2.02 |
| 11 | 695.737 | 3.31 |
| 12 | 768.738 | 2.28 |
| 13 | 799.037 | 2.47 |

The modes of vibrations were determined for each pole, allowing the interpretation of the vibratory motion of the object at a certain frequency. Animation was generated to show the movement of the machine tool at each natural frequency. Three modes of vibration were identified with a possible

negative effect on the vibrostability of the machine tool, characterized by the significance of motion and a significant value of the amplitude of the dynamic compliance function:

- Mode 3 at 200 Hz, characterized by significant antiphase vibration of the workpiece and the tool;
- Mode 4 at 256 Hz, with a significant amplitude of vibration of the workpiece; and,
- Mode 6 at 370 Hz, also manifested by the significant vibration of the workpiece.

The study revealed that the higher compliance to self-excited vibrations was not caused by the changes in the guide connection but by element used to mounting of spindle. The modification of this structural element of the MDS system of the lathe effectively removed the cause of self-excited vibrations.

### 2.2. Parametric self-oscillation in thread milling

The second example of applying the proposed methodology for the effective search of "weak element" in the MDS system of the machine tool referred to the determination of the reason of intense self-excited vibrations generated during thread milling – Fig. 5. It was provisionally assumed that the reduction of the vibrostability of the lathe MDS system was caused by previously made modifications.

First, the analysis involved factors associated with the thread milling technology used. It was checked for the proper application of technological parameters of cutting, machining program, the tool, its chucking and overhang value, as well as the quality of the workpiece clamping. No cause with a possible negative effect on the vibrostability of cutting process could be found. Then, the marks of machining on the workpiece were examined and correlated with the frequency of generated self-excited vibrations.

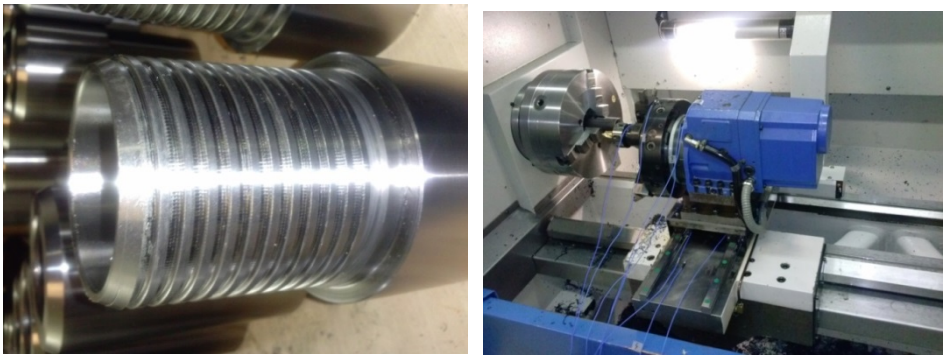

Fig. 5. a) Path of thread milling in unstable conditions; b) The general view of the machine with mounted sensors

The frequency of 1032 Hz and its harmonics, dominant in the obtained spectrum of accelerations, is very high. In most cases, self-excited vibrations are manifested at frequencies close to the frequency corresponding to one of the structural modes of machine tool body machine. Body elements are made of cast iron and usually vibrate in the range below 300 Hz. A detailed comparison of the vibration levels led to the conclusion that at a frequency of 1032 Hz, which the largest amplitude of the vibrations, can be observed on the upper surface of the tool turret and on the steel base to which the entire turret was attached. Attempts at turning with a very similar tool with an almost identical setting of the MDS system elements, differing only in the side of tool approach, resulted in stable machining. Vibrations in the work-piece branch of the force chain were negligible. Even when self-excited vibrations were observed, elevated levels of vibration were not observed on the spindle elements.

Based on the aforementioned considerations and measurements, the self-excited vibrations were identified as parametric (mode coupling) – Figure 2b. Such vibrations are observable when the resultant cutting force direction coincides with the direction of the greatest compliance of the MDS system of the lathe, measured at the point of contact of the tool and workpiece. The determination of stiffness ellipsoid mentioned in the Section 1 would require a much more complex research program, and it was not feasible due to time constraints and available machine tool accessories. Parametric oscillations occur at a frequency lower than one of the natural frequencies, while regenerative ones are generated at a frequency greater than one of the natural frequencies [3]. This conclusion could be drawn only based on the impact test performed in the subsequent step, the results of which are shown in Figure 6.

Fig. 6 shows the results of the impact test for force applied to the tool. The dominant resonance can be seen at the frequency of about 1129 Hz, similar to that determined dominant frequency spectrum of the signal recorded during self-excited vibrations. In addition, the analysis of the various transfer functions allowed concluding that the greatest amplitudes of vibration occurred in the upper part and the base of the tool turret, on a steel element to which they were attached rolling elements in guideway connection. The force acting on the housing of the tool turret showed weak coherence between the designated signals, similar to the situation when the force was applied to the lower part of the guide. This demonstrates the good properties of the damping elements made of cast iron. Detailed analysis of the experimental data and the analysis of the MDS system of the machine tool led to the identification of the steel element, used to attach the rolling element, as the “weak element” – Fig. 7.

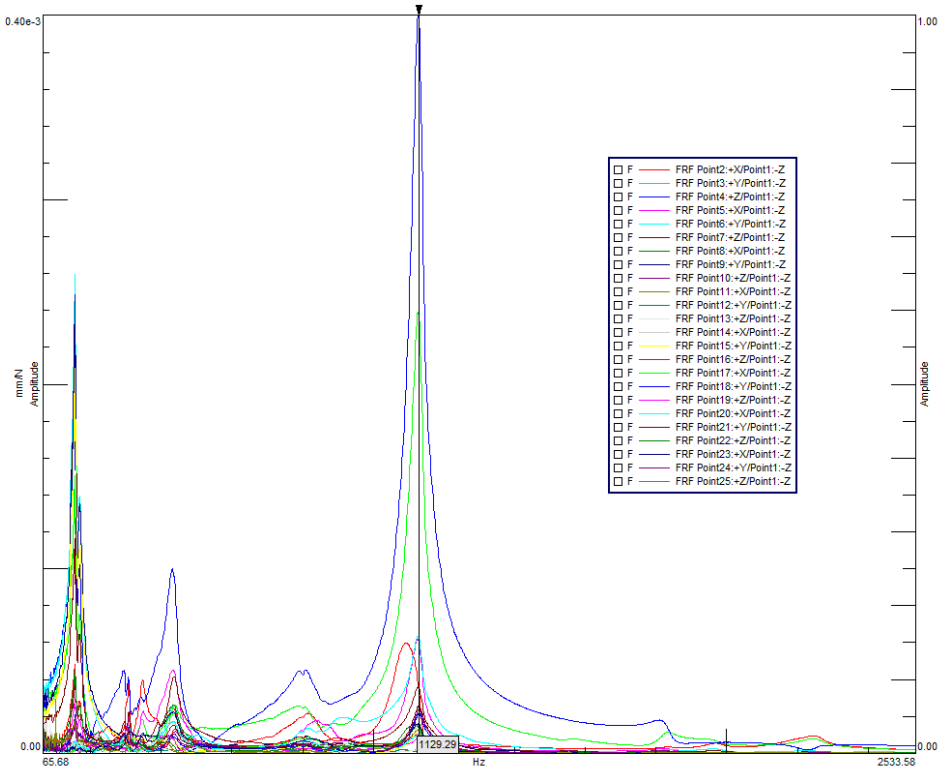


Fig. 6. Amplitude-frequency characteristics obtained in the pulse test for force acting on the tool

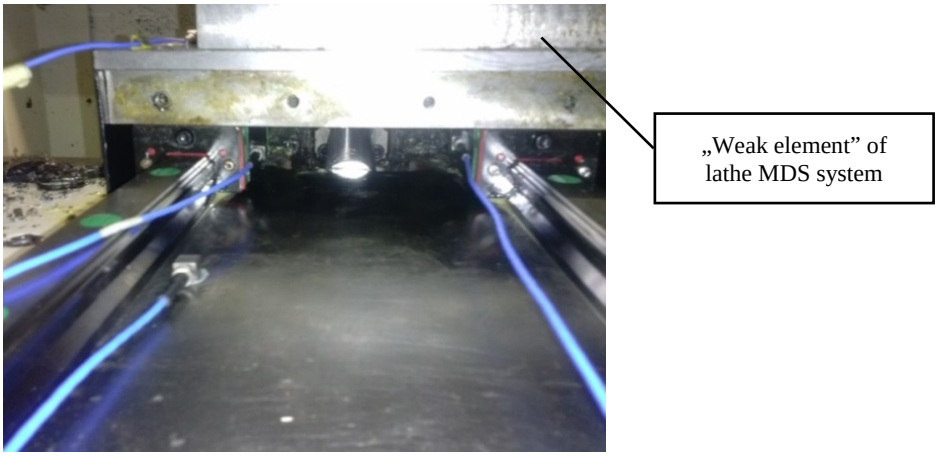


Fig. 7. “Weak element” of lathe MDS system

In consultation with the manufacturer, it was established that the original connecting element was made of cast iron. The replacement of sliding guides into rolling guides required the modification of the element; and, in order to lower the cost of the product, it was made of steel (as no additional casting was needed). The result was an unintended negative change in the dynamic properties of the entire MDS system of the machine tool.

The formulated conclusion allowed the manufacturer to take specific measures to stiffen and increase the damping of the element. The changes brought about the complete elimination of the problem of chatter. Therefore, it was shown that a seemingly small change in the MDS system resulted in the loss of its vibrostability for a particular relative configuration of the resultant cutting force and the stiffness ellipsoid, and also resulted in the activation of chatter mechanism.

### 2.3. Self-excited vibrations in the process of milling on the machining centre

Another example of the application of the methodology indicating the "weak element" in the machine tools based on symptoms observed during operation was to the search for the causes of self-oscillation during milling performed with the use of the fixed-axis machining centre. This problem was revealed in the marks of unstable machining, on one of the side surfaces of the workpiece, resulting from a particular spatial configuration of movements of individual body elements – Fig. 8.

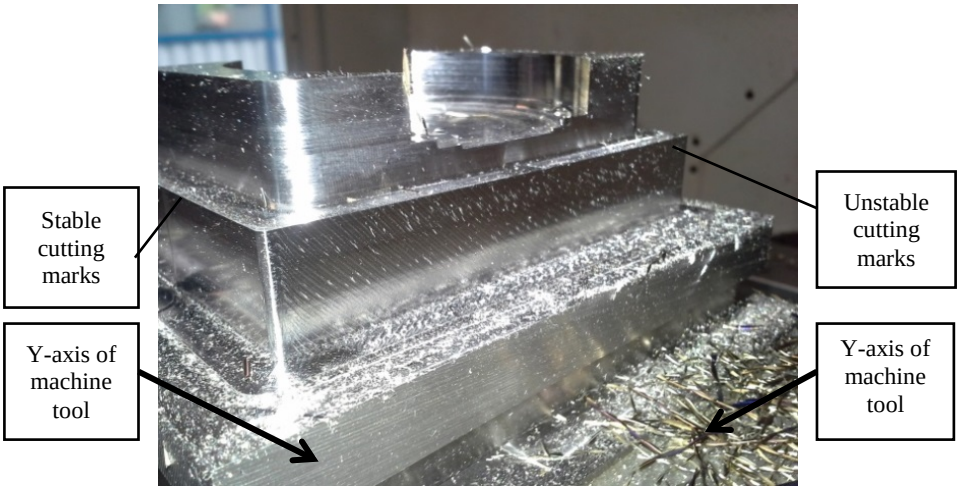


Fig. 8. Machining marks on the walls of the tested object (machining stability dependent on the direction of machining)

The machined surfaces with marks of vibration were examined prior to the research. It was agreed that probably the loss of the MDS vibrostability occurred via the regeneration effect. In order to unambiguously confirm the causes of vibration, an experimental research program consisting the following was initiated:

- Cutting test with the use of the cuboid object, with a tool with a small overhang: In this test, the depth of cut was $a_p$ = 18 mm, while the incremental width of cut in subsequent tests was $a_e$ = 0.1–1 mm, and the aim of this study was to identify the frequency of chatter.
- Impact test: the purpose was to determine the dynamic characteristics of the machine and to find the resonant frequency with the value close to the recorded frequency of self-excited vibrations. This was to enable the selection of spindle speed that would ensure machining stability.
- Cutting with the changed rotational speed: This stage of the study was to confirm the thesis that the cause of the vibration lies in the phenomenon of regeneration effect.
- Cutting and impact test using a tool with a large overhang: This stage was to determine the dynamic properties of the machine tool with a tool clamped in the spindle, with increased compliance and select machining technology.
- Modal analysis of the milling machine: The aim was to identify the "weak element," i.e. a structural element, that is responsible for reducing the dynamic stiffness of the machine tool.

In the first place, it was determined if the vibrations were related to the tool or workpiece. A comparison of the amplitudes of vibration showed the dominance of vibrations on the tool. Then the self-excited vibrations frequency was determined by comparing the frequency spectra for the machining with incremental milling width. The observed frequencies of harmonic vibrations resulted from the spindle speed and the number of cutting edges. The frequencies of self-excited vibrations were related to the frequency corresponding to the structural form of vibrations (and do not depend on the frequency of cutting). The frequency of chatter was 1166 Hz, which is confirmed by the signal spectrum of vibration acceleration, measured on the workpiece – Fig. 9.

Next, the impact test was performed with the purpose of correlating the chatter frequency with the frequency corresponding to the structural mode of the machine tool. Fig. 10 shows the FRF's (frequency response functions) for the X and Y axes of the machine tool, which shows that the mode of vibration at 1079.79 Hz is likely responsible for the formation of chatter.

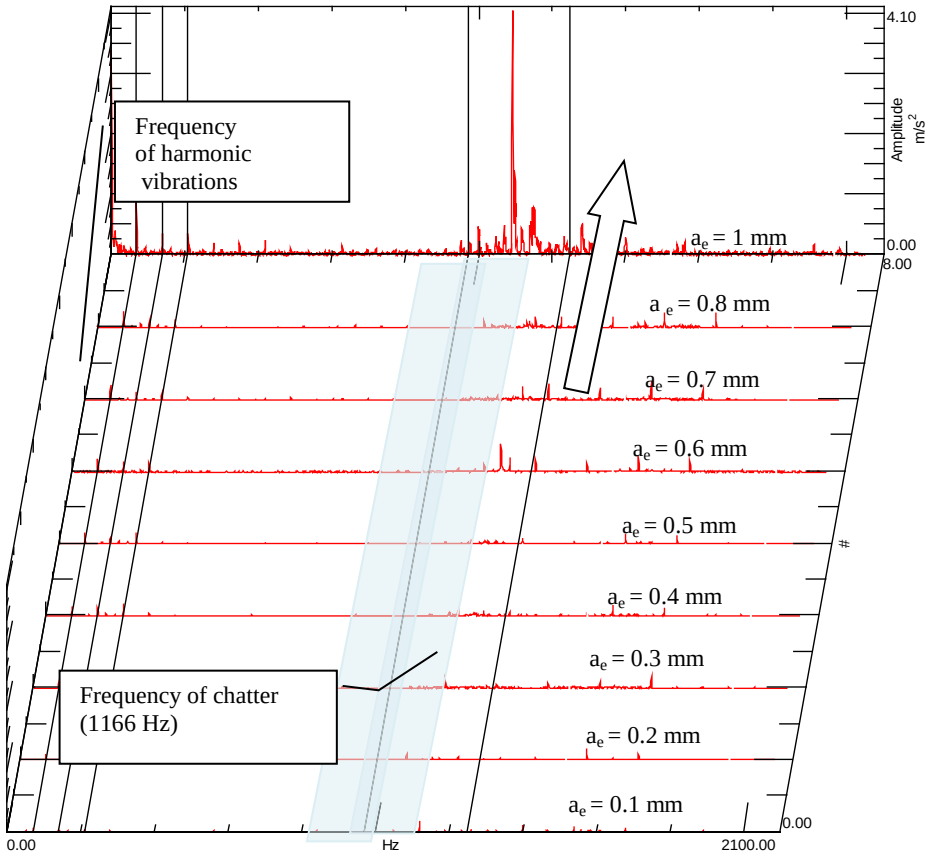


Fig. 9. Spectra of the vibration acceleration signal with a variable width of cut, as recorded on the spindle

Based on the known structural frequency, the rotational speed of the tool was selected to ensure the stability of machining. It can be determined based on the theory of chatter (temporal relations between the waves of primary and secondary rotation of tool or workpiece [14]. Vibrostability was obtained at the speed of 1477 rpm. In the next step, a cutting test with the pre-determined speed was performed. The observed significant difference in the levels of vibrations recorded for the same depth of cut (18 mm) and the same width of cut (1 mm), but at different speeds (1400 and 1477 rpm), confirmed the chatter was generated via the regeneration effect.

In the next step, a test was performed for the tool with a high compliance that is used for molding shells machining. The instability of machining (high levels of vibration) was observed already for very small sections of cut ($a_p$ = 0.15 mm, $a_e$ = 0.1 mm). Based on the recorded vibration signals, it was determined that the chatter frequency in this case was equal 389.95 Hz – Fig. 11b.

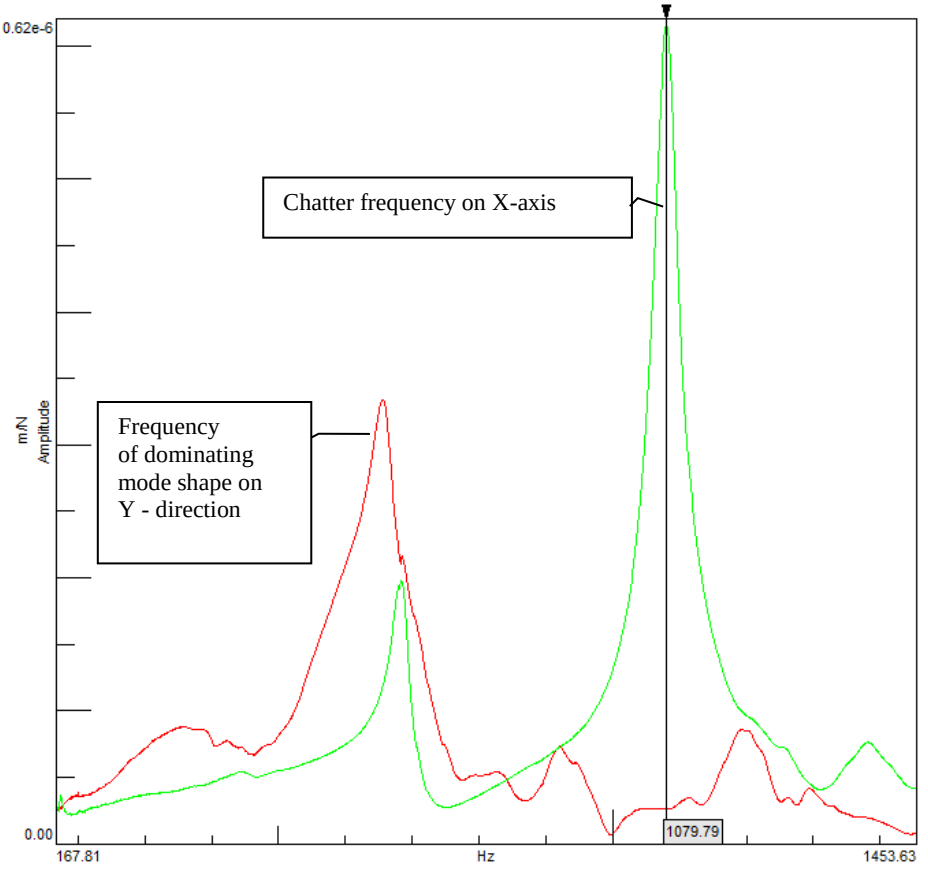


Fig. 10. Frequency response functions of the machine tool with a clamped machine tool with a small hangout, determined on X and Y axes of the machine tool

Based on the frequency response function of the machine tool with a long overhang of tool, it was determined that the chatter may be caused by the modes of vibrations at two frequencies (377 Hz, 391 Hz). This makes it difficult to choose the stable rotational speed. The frequency of chatter, and therefore the rotational speed ensuring the stability of machining, will therefore vary depending on the change of the tool.

Selection of stable cutter speed, individually for each tool, would require impact testing for each individual tool. The implementation of this idea in an industrial environment would be very difficult and sometimes impossible. It was therefore necessary to indicate the structural element whose change would have the greatest impact on the improvement of the dynamic properties of the machine tool, and thereby increase its vibrostability. The modification of the element should increase the stability of machining, irrespective of the cutting tool.

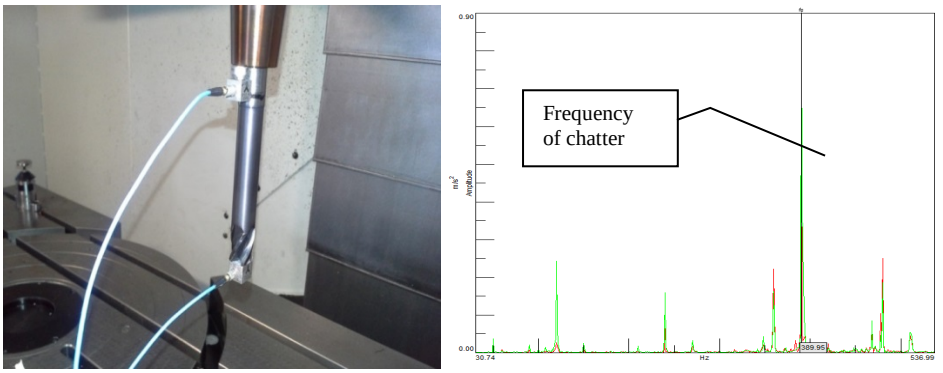


Fig. 11. a) Tool with a long overhang, ready for the impact test; b) the spectrum of the acceleration signal obtained during unstable machining with the use of the tool with a large overhang

For this purpose, based on the modal test, the modes of vibration with the greatest impact on the relative vibration of the tool and workpiece were determined. The frequencies of these modes are summarized in Tab. 2.

Table 2. Modal model of 5-axis machining centre

| Pole | Frequency [Hz] | Modal damping [%] |
|---|---|---|
| 1 | 116.386 Hz | 5.32 |
| 2 | 171.233 Hz | 3.55 |
| **3** | 426.137 Hz | 3.28 |
| **4** | 448.682 Hz | 2.10 |
| 5 | 870.980 Hz | 1.93 |
| **6** | 885.739 Hz | 0. 85 |
| 7 | 994.418 Hz | 4.65 |
| 8 | 1153.778 Hz | 0.18 |

Detailed analysis of the animation of the modes of vibration, amplitudes of displacements, and phase relationships allowed the identification of the "weak element", namely, the drive of the B-axis of the milling centre. These conclusions formed the basis of modifications performed in the structural system of machine tool.

## Summary

The paper presents a methodology for the search of a "weak element" in the mass-damper-spring system of the machine tool under operating conditions, using experimental modal analysis. It should be noted that this methodology might be mainly used when the user, not knowing the dynamic properties of the

machine tools, encounters the problem of intense chatter, which they are not able to solve. It should be emphasized that each case is different, which should be considered in developing any research program. Yet, the examples of the practical application of the developed methodology (Section 2) indicate its potential in improving the vibrostability of machining. This can be done by selecting a "weak element" of the system and to identify the MDS machine design changes, the introduction of which will lead to an improvement in its dynamic properties.

**References**

1. Altintas Y., Budak E.: Analytical Prediction of Stability Lobes in Milling. Annals of CIRP. 1995, 44, pp. 357–362.
2. Bodnar A.: Diagnostyka drgań samowzbudnych w systemie obrabiarka – proces skrawania. Monografia habilitacyjna (po polsku). Wydawnictwo Uczelniane Politechniki Szczecińskiej, 2006.
3. Budak E., Altintas Y.: Analytical prediction of chatter stability in milling-Part I: General formulation. Journal of Dynamic Systems, Measurement, and Control, Trans. ASME. 1998, 120, pp. 22–30.
4. Iglantowicz T., Lak S., Sobkowiak E.: Stanowisko do badań dynamicznych obrabiarek. Prace Naukowe Politechniki Szczecińskiej. Instytut Budowy Maszyn, 1973, 2, s. 305–310.
5. Iglantowicz T., Skrodzewicz J., Szwengier G.: Komputerowe wspomaganie doświadczalnych badań charakterystyk układów nośnych obrabiarek. Prace Naukowe Politechniki Szczecińskiej. 1992, 8, s. 91–110.
6. Marchelek K., Tomkow J.: Vibrostability of a multidimensional machine tool-workpiece-tool system, Part II: An example of vibrostability analysis made on a vertical lathe. Journal of Vibration & Control. 1998, 4(2), pp. 113–130.
7. Marchelek K., Tomkow J.: Vibrostability of a multidimensional machine tool-workpiece-tool system, Part I: Modeling the mechanical structure and cutting process. Journal of Vibration & Control. 1998, 4(2), pp. 99–112.
8. Marchelek K.: Dynamika obrabiarek. WNT, Warszawa 1991.
9. Pajor M., Okulik T., Marchelek K., Chodźko M.: Badania własności dynamicznych układów korpusowych obrabiarek w procesie projektowo-konstrukcyjnym. Modelowanie Inżynierskie. 2008, 4, 35, s. 85–92.
10. Parus A.: Kształtowanie właściwości dynamicznych systemu obrabiarka––proces skrawania za pomocą dodatkowych układów mechatronicznych. Monografia habilitacyjna (po polsku). Wyd. Zapol. Szczecin 2012.
11. Dhupia J., Powałka B., Katz R., Ulsoy A.: Dynamics of the arch-type reconfigurable machine tool. International Journal of Machine Tools and Manufacture, 2007, 47(2), pp. 326–334.

12. Tlusty J., Ismail F.: Special aspects of chatter in milling. ASME Journal of Vibration, Stress and Reliability in Design, 1983, 105, pp. 24–32.
13. Tobias S.A., Fishwick W.: Theory of regenerative machine tool chatter. The Engineer, London, 1958, 205, pp. 199–203 (Feb. 7), pp. 238–239 (Feb. 14).
14. Tomków J.: Wibrostabilność obrabiarek. WNT, Warszawa 1997.
15. Wiercigroch M., Budak E.: Sources of nonlinearities, chatter generation and suppression in metal cutting. Philosophical Transactions of the Royal Society London. 2001, 359, pp. 663–693.

**Poszukiwanie słabych ogniw w systemie obrabiarka–proces skrawania ze względu na jego wibrostabilność, na podstawie symptomów eksploatacyjnych**

**Słowa kluczowe**

Obrabiarka, analiza modalna, drgania chatter, stabilność.

**Streszczenie**

W artykule przedstawiono metodologię poszukiwania „słabego ogniwa" w dynamicznym systemie, składającym się z obrabiarki oraz procesu skrawania, z użyciem metod eksperymentalnej analizy modalnej. Prace te zostały zainspirowane koniecznością rozwiązania rzeczywistych problemów obróbkowych, które miały miejsce w przemysłowej eksploatacji obrabiarek różnego typu. Koniecznym stało się zidentyfikowanie przyczyn utraty stabilności obróbki oraz wskazanie „słabego ogniwa" w układzie masowo-dyssypacyjno-sprężystym obrabiarki. W konsekwencji określono zakres wymaganych zmian konstrukcyjnych oraz zweryfikowano ich skuteczność. W artykule wykazano również praktyczną efektywność zaproponowanej metodyki prowadzenia badań obrabiarek.

INNOVATIVE ECONOMY
NATIONAL COHESION STRATEGY
INSTITUTE FOR SUSTAINABLE TECHNOLOGIES
NATIONAL RESEARCH INSTITUTE IN RADOM
EUROPEAN UNION
EUROPEAN REGIONAL DEVELOPMENT FUND

Project co-financed by the European Union from the European Regional Development Fund

**Piotr GARBACZ, Bartłomiej BURSKI, Wojciech MIZAK**
Institute for Sustainable Technologies
– National Research Institute, Radom
piotr.garbacz@itee.radom.pl
bartlomiej.burski@itee.radom.pl
wojciech.mizak@itee.radom.pl

# AUTOMATIC SYSTEM FOR CREATING 3D OBJECT MODELS

**Key words**

3D object models, 3D sensor, RoboEarth platform.

**Abstract**

Three-dimensional models can be used in object recognition as references for the identification systems. The RoboEarth cloud-robotics platform contains additional algorithms both for object recognition and model creation. The article describes an automated system developed in order to improve the process of creating point cloud object models based on software provided with the RoboEarth platform. The process is performed using a special template with markers providing information about the localisation and orientation and recording the object from different angles. This can be done either by rotating the sensor or the template with the object. By incorporating a measuring table rotated by a stepper motor as well as rails for precise sensor mounting this process can be automated. All models were based on typical household items. In order to determine the necessary parameters for generating models, the distance between the sensor and the template, the number of steps of the motor, and the number of measurements per step was checked. The quality of the models was

verified by measuring correspondences using object recognition software from both different angles and distances. The research performed showed that an automatic approach wields better results than manual registration and can be used to increase the quality of the 3D models.

## Introduction

Object detection can be described as locating and identifying items in one's vicinity. Like many other tasks it is considered trivial by humans but requires the implementation of complex and computation demanding algorithms as well as large data storage capabilities for machines. Despite those drawbacks, object detection can be found in many applications, e.g. video surveillance systems [1] or mobile and service robotics. In order to increase their interaction with their surroundings, it will be necessary for the machines to be able to recognise objects in their vicinity. The identification process is often performed with the help of reference objects, stored inside a database, either local or global. Those reference objects can take different forms including three-dimensional models, two dimensional drawings or photographs, or semantic descriptions of the characteristics of the object of interest [2, 3].

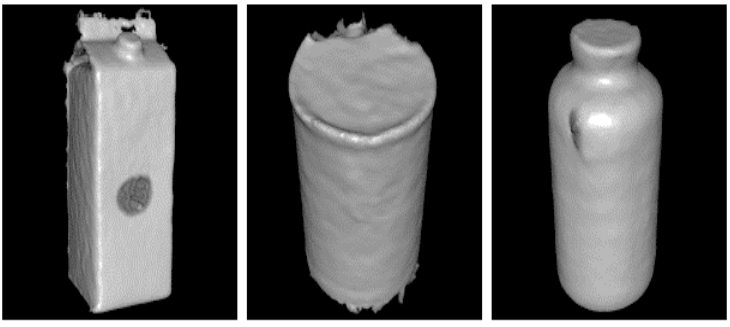

Fig. 1. Example unmeshed models generated for object recognition [3]

This article describes the development of an automated system for generating object 3D models as well as the tests performed in order to assess the quality of the obtained data and improve the results of the generated models. In order to test the developed platform, software components for generation and object recognition were used. The components chosen are a part of the RoboEarth platform that was designed to help offload complex computation and data storage from robots and into servers, but it also provides additional modules [4]. The described system is based on a Microsoft Kinect depth sensor mounted on a regulated base, which allows one to change the distance and angle between the cameras and the reference object. The second important element of this system is a rotary table incorporated in order to view the scanned item from

different directions. The performed tests included generating models with different registration parameters and checking the success of object detection based on the number of correspondences between the model and the object identified.

## 1. Method description

The principle behind 3D object model generation is to scan the reference object from different directions in order to obtain detailed information about its size, shape, and texture. The developers of the object recorder provided with the RoboEarth platform propose a method based on using special patterns that help identify the localisation and orientation of the item in relation to the marker template (Fig. 2).

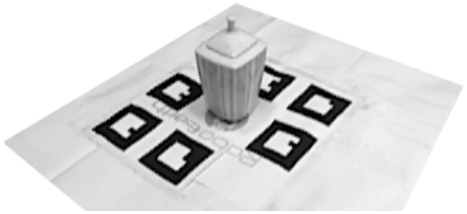

Fig. 2. Reference object with the marker pattern

Three-dimensional model generation can be performed using two different approaches, either by moving the RGB-D camera around the object or by rotating the pattern with the item placed upon it in front of a fixed sensor. The second method described has the advantage of generating models that are identically illuminated on all sides thanks to the fixed direction from which the camera observes the scene. Each measurement generates a point cloud limited to the area limited by the patterns. Those points represent the spatial localisation of the registered fragment of the item inside the coordinate system created by the object recording software. During the recording process, point clouds from different measurements are gathered and merged into a 3D model of the object. Additionally, the resulting model is also textured by incorporating data acquired using the RGB camera of the sensor. In the proposed method, the object is rotated at a fixed speed. The object model will be generated during up to three full revolutions of the measuring table.

## 2. RoboEarth platform

The RoboEarth platform was designed by a consortium of European Universities and Philips and is an example of a Platform as a Service cloud

environment. This system was described for the first time in 2011 [5], and an early version was made publicly available in late 2013. The main goal of this project is to expand the functionality of robots by creating a global knowledge base for the machines and the migration of heavy computation into efficient servers [4].

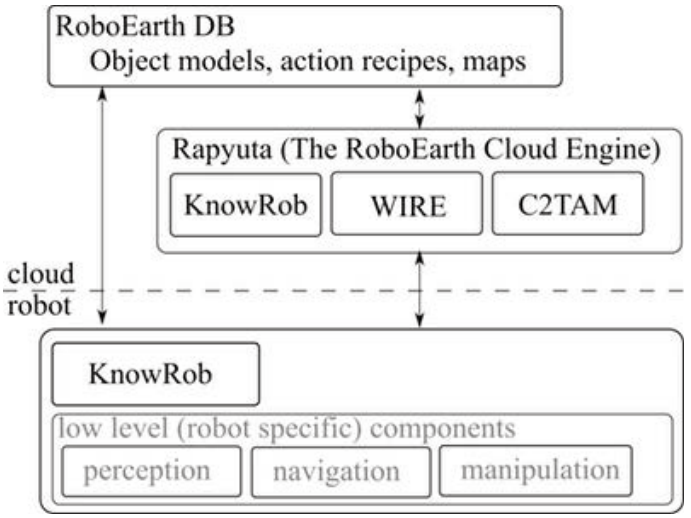


Fig. 3. Software components of the RoboEarth platform [4]

RoboEarth is not a uniform software platform but consist of up to six individual software components including a cloud engine, database, mapping software, and object detection software. The last component is capable of locating items in the vicinity of the robot and of generating 3D models of reference objects. By using the aforementioned pattern, the measurements are limited to the area designated by the markers. This helps limit the computation and storage resources because of the lower amount of points amassed. The object software was developed to cooperate with the Microsoft Kinect depth sensor.

## 3. Measurement platform

The authors of the RoboEarth platform propose a manual method for model generation. This means positioning the camera or pattern by hand in order to observe the item from different directions. Due to the scarce additional information provided by the software designers concerning the scanning process and about obtaining satisfactory models, an automatic system was developed.

### 3.1. Microsoft Kinect Sensor

To obtain the desired 3D models, a sensor capable of depth and colour registration has to be used. Out of the available solutions, the Microsoft Kinect has been selected for implementation in the proposed system. Due to its low price as well as good parameters, and the availability of hardware drivers, and software development kits, it gained popularity in the research field [6, 7, 8, 9].

The Microsoft Kinect is composed from the following components (Fig. 4):

- RGB colour camera (640x480 px resolution, fixed 30 FPS frequency),
- IR emitter,
- IR depth sensor, and
- Microphone array.

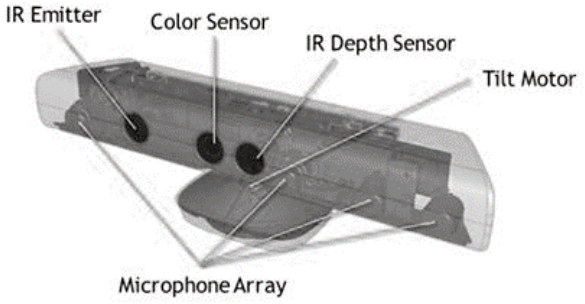


Fig. 4. Components of the Microsoft Kinect depth sensor [10]

Depth measurement is achieved by performing an analysis of the pattern emitted by the IR emitter and registered using the IR depth sensor. The additional RGB colour camera allows for applying textures of the observed surroundings to the generated point cloud. The accuracy of the Microsoft Kinect is not officially disclosed by the producer; however, available studies [11] describe the measurement accuracy at 1 mm for lengths between 500 and 1500 mm. Table 1 presents the basic parameters of the Kinect 3D sensor.

Table 1. Parameters of the Kinect 3D sensor [12]

| Parameter | Value | Unit |
|---|---|---|
| Horizontal view angle | 57 | [°] |
| Vertical view angle | 43 | [°] |
| Observation distance | 1.2–3.5 | [m] |
| Resolution | 640x480 | [px] |
| Frequency | 30 | [FPS] |

### 3.2. Model Registration Module

As described earlier, registrations are performed by scanning the reference object from different directions. In order to automate this process and analyse the possibility of improving the generated models, a dedicated registration module has been developed. Figure 5 highlights the primary components of the proposed solution: the rotary table on which the object is placed, and a regulated support for the Kinect that allows to position the sensor in relation to the object.

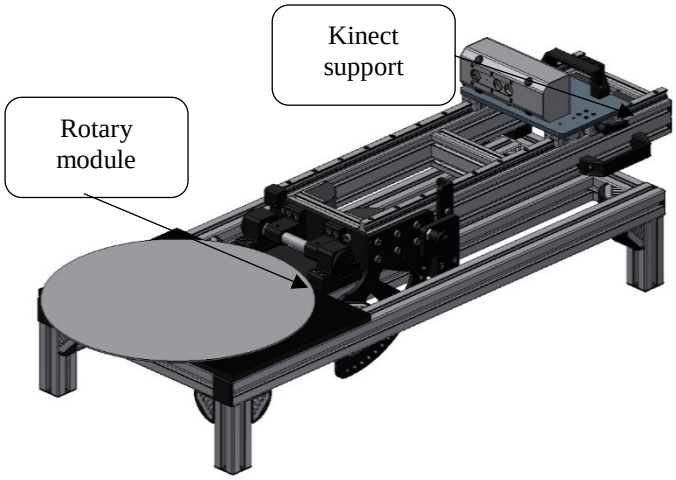


Fig. 5. Model of the registration module

The primary element of the rotary module is the measurement table with the marker patterns applied, on which the registered object is placed during model generation. The ability to view the object from different directions is ensured by a stepper motor. Another key element is the regulated Kinect support. This module allows altering both the distance and the angle between the reference object and the sensor. The distance can be regulated between 150 mm to 1200 mm, while the angle can be set from 0° to 90° with a step of 7.5°. Both of the parameters have to be set manually by the operator.

## 4. Experimental studies

The main goal behind the proposed automated system is the improvement of the quality of the recorded models. As a proof of concept, different 3D models were generated varying in the rotation speed and the amount of full rotations. The target frequency of the stepper motor was set from 2 Hz up to 8 Hz, and the number of full rotations varied between 1 and 3. The distance and angle of the

sensor in relation to the rotating table was set in accordance to the information from the developers of the object recording software. In order to achieve the best resolution, the distance was fixed at 600 mm, which is the minimal working distance for the Kinect sensor. The angle was set at 7.5°, which guarantees that at least three markers are visible at any time during the measurements. As a result of the analysed parameters, nine models of the example object were generated. An example model obtained is presented in Figure 6.

Fig. 6. Example model of a juice box

**4.1. Verification tests**

The generated models were used during verification tests in order to select the optimal parameters of the system. To assess the quality of the virtual representations of the reference items, the object recognition software provided with the RoboEarth platform was used. For each model, the distance between the sensor and the measuring table was changed between 600 mm, 900 mm, and 1200 mm. The correspondences found between the real object and the generated 3D model were used to assess the quality of the models. Two key-points are considered correspondent if their localisation both in the current image of the object of interest and the reference model differ by only a set, small threshold. Results obtained for three models, differencing in the number of rotations used in the generation process are presented in Table 2. The lack of information about the correspondences found means that the object could not be recognised.

Table 2. Example results of found 3D correspondences between the object and its model

| Distance [mm] | Model | model 1<br>2 Hz<br>1 rotation | model 2<br>2 Hz<br>2 rotations | model 3<br>2 Hz<br>3 rotations |
|---|---|---|---|---|
| | Rotation of the object [°] | Found correspondences | | |
| 600 | 0 | 17 | 14 | 15 |
| | 90 | 22 | 14 | 15 |
| | 180 | 22 | 17 | 18 |
| | 270 | 17 | 15 | 16 |
| 900 | 0 | 17 | 17 | 13 |
| | 90 | 10 | 11 | 10 |
| | 180 | 12 | 15 | 18 |
| | 270 | 10 | 11 | 13 |
| 1200 | 0 | 10 | 10 | 10 |
| | 90 | - | - | - |
| | 180 | - | 10 | 10 |
| | 270 | - | - | 11 |

By analysing the acquired data, it was possible to compare the obtained models and determine the optimal process for generating object representations. All models used were able to provide the information necessary to identify the test object for the minimal distance. Increasing the distance made the simpler representations too inaccurate to provide satisfying results. As expected, using more detailed models gave better results for greater distances between the object and the sensor. However, if the distance exceeded 1000 mm, successful detection was problematic for all models regardless of size. An image presenting the detection results is presented in Figure 7. The first image shows the pre-recorded reference data used for object recognition. The second one displays the current image acquired from the Kinect sensor. Additionally, both images are enriched with key-points used in the object identification process. They are displayed as black points surrounded by circles varying in size. The horizontal lines beginning in key-points in both images represent the correspondences found. In the top image, additional, insignificant (for the detection) data is also visible.

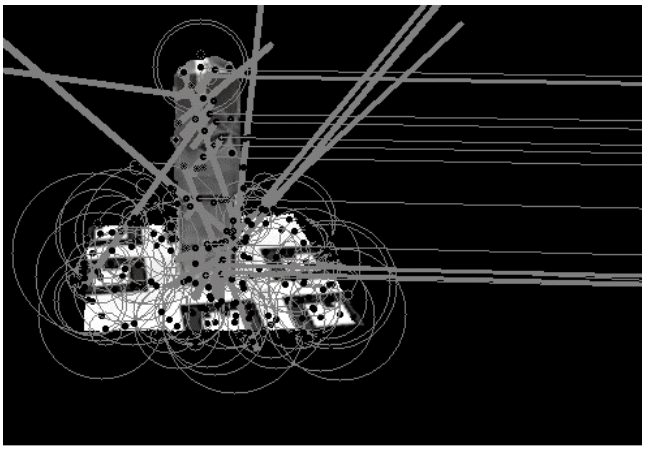

a)

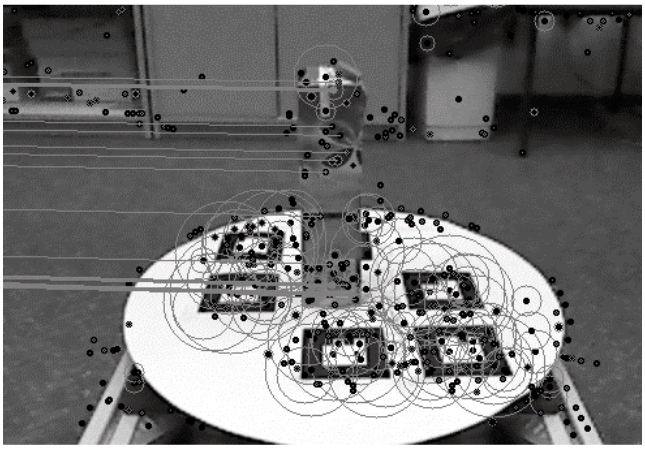

b)

Fig. 7. Detection results of the test object with visible correspondences: a) reference data b) sensor image

The best results were obtained for a model generated during 3 full rotations with the frequency of the stepper motor at 2 Hz. On the other hand, this representation had a size of 630 MB and consisted of 123 separate point clouds. As a result, it took a significant amount of time to load and analyse. The simplest models had to be discarded due to the subpar results obtained for greater distances. Satisfying results could only be achieved for the minimal distance. For similar models generated under different conditions, e.g. 2 Hz and 1 rotation, 4 Hz and 2 rotations and 8 Hz and 3 rotations, which all consisted of 45–50 point clouds, the identification process wielded similar results. However, lower

frequencies allow gathering more point clouds during a single rotation as opposed to multiplying the measurements during subsequent rotations.

In conclusion, two rotations were chosen with the frequency of 2 Hz per step as the optimal model generation method. This approach allows obtaining a compromise between the quality and size of the 3D object model. The lower frequency makes it possible to obtain more scans during a single rotation. The second move is implemented to increase the quality of the texture of the object.

**Summary**

RGB-D sensors allow simultaneously acquiring data about depth and colour. This creates an opportunity to use such devices like the Microsoft Kinect in object scanning and 3D model generation. Commercially available software exists which assists the user during the process. In order to further relieve the operator, an automated system has been developed composed of a regulated support for the sensor and a rotating table. This system allows for the generation of 3D point-cloud models of objects enriched with information about its texture colour. The created models can be used in various applications, including object recognition, or can be further converted into other formats, e.g. CAD models. In comparison to a manual approach, during which the operator is required to manually change the scanning direction, the process is repeatable and gives more precise results. Several tests were performed in order to optimise the scanning phase. The tests focused on the influence of the rotation and amount of data acquired per step as well as the distance and angle between the Kinect sensor and scanned object. As a result, a single method for model generation was chosen which allows for maintaining a good quality of the models while limiting the memory required for storage.

Future work will include additional tests in order to further improve the quality of the point-clouds. Other parameters, which can have an influence on the resulting model, will be tested, including the illumination of the scene, the impact of natural and artificial light, and the texture and material of the registered object. The system can be modified in order to allow for an automatic regulation of the sensor position. This would allow scanning the items from different directions and from varying angles. Several practical implementations of the system are also considered, e.g. in mobile robotics or CAD model generation. In the first example, a mobile robot can be tasked with locating specified objects in its vicinity. In order to offload the computation heavy recognition process from the robot, the described RoboEarth platform can be incorporated into the system. Using the automatic system as a CAD model generator will require the incorporation of additional software components for converting the acquired point-cloud.

*Scientific work executed within the Strategic Programme "Innovative Systems of Technical Support for Sustainable Development of Economy" within Innovative Economy Operational Programme.*

**References**

1. Nascimento J.C., Marques J.S.: Performance Evaluation of Object Detection Algortithms for Video Surveillance, IEEE Transactions on Multimedia 8(4), 2006.
2. Marszałek M., Schmid C.: Semantic Hierarchies for Visual Object Recognition: IEEE Conference on Computer Vision and Pattern Recognition, 2007.
3. Krainin M., Curless B., Fox D.: Autonomous Generation of Clomplete 3D Object Models Using Next Best View Manipulation Planning, IEEE International Conference on Robotics and Automation (ICRA), 2011, pp. 5031–5037.
4. RoboEarth website: http://www.roboearth.org.
5. Waibel M., Beetz M., Civera J., D'Andrea R., Elfring J., Gálvez-López D., Häussermann K., Janssen R., Montiel J.M.M., Perzylo A., Schießle B., Tenorth M., Zweigle O., van de Molengraft R.: RoboEarth – a World Wide Web for Robots, IEEE Robotics and Automation Magazine (Volume: 18, Issue: 2), IEEE 2011.
6. Gośliński J., Owczarek P., Rybarczyk D.: The use of Kinect sensor to control manipulator with electrohydraulic servodrives. Pomiary, Automatyka, Robotyka 17(2), 2013, pp. 481–486.
7. Warade S., Aghav J., Petitpierre C., Udayagiri S.: Automated Training and Maintenance through Kinect. International Journal of Computer Science, Engineering and Applications 2(3), 2012.
8. Le B., Nguyen A., Zhu Y.: Hand Detecting and Positioning Based on Depth Image of. International Journal of Information and Electronics Engineering 4(3), 2014, pp. 176–179.
9. Zhang X., Yan J., Feng S., Lei Z., Yi D., Li S.: Water Filling: Unsupervised People Counting via Vertical Kinect Sensor: IEEE Ninth International Conference on Advanced Video and Signal-Based Surveillance, 2012, pp. 215–220.
10. Holmquest L.: MSDN Magazine. 3D Sight with Kinect. http://msdn.microsoft.com/en-us/magazine/jj851072.aspx
11. Kozono K., Aoki M., Ono M., Kamikawa Y., Arimura H., Toyofuku F.: Accuracy Evaluation of Depth Data in Microsoft Kinect: Medical Physics 6/39, 2012, pp. 36–46.
12. Nima R.: Thesis: Industrial Applications of Microsoft Xbox Kinect Sensor., SOUTHERN ILLINOIS UNIVERSITY AT EDWARDSVILLE, 2013.
13. Nanotech website: http://www.nanotech.com.

**Automatyczny system generowania modeli 3D**

**Słowa kluczowe**

Modele obiektów, Sensory 3D, platforma RoboEarth.

**Streszczenie**

Trójwymiarowe modele znajdują zastosowanie w procesie detekcji jako obiekty referencyjne dla systemów identyfikacji. Platforma RoboEarth, której zadaniem jest obsługa chmur obliczeniowych dla zastosowań w robotyce, zawiera algorytmy umożliwiające zarówno rozpoznawanie obiektów, jak i generowanie ich modeli. W artykule przedstawiono zautomatyzowany system opracowany w celu poprawy procesu generowania modeli 3D obiektów, z wykorzystaniem oprogramowania platformy RoboEarth. Proces generowania modeli jest wykonywany z zastosowaniem specjalnych znaczników określających orientację i położenie obiektu oraz rejestrowaniu chmur punktów z różnych punktów odniesienia. Zmiana punktu odniesienia może być dokonana poprzez przemieszczenie sensora lub obrót obiektu. Opracowany system umożliwia automatyzację tego procesu poprzez zastosowanie obrotowego stolika pomiarowego napędzanego silnikiem krokowym. Ze względu na występowanie czynników, które mają wpływ na jakość generowanego modelu oraz w konsekwencji późniejszy proces detekcji obiektów, wykonano badania mające na celu określenie właściwych parametrów opracowanego systemu. Rezultaty przeprowadzonych badań zostały przedstawione w artykule wraz z przykładowymi wynikami detekcji obiektów.

INNOVATIVE ECONOMY
NATIONAL COHESION STRATEGY
INSTITUTE FOR SUSTAINABLE TECHNOLOGIES
NATIONAL RESEARCH INSTITUTE IN RADOM
EUROPEAN UNION
EUROPEAN REGIONAL DEVELOPMENT FUND

Project co-financed by the European Union from the European Regional Development Fund

**Jordan MĘŻYK**
Institute for Sustainable Technologies – National Research Institute, Radom
jordan.mezyk@itee.radom.pl

# MONITORING MATERIAL JOINING PROCESSES WITH USE OF ADVANCED VISION METHODS

**Key words**

Friction stir welding, quality inspection, optical inspection, thermal imaging.

**Abstract**

The article presents a method and a system for monitoring the processes of joining the materials with use of advanced vision techniques. The method and system are intended for use with the FSW joining method or similar techniques. The monitoring method consists in using a dual vision system comprised of a visible light camera and an infrared camera. The images recorded by both vision tracts are used to monitor the parameters of the process and to identify possible non-conformities of the weld. The developed system allows the monitoring of the process during the production of the joint with non-destructive, contactless techniques. The construction of the system allows its portability and adaptability for different types of FSW machines. Typical applications of the system include the monitoring of welding processes in the production line as well as laboratory testing for the development of the welding techniques.

## Introduction

The article presents the authors' method for monitoring the Friction Stir Weld (FSW) process. The FSW method [1, 2, 3] is a modern and still not very popular

method of joining two materials by "stirring" them after previous plasticisation with use of a proper tool. The rotary movement of the tool and its pressure against the welded surface generate friction and local heating of the materials that causes plasticisation. Next, the tool is moved linearly along the path of the expected weld, while the tool's pin stirs the materials and the tool's shoulder compresses the material in the produced weld. The important feature of the process is that the heated materials do not transform into liquid state and remain in the solid state. The method allows joining materials that are hard to arc weld or simply unweldable, including welding of different types of materials together.

## 1. Research problem and research method

There are few critical parameters to the welding process, which are spindle speed $v_n$, welding speed $v_z$, tilt angle $\alpha$, and the plunge force $F_p$. A poor choice of the parameters may result in producing faulty or just non-conformant welds. Non-conformant welds are not necessarily bad welds, but being merely mechanically strong it does not fulfil the requirements of the standard [4].

Typical non-conformances include excessive burrs, discontinuities, cracks, or an uneven edge of the weld. The following images present some examples of non-conformances (Fig. 1).

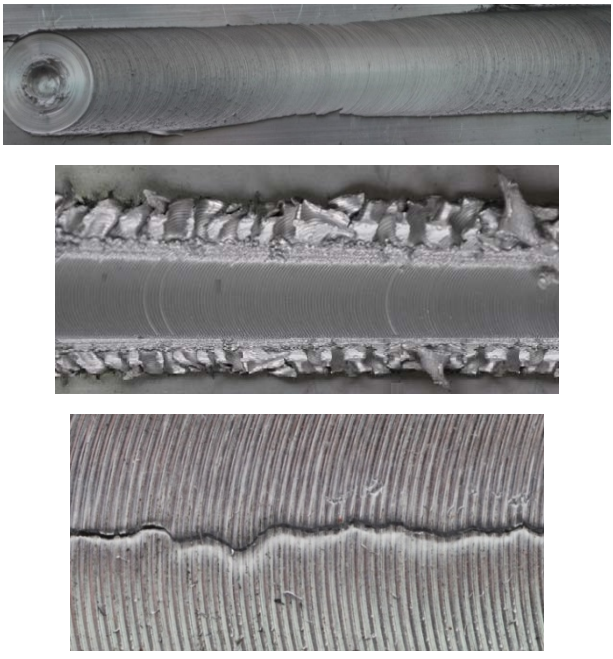

Fig. 1. Sample non-conformances in FSW process: (top to bottom) uneven edge of the weld, excessive burr on the edges, crack as an effect of overheating

In case of FSW welding, the quick and continuous inspection of the process should allow the elimination of produced faults in an automated manner already in the welding stand and allow the elimination of faulty elements. The authors of the article propose the method for monitoring the FSW process with use of a hybrid vision method, which is the recording of the image of the weld with use of thermovision camera and visible light camera (Fig. 2).

The surface of the welded material is observed by a matrix infrared camera to assess the temperature field behind the tool and with a line-scan camera that observes the surface of the material to observe the geometry of the weld.

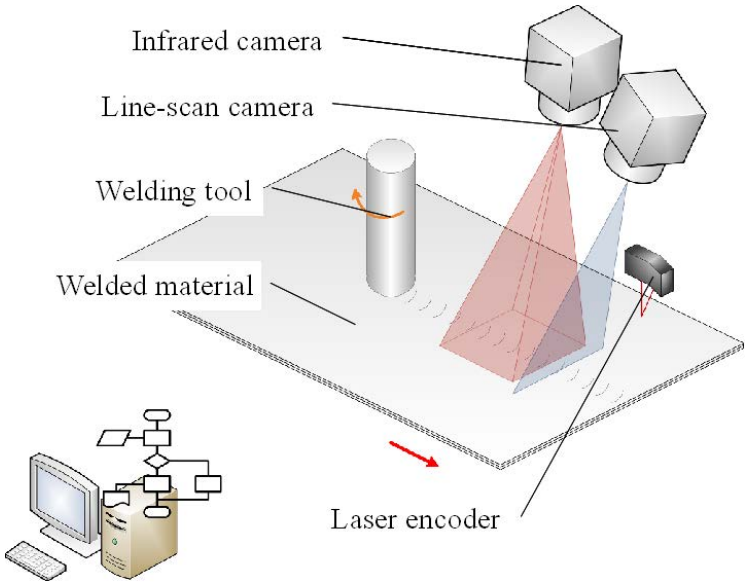


Fig. 2. The principle of the hybrid monitoring method for FSW process

The article presents selected results of introductory research performed with the use of only infrared imaging. The research on the monitoring of the FSW process of different types of materials was performed on a research stand built on the conventional vertical mill FYF32JU2. The stand was equipped with a process monitoring system based on the thermal imaging camera Flir SC5200 [5, 6], with a cooled InSb sensor for short wave IR that is for 2.5–5.1 μm. The measurement range is divided into three sub-ranges: 5–300°C, 25–600°C and 300–1500°C. The camera was controlled by the manufacturer's software "Altair". A photograph of the stand is presented in Figure 3.

Fig. 3. The view of the research stand for monitoring the FSW process with installed thermal imaging camera

## 2. Results

Several recordings of the process were made for different rotary and linear speeds of the tool. That allowed production of both correct and faulty welds that included non-conformances, such as excessive burrs, discontinuities, or an uneven edge of the weld. The recorded thermal sequences allow identification of the faults and non-conformances of the weld during the welding process. The application of thermal imaging camera also allows the detection of sub-surface faults.

A sample image from the camera recorded during correct process of FSW welding is presented in Figure 4, and Figure 5 presents a sample profile of the temperature during along the measurement line.

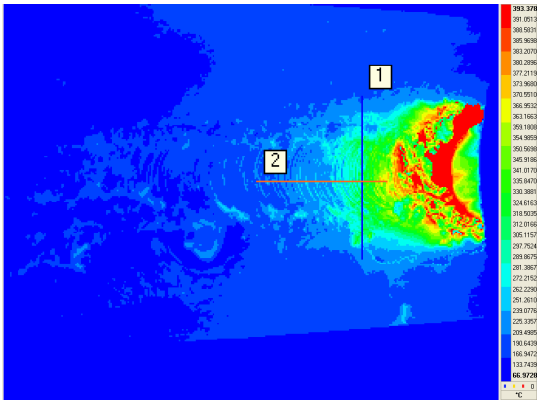


Fig. 4. The results of the measurement of the temperature with use of the camera: the thermogram from the FSW welding process

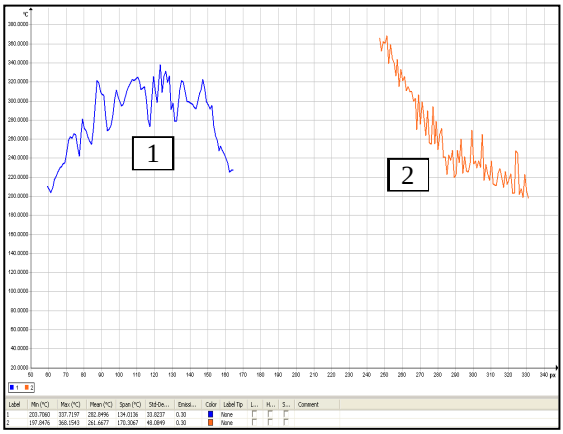


Fig. 5. The results of the measurement of the temperature with use of the camera: the profiles of the measured temperature along the measurement lines (see Fig. 4)

One of the characteristic phenomena in case of FSW welding is the appearance of excessive burr on both sides of the weld. There are also situations when part of the burr (a shaving) is pushed out behind the tool and stays on the surface of the weld causing disturbances during the measurement with the camera. Such disturbances are clearly visible on the thermograms and on the temperature profiles in the form of a local momentary decrease or increase of the temperature. The image from the camera and profile with the disturbance are presented in Figures 6 and 7.


Fig. 6. Thermogram with recorded disturbance in form of a shaving

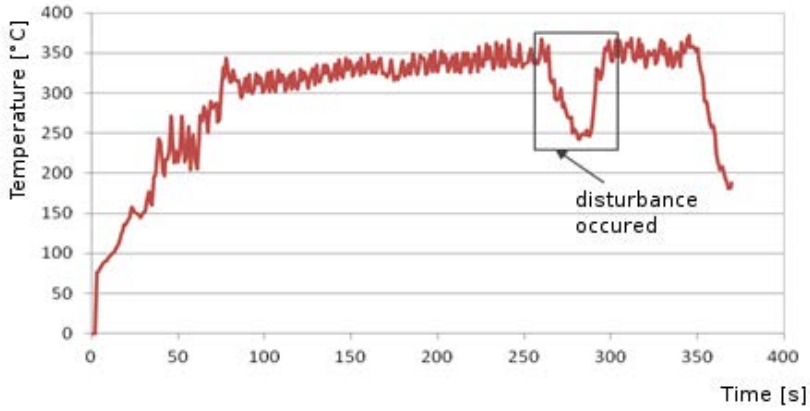


Fig. 7. The profile of the temperature with a marked result of the disturbance in form of a shaving

The recorded temperature profile (Fig. 7) has a clear "pit" that shows the presence of foreign material in the range of the observation of the surface of the weld.

The applied system intended for monitoring the FSW processes, built on the basis of the thermal imaging camera also allows the detection of sub-surface faults, such as empty spaces under the layer of the metal, cracks or the thermal results of tool's pin fracture, which are visible on the infrared camera but visible to the human eye. The view of the weld after the process, the thermogram of the surface of the weld recorded during process, and the temperature profiles along lines 1 and 2 are presented in figures 8 and 9.

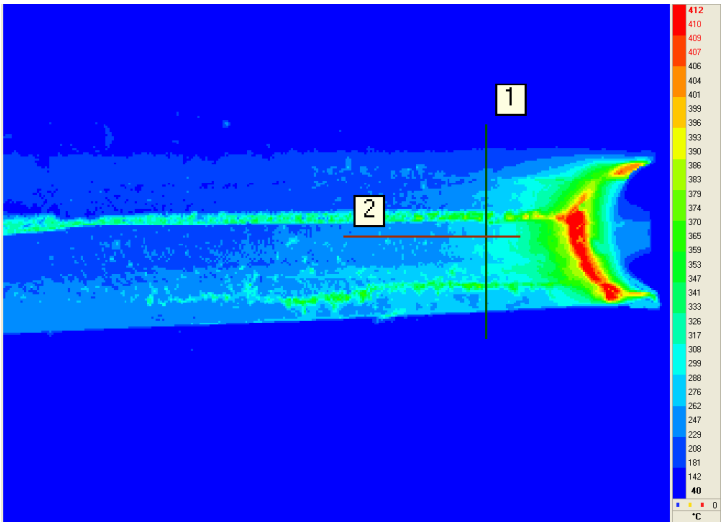


Fig. 8. Detection of sub-surface faults: thermal image of the surface during the process (see Fig. 9)

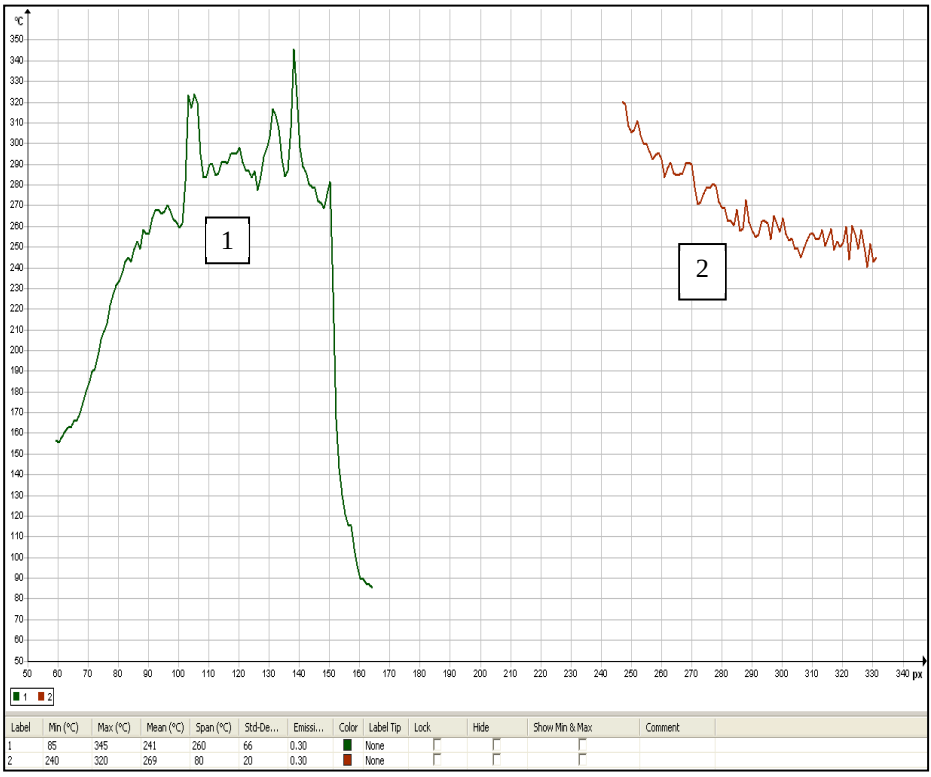


Fig. 9. Detection of sub-surface faults: temperature profiles along the lines 1 and 2 (see Fig. 8); marked is a temperature peak that shows the sub-surface cavity

Another example of sub-surface fault detection is shown below. The surface of the weld (Fig. 10) is unequal, but the weld itself seems continuous. Visual observation does not show excessive non-conformities.

Fig. 10. The view of the weld surface

The observation of the weld using thermal imaging camera (Fig. 11) shows that there exists some irregularity in the structure of the weld.

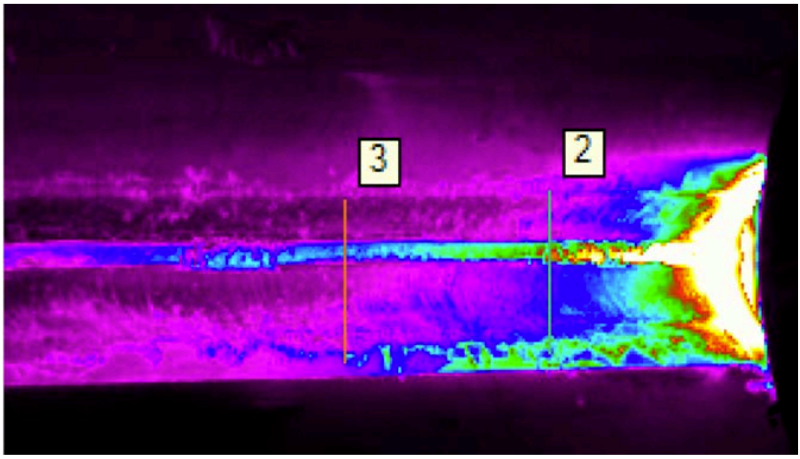


Fig. 11. Thermal image of the surface during the process (see Fig. 10)

The irregularity shows as a line of increased temperature along the path of the tool. The analysis of the temperature profiles along lines 2 and 3 indicates obvious variations of temperature.

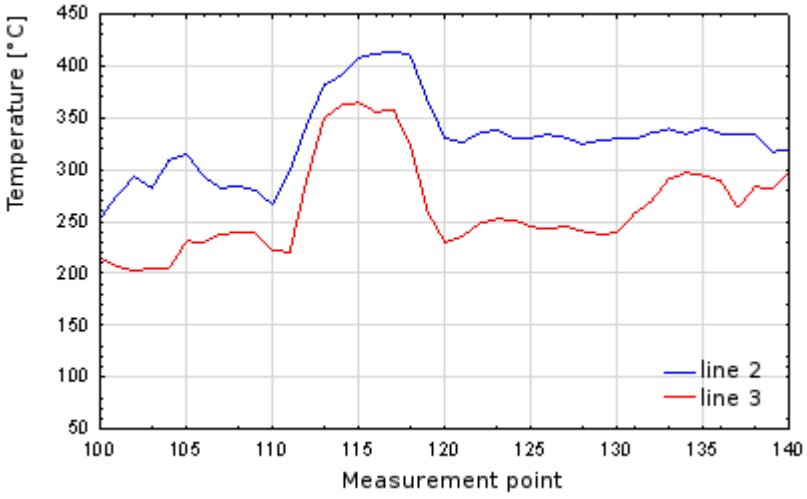


Fig. 12. Temperature profiles along the lines 2 and 3 (see fig. 11)

The assessment of the weld should be unequivocal – the weld is faulty.

## Conclusion

The presented monitoring method for the friction stir welding process consists in the utilisation of information contained in the images of the weld recorded in infrared band and visible light band. The proposed hybrid inspection system, thanks to its modular and flexible structure, may be adapted to all kinds of FSW types and FSW machinery. A crucial element of the system is a database with a pattern catalogue as well as non-compliances catalogue.

The method is intended for FSW processes, but its general principle of using two light wavelengths allows its application for other uses, such as arc-welding process monitoring, the assembly of components at high temperatures, and the testing of products at high temperatures.

*Scientific work executed within the Strategic Programme "Innovative Systems of Technical Support for Sustainable Development of Economy" within Innovative Economy Operational Programme.*

## References

1. Lohwasser D., Chan Z.: Friction Stir Welding. From basics to applications. Woodhead Publishing Series in Welding and Other Joining Technologies No. 66, USA 2010.
2. Birsan D., Visan D., Mircea O.: Temperature monitoring in friction stir welding using thermovision method. The Annals of "Dunarea de Jos" University of Galati, Fascicle XII, Welding Equipment and Technology, 2009, pp. 45–49.
3. Dawes C.J.: An introduction to friction stir welding and its development. Welding & Metal Fabrication, UK, 1995.
4. ISO 25239-5:2011 Friction stir welding – Aluminium – Part 5: Quality and inspection requirements.
5. Minkina W., Dudzik S.: Infrared Thermography: Errors and Uncertainties. John Wiley & Sons, UK, 2009.
6. www.flir.com.
7. www.basler.com.

**Monitorowanie procesów łączenia materiałów z wykorzystaniem zaawansowanych metod wizyjnych**

**Słowa kluczowe**

Zgrzewanie tarciowe z mieszaniem materiału FSW, kontrola jakości, optyczna inspekcja, analiza termograficzna.

**Streszczenie**

W artykule zaprezentowano metodę oraz system do monitorowania procesów wytwarzania połączeń materiałowych z użyciem zaawansowanych technik wizyjnych. Metoda oraz system przeznaczone są do wykorzystania z technologią zgrzewania tarciowego z mieszaniem materiałów (FSW – ang. *Friction Stir Welding*) lub podobną. Metoda monitorowania polega na wykorzystaniu dualnego systemu wizyjnego składającego się z kamery światła widzialnego oraz kamery termowizyjnej. Obrazy rejestrowane w obu torach optycznych wykorzystywane są do monitorowania parametrów procesu oraz do identyfikacji potencjalnych niezgodności powstałej spoiny materiałowej. Opracowany system pozwala na monitorowanie procesu łączenia on-line z wykorzystaniem nieniszczącej, bezkontaktowej techniki pomiarowej. Konstrukcja systemu umożliwia jego montaż i adaptację do różnych typów maszyn do zgrzewania tarciowego. Typowe zastosowania dla prezentowanego rozwiązania obejmują monitorowanie procesów zgrzewania na liniach produkcyjnych oraz badania laboratoryjne, których celem jest rozwój technologii zgrzewania tarciowego.

**Jarosław ZDROJEWSKI, Sławomir BUJNOWSKI,**
**Ryszard WOCIANIEC, Adam MARCHEWKA**
UTP University of Science and Technology, Bydgoszcz
jaroslaw.zdrojewski@utp.edu.pl, slawomir.bujnowski@utp.edu.pl,
ryw@utp.edu.pl, adam.marchewka@utp.edu.pl

# MULTI CAMERA OPTICAL SYSTEM FOR ALIGNMENT AND INSPECTION DURING PCB MANUFACTURING PROCESSES

**Key words**

Panel and film alignment, camera, optical inspection, supervision of the manufacturing process.

**Summary**

The paper presents a method of multipoint alignment using optical inspection of printed circuit board layers during manufacturing processes and exposure stage. The presented system is based on eight movable monochrome CCD cameras that supplies input data for the complex registration system. The article presents an analysis of the results of experiments for selected types of targets using the proposed location optimization method, allowing the evaluation of the correctness and stability of the system. The paper also presents an analysis of the efficiency and limitations of the proposed approach. In the article, the advantages of using the proposed method in the PCB manufacturing process are discussed.

## Introduction

Printed circuit board manufacturing processes are complex. To get the proper results, the board has to go through many production stages. One of them, exposure (or printing), is crucial. It entails copper pattering on each layer, masking the pads and contacts, coating the layers, and making the pads and contacts "solder ready." Basically, the manufacturing cycle begins with the project files, including the specifications sent to the producer. It is conducted in a technological process consisting of following stages: exposure, development, etching, building assembly, lamination (for multilayer circuits), drilling, plating, solder masking, and label printing [2]. The whole process gets even more complicated when some connections in the multilayer printed circuit board are made using buried or blind holes. The majority of these stages require continuous control, which is mostly conducted automatically in optical measuring devices. The geometry and electrical parameters of the constructed circuit are measured to keep observed deviations within defined tolerance limits in order to reach the quality of the final product through applying the required corrections to the technological process [4].

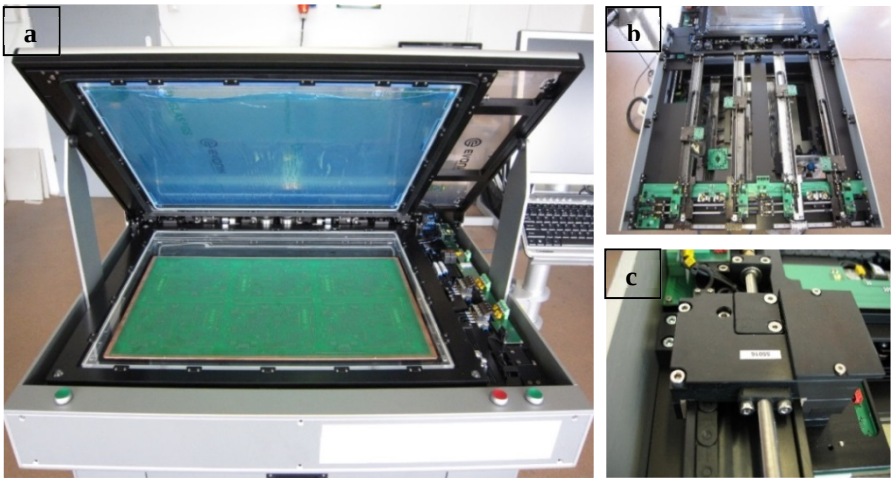


Fig 1. Exposure system: a) alignment frame and solder mask panel ready for registration ad exposure, b) multi camera optical system for alignment and inspection, c) top view of then registration camera

The printing process is realized using exposure machines, currently being very sophisticated tools to expose a single layer of the circuit and to maintain alignment, control geometry, and track-layer position by a complex alignment process using a multi-camera optical system. A good example of the system is the printer shown in Figure 1a. The presented system is able to lead not only double-sided printing but also active registration of both sides – film alignment to the marks located on the panel. To have this ability, it has two separated sets of cameras. Each set belongs to a given side of panel and is dedicated to grab

images and measure panel and film marks using image processing software [1, 8, 9, 10]. The data of the measured marks is directly used in the control process during alignment to move the axes assigned to the given film frame.

In the configuration of the system presented in Figures 1b and c, all cameras move in the X and Y direction with a range limited by specified minimal and maximal panel size. All four cameras located on the left can reach and measure some features on the left side of the panel, right ones on the right. A similar split exists for the top and bottom camera groups. Because the printer has to deal with fiducial targets, the system is using LED based illumination, and the etched marks are visible thanks to the reflection light bouncing back from the mask covered copper to the camera.

## 1. Films alignment based on multi reference marks

The registration system should be a compromise between the number of measurement points on the board, the number of cameras used, and the time needed to evaluate input data, which includes images from all sources [5]. Taking into account the requirements and the experience of production techniques for manual registration, two solutions were considered. The first uses two cameras per panel side and two marks on the board layout and films. In this case, the marks are located centrally in the symmetry axis of the two shorter sides of the panel. The second solution assumes the use of four cameras per panel side and appropriate marks located in the corners of the board. In general, if printer is running double-sided exposure and alignment on both side is required, two or four registration marks on the bottom of the panel and the same two or four on the top are needed.

Regardless of the number of marks and number of cameras, film positioning is aimed at optimization. Optimization the task of minimizing the position deviations, which depend on both instable film size and the variable location of the panel holes used as registration marks.

System can operate in two different tolerance modes [3]: dimensional deviations (film to board) and alignment deviation. The basic mode is the mode of DA (Dimensions/Alignment) in which dimensional tolerance [7] and the alignment tolerance are defined separately. In this mode, the measuring system will calculate the position of the registration marks based on processed input images from the cameras. Using this data, the system will separately calculate dimensional deviations for both the films and the alignment deviations film to board or film to film. All calculated values will be compared with a given tolerance level. If the dimensional deviation is greater than the dimensional tolerance (DT), the system will stop the registration procedure and an error message describing the reason will be presented to the operator. In the case of crossing the tolerance limit for the alignment deviations (AT), the registration

process will be repeated and new deviations will be compared once more with the given tolerance values.

## 2. Experimental results

At the start of the research, it was assumed that, during the production process, a comparison between single and double camera layer mode has to be made. To reach this goal, a special type of target was introduced. It was crucial to have good alignment conditions for configuration of the 8 cameras, and it was necessary to have access to the data [6], usually supplied by a single set of sources based on 4 corner marks and holes on the top film.

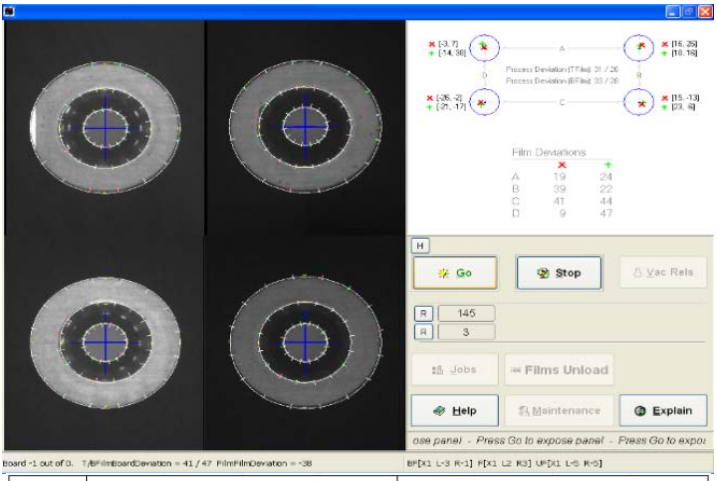


| Panel | Top view | | | | Bottom view | | | |
|---|---|---|---|---|---|---|---|---|
| nb | x | yl | yr | pd | x | yl | yr | pd |
| 1 | -6 | 14 | 9 | 30 | -7 | 12 | 12 | 37 |
| 2 | 4 | 12 | 15 | 38 | 1 | 10 | 15 | 45 |
| 3 | -12 | -7 | 11 | 33 | -14 | -8 | 12 | 40 |
| 4 | -6 | -6 | -2 | 25 | -9 | -3 | 3 | 32 |
| 5 | -12 | 1 | 3 | 27 | -14 | -5 | 2 | 34 |
| 6 | -13 | 2 | 13 | 30 | -15 | 3 | 13 | 37 |
| 7 | -6 | -12 | -13 | 34 | -9 | -11 | -14 | 41 |
| 8 | -3 | -13 | -2 | 33 | -7 | -13 | -6 | 41 |
| 9 | -12 | -8 | -1 | 31 | -9 | -7 | -2 | 38 |
| 10 | 12 | -3 | -11 | 32 | 12 | -5 | -10 | 39 |
| AVG | -5,35 | -2,01 | 2,15 | 31,20 | -7,10 | -2,72 | 2,50 | 38,31 |
| B/T % | | | | | 1,33 | 1,35 | 1,16 | 1,228 |

Fig. 2. Results showing the results screen of the control program and table including a comparison of alignment error and process deviations

Final verification was made on the optical measuring machine, where each single side was measured independently. Results of the research process are presented on Figure 2. Figure 2 shows the ratio of the reduction of two important

factors. The average value of the align error was reduced by 28.1%, and process deviation was reduced by 22.8%. The presented data do not include the values representing bottom film alignment, because the conditions for this layer have not been altered from standard operation. It is important to notice that outer layer exposure was made on the same printer and the level of error reduction is basically limited by the precision or imprecision accepted in the previous production stage. Of course, in any case, imprecision represented by alignment error is limited by alignment strategy tolerances defined in the job.

## Conclusion

The multi-camera optical system for alignment and inspection supports production quality control and provides opportunities for measurable benefits in terms of minimizing both the alignment error and impact of films and panel dimensional deviation. In comparison to the standard single side camera setup, significant improvement for the top film position in relations to the etched top outer layer was noticed. Beside an enhanced hardware configuration, stable and reproducible operation was observed. Threats to the proper operation of the registration process are interferences from external friction, which is a side effect of the sticky mask panel surface and the bottom film. Those limitations have a large impact in the situation when the alignment process has to be repeated under conditions defined by job tolerances.

Applying of multi-camera optical system for alignment and inspection in the process of printing mask panels allows one to enhance registration capability, alignment process control, and printing feedback in better selectivity and accuracy compared to the regular procedure. Final alignment quality can be ensured and verified right before printing.

The use of the multi-camera optical system for alignment and inspection allows obtaining significantly better mask printing results. The achieved reduction in process deviation displays the possibility for a strong recommendation for the mask printing applications.

## References

1. Choraś R.S.: Komputerowa wizja. Metody interpretacji i identyfikacji obiektów, Akademicka oficyna wydawnicza EXIT, Warszawa 2005.
2. Coombs C.F.: Printed Circuit Handbook 6th Edition, McGraw-Hill 2007.
3. Marchewka A., Zdrojewski J.: Film Alignment Before Solder Mask Exposure, Image Processing & Communications Challenges 3, AISC 102, Springer Heidelberg 2011, pp. 387–393.
4. Ohlig B.: Registration and Knowledge Through and Across Your Panel, CircuiTree 2002.

5. Wocianiec R., Zdrojewski J.: Film Position Optimization Before Exposure, Image Processing & Communication An International Journal 2010, vol. 5, no. 2, pp. 35–46.
6. Zdrojewski J., Marchewka A., Pérez de Prado R.: Registration and Analysis of Data during Registration and Exposure Process, Image Processing & Communications Challenges 6, Advances in Intelligent Systems and Computing 2015, vol. 313, pp. 237–243.
7. Zdrojewski J., Marchewka A.: Phototool geometry verification, Proceedings of the 8th International Conference on Computer Recognition Systems CORES, Springer-Verlag, Berlin Heidelberg 2013, pp. 501–509.
8. Marciniak T., Lutowski Z., Bujnowski S., Boroński D., Giesko T., „Application of Digital Image Correlation in Fatigue Crack Analysis", Materials Science Forum Vol. 726 – Fatigue Failure and Fracture Mechanics, 2012 Trans Tech Publications, pp. 218–222.
9. Marciniak T., Lutowski Z., Bujnowski S., Boroński D., Czajka P., „Dual-Band Experimental System For subsurface Cracks Testing", Materials Science Forum Vol. 726 – Fatigue Failure and Fracture Mechanics, 2012 Trans Tech Publications, pp. 222–226.
10. Boroński D., Giesko T., Marciniak T., Lutowski Z., Bujnowski S., „Detekcja i pomiar długości pęknięcia zmęczeniowego z zastosowaniem systemu FatigueVIEW", Przegląd Mechaniczny 4/2014,2014 IMBiGS, s. 21–27.

**Wielokamerowy system pozycjonowania klisz w procesie wytwarzania PCB**

**Słowa kluczowe**

Pozycjonowanie klisz i paneli, kamera, inspekcja optyczna, nadzór procesu wytwarzania.

**Streszczenie**

W artykule opisano metodę wielopunktowego pozycjonowania przy użyciu inspekcji optycznej warstw obwodu drukowanego w czasie wytwarzania i na etapie naświetlania. Prezentowany system zbudowano w oparciu o osiem przemieszczalnych, monochromatycznych kamer CCD dostarczających dane wejściowe do złożonego układu pozycjonującego. W artykule przedstawiono analizę wyników eksperymentów dla wybranych typów znaczników i zadanej metody optymalizacji, co pozwoliło na ocenę poprawności zachowania i stabilności układu. Artykuł zawiera analizę efektywności i ograniczeń przedstawionego rozwiązania. Poddano dyskusji zalety użycia zaproponowanej metody w wytwarzaniu PCB.

INNOVATIVE ECONOMY
NATIONAL COHESION STRATEGY
INSTITUTE FOR SUSTAINABLE TECHNOLOGIES
NATIONAL RESEARCH INSTITUTE IN RADOM
EUROPEAN UNION
EUROPEAN REGIONAL DEVELOPMENT FUND

Project co-financed by the European Union from the European Regional Development Fund

**Wojciech JÓŹWIK, Szymon ZACHARSKI**
Institute for Sustainable Technologies – National Research Institute, Radom
wojciech.jozwik@itee.radom.pl
szymon.zacharski@itee.radom.pl

# COMPARISON OF THE RESULTS OF TESTS ON AXISYMMETRIC ELEMENTS CONDUCTED ON AN INDUSTRIAL AND LABORATORY TEST STAND AND EMPLOYING AN EDDY CURRENT METHOD

**Key words**

Eeddy current, defect detection, bearing ring.

**Abstract**

The aim of the study was to compare the test results obtained at the stand intended for the industrial inspection of the quality of bearing rings with the results of tests performed on the laboratory stand. The tests concerned four inner bearing rings. In three of them, artificial defects were made, while the fourth ring played the role of a model ring. Both the inner and outer surface of the ring was scanned at the time of the test.

The tests on both the industrial and laboratory stand revealed a lower level of signal for an inner defect that resulted from the distance between the measurement head and the tested surface.

The results of tests formed the basis for the determination of the border values of the measurement signal categorising the ring as faulty. Due to the different level of the signal for the outer and inner surface, the authors proposed that the border values should be determined separately for each surface. The obtained results enabled the development of the calibration method for the system of automatic inspection of the quality of the bearing rings.

## Introduction

The production of the bearing ring is a multistage process including forging, turning, quenching, and grinding. Inaccurate execution of the process can lead to material defects in the end product, i.e. the bearing ring. The discontinuities in the form of blisters, cracks, or non-metallic inclusions can result in a stress concentration that in turn can damage the ring and lead to industrial or transport accidents.

There are a number of non-destructive test methods that enable the inspection of bearing rings, e.g. optical inspection, magnetic-powder method, ultrasound, X-ray (tomography), and the eddy current method. The problems with the application of optical inspection lie in the difficulty to detect subsurface defects of the bearing ring. Selected literature [1] shows that the presence of grinding smudges on the surface of the ring indicates the presence of a subsurface defect. This issue has not been fully recognised yet, and it needs to be further studied. The methods that enable the detection of subsurface material discontinuities are the magnetic-powder method and ultrasound defectoscopy. However, these two methods cause fouling the tested surface. The method that helps one to properly define the location of the defect and its dimensions is the X-ray method. Unfortunately, the use of this method needs to be governed by very strict health and safety regulations. Moreover, X-rays and computed tomography (CT) are time-consuming methods, and the synchronisation of the devices employing them with the cycle of the production line would require simultaneous operation of many stands. Therefore, the method of eddy currents seemed to be the most appropriate as far as the inspection of bearing rings was concerned [2]. This was due to the fact that it can detect both surface and subsurface defects [3], does not call for the use of the coupling agent or other operating fluids, and does not need the measurement head to be in the direct contact with the object tested. Additionally, this is a quick test method.

## 1. Application of the eddy current method in quality inspection of goods

The eddy current method is widely used in devices intended for the inspection of the quality of final products. The main challenge is the proper

interpretation of the signal generated by the defectoscope. Paper [4] describes an algorithm of the interpretation of the scanning signal of a pipe constituting an element of a nuclear reactor. The objective of the study was to develop the algorithm enabling the determination of the kind of defect in an axisymmetric element. In this case, the tests need to be conducted for many frequencies of a transducer. Paper [5] describes a device intended for semi-automatic, cyclical inspection of the wheels of airliners. The scanning is automatic at a manual installation of the wheel in the testing machine. The time of the test was shortened to 4 minutes per wheel, and the results were compared with the results obtained when the ultrasound method was used. At the time of the verification of the system, a faulty wheel was found, whose defect was also observed during the tests complying with the current regulations.

Paper [6] presents an idea on how to use the eddy current method for automatic control of carbon fibre reinforced composites (CFRP) obtained through the automatic fibre placement (AFP). The authors indicated that the eddy current method has a great potential in the automatic detection of changes in the structure of carbon fibres in the composite.

## 2. Test objectives and research instrumentation

The objective of the study was to verify the possibility to detect material discontinuities by the system intended for automatic inspection of the quality of bearing rings. For that purpose, the readings of the eddy current defectoscope were compared in industrial and laboratory environments. The tests conducted in the industrial environment were performed using a stand for industrial inspection of the quality of bearing rings developed at the Institute for Sustainable Technologies – National Research Institute. The system is intended for the automatic inspection of rings of tapered roller bearings [7, 8].

During previous tests performed on the laboratory stand, the authors decided that the measuring head should be placed in a grip guaranteeing constant contact with the tested ring [9] and that the scanning should be conducted at the transducer frequency of 0.06 kHz [10]. A drop in the frequency means that the depth of the eddy current penetration into the tested material is greater, which enables the detection of subsurface material defects [11]. Paper [12] shows that the eddy current method helps one to detect 45μm deep corrosion losses. The detection of small surface defects needs the frequency of the transducer to be in the range of 5–25 kHz, which prevent detection of subsurface defects.

A kinematic draft of the measurement system for inner bearing ring tests is presented in Fig. 1. The laboratory tests were performed on the stand shown in Fig. 2. The ring was placed in a three-jaw chuck powered by the servomotor.

The tests were conducted for the rotational speed of the ring of 60 rpm. The previous work indicated that the increase in the rotational speed facilitates the detection of both surface and subsurface defects [10]. The determination of the rotational speed is necessary for the detection of a defect, the reduction of vibrations of the industrial test stand, and the required efficiency of the inspection process.

At the time of laboratory and industrial tests, an SSEC III PC eddy current defectoscope was used. The device is equipped with a digital output and two analogue outputs determining the real and imaginary part of the readings of the measuring head. The analogue signal is generated in a voltage form in the range of 1000–1000 mV, and it is used for the communication with the external devices. The digital signal is intended for the communication between the defectoscope and the PC, and through it, the user sets up the operation of the measuring device.

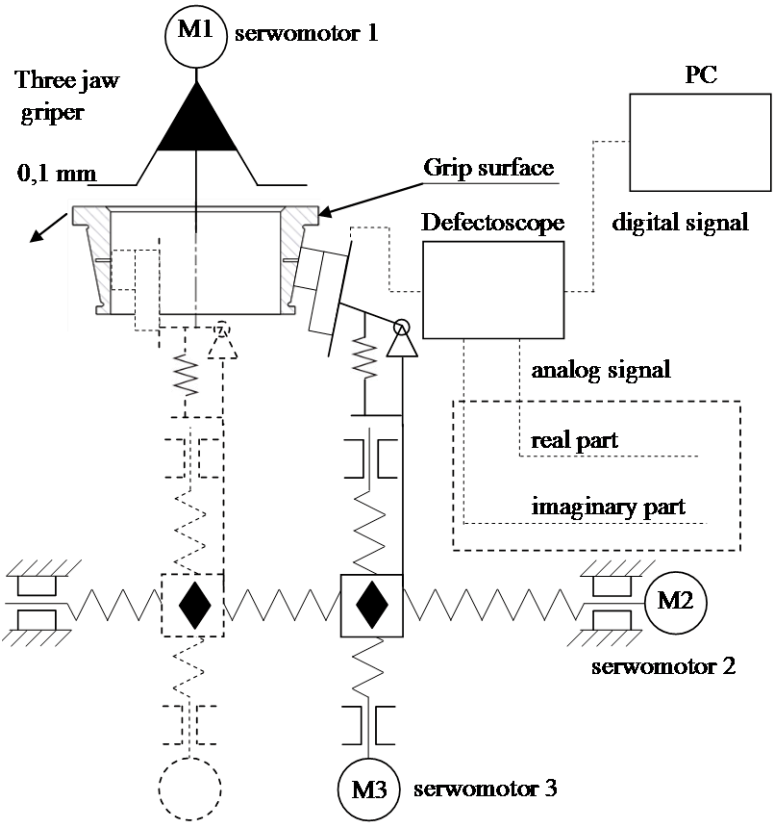


Fig. 1. Schematic of the measurement stand in the industrial stand

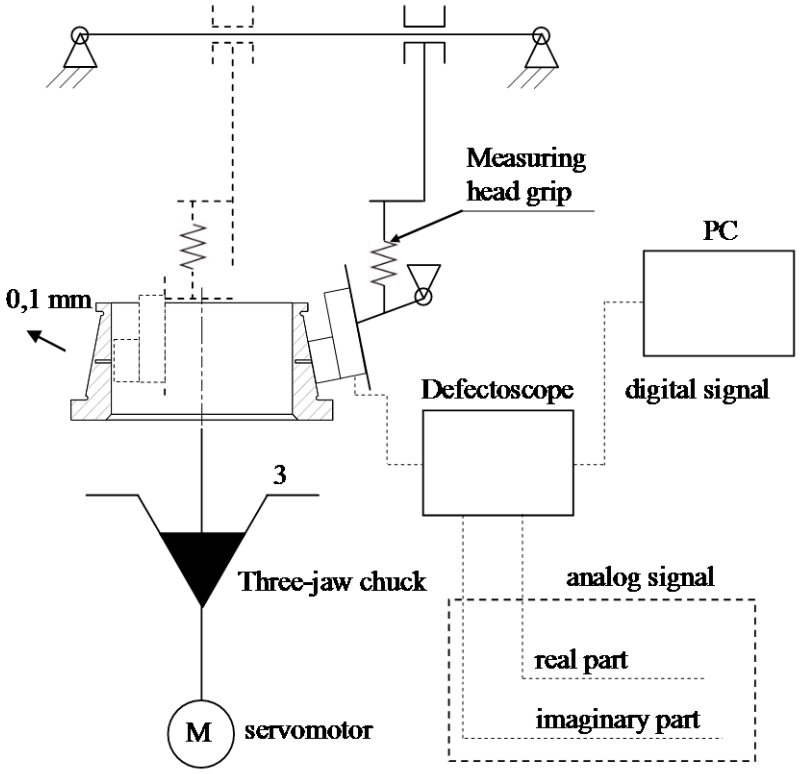


Fig. 2. Schematic of the laboratory stand

## 3. Test object

The tests were conducted for four inner rings of the tapered roller bearing. In three of them, artificial test defects were made, while the fourth was used as a model ring. The test defects in the form of blind holes were made to reconstruct real defects created during the technological process. The studied rings are presented in Figures 3–6.

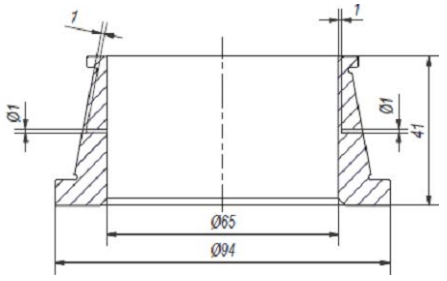


Fig. 3. Ring 1

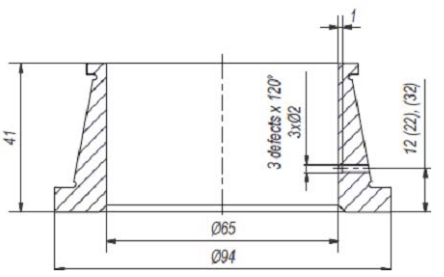


Fig. 4. Ring 2

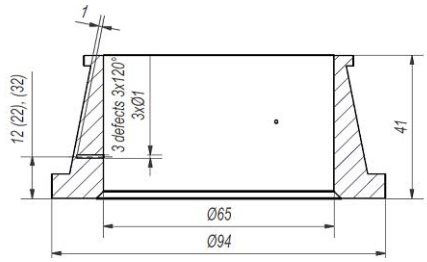


Fig. 5. Ring 3

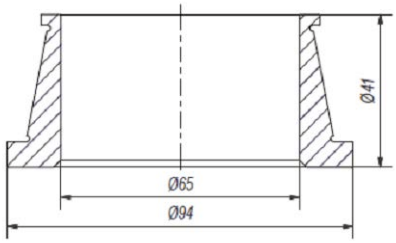


Fig. 6. Ring MR

## 4. Tests on a laboratory stand

The tests were performed for the inner and the outer surface of the ring. There were five measurements conducted for each ring. The examples of the results are presented in Figures 7–14. The values that were measured included the size of the defect for the real and the imaginary component, which was defined as the peak-to-peak value of the signal. In order to improve the transparency of the graphs, the value of the imaginary component was reduced by the constant value of 400 mV.

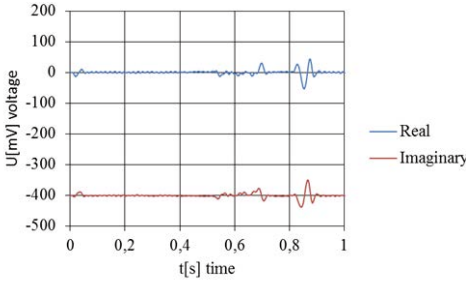


Fig. 7. Ring 1 test from the inside

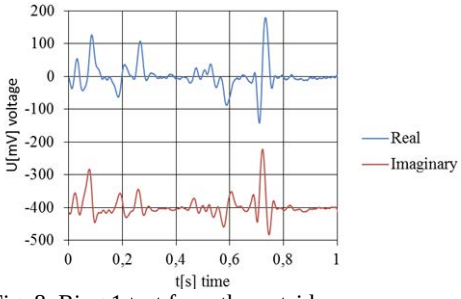


Fig. 8. Ring 1 test from the outside

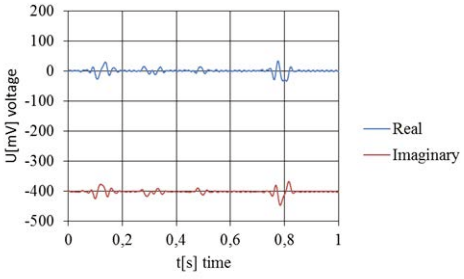


Fig. 9. Ring 2 test from the inside

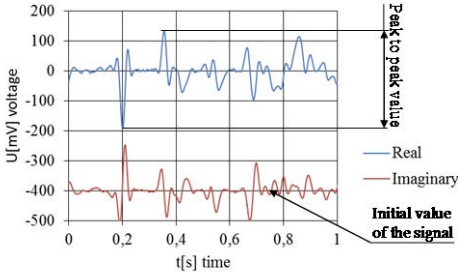


Fig. 10. Ring 2 test from the outside

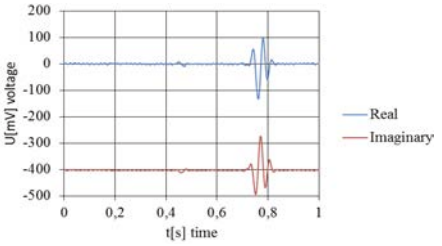


Fig. 11. Ring 3 test from the inside

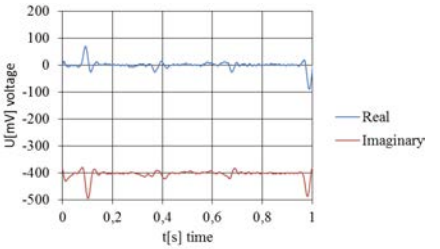


Fig. 12. Ring 3 test from the outside

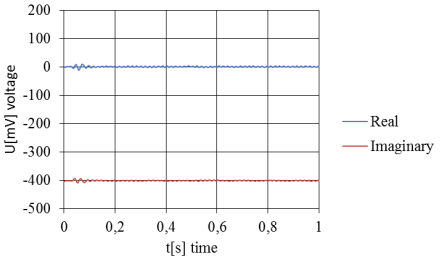


Fig. 13. Model ring test from the inside

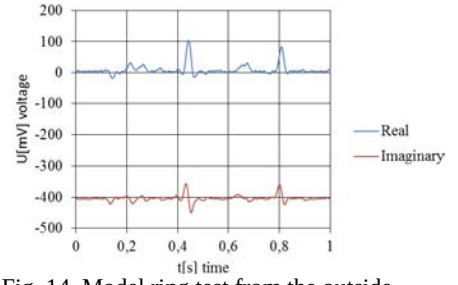


Fig. 14. Model ring test from the outside

The authors observed that for Ring 1 and the model ring (MR) the peak-to-peak value of the signal was lower in the case of the inner surface. The cause for the differences is the distance of the middle point of the measuring head from the tested surface [10], which in the case described was 0.6 mm (the width of the measuring head = 13 mm, the diameter of the ring = 65 mm). The collective results of the tests on the laboratory stand are presented in Table 1.

Table 1. Collective results of tests on the laboratory stand

| | | Peak-to-peak value [mV] | | | |
|---|---|---|---|---|---|
| | | Scanning of the outer surface | | Scanning of the inner surface | |
| Value | Ring | Real | Imaginary | Real | Imaginary |
| Arithmetic mean | 1 | 305.8 | 280.2 | 89 | 93.2 |
| | 2 | 316.2 | 259.4 | 78.4 | 73.6 |
| | 3 | 155.4 | 136 | 223.8 | 217.4 |
| | MR | 108.6 | 105.4 | 19.4 | 17.2 |
| Standard deviation | 1 | 19.7 | 17.8 | 5.1 | 4.8 |
| | 2 | 13.4 | 9.1 | 8.2 | 4.6 |
| | 3 | 3.6 | 18 | 3.3 | 3 |
| | MR | 10.1 | 7.1 | 1.1 | 1.5 |
| Minimum value | 1 | 284 | 261 | 84 | 88 |
| | 2 | 295 | 247 | 67 | 68 |
| | 3 | 150 | 115 | 220 | 214 |
| | MR | 98 | 94 | 18 | 15 |
| Maximum value | 1 | 331 | 304 | 97 | 97 |
| | 2 | 327 | 271 | 87 | 79 |
| | 3 | 159 | 156 | 229 | 221 |
| | MR | 122 | 113 | 21 | 19 |

## 5. Tests on the industrial stand

Each ring was tested five times. One measurement concerned the full ring test (scanning of the inner and outer surface). The examples of the measurements are presented in Figures 15–18.

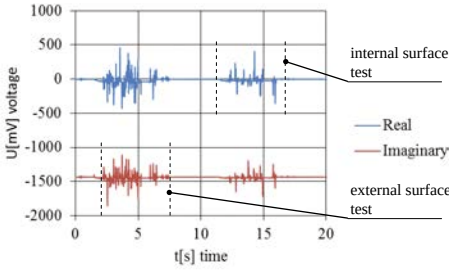


Fig. 15. Test of Ring 1

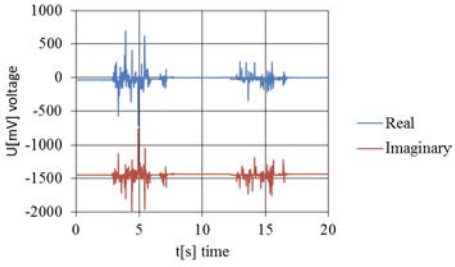


Fig. 16. Test of Ring 2

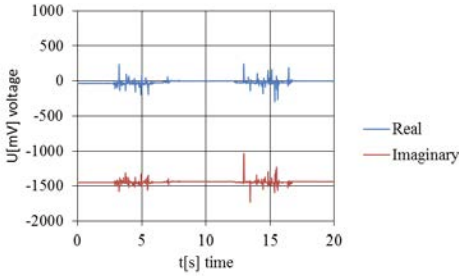


Fig. 17. Test of Ring 3

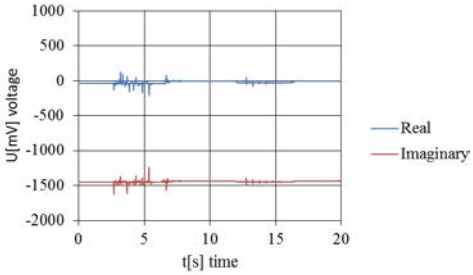


Fig. 18. Test of Model Ring

For each measurement the following statistical values were defined: the highest, arithmetic mean, and the standard deviation. The cumulative results of the test are presented in Table 2.

Table 2. Cumulative results of tests on the industrial stand

| | | Peak-to-peak value [mV] | | | |
|---|---|---|---|---|---|
| | | Scanning of the outer surface | | Scanning of the inner surface | |
| Value | Ring | Real | Imaginary | Real | Imaginary |
| Arithmetic mean | 1 | 818.8 | 795.2 | 689.2 | 404.6 |
| | 2 | 1253.6 | 1417.8 | 643.6 | 606.6 |
| | 3 | 334.6 | 343.4 | 627.2 | 738.8 |
| | MR | 319.8 | 321 | 104.8 | 103.2 |
| Standard deviation | 1 | 50.5 | 54.8 | 59.9 | 73.1 |
| | 2 | 143.3 | 111.7 | 104.1 | 82.8 |
| | 3 | 100.7 | 79.2 | 166.6 | 142.2 |
| | MR | 20.6 | 24 | 16.3 | 13 |

| | | Peak-to-peak value [mV] | | | |
|---|---|---|---|---|---|
| | | Scanning of the outer surface | | Scanning of the inner surface | |
| Value | Ring | Real | Imaginary | Real | Imaginary |
| Minimum value | 1 | 744 | 742 | 620 | 317 |
| | 2 | 1065 | 1320 | 532 | 496 |
| | 3 | 217 | 246 | 477 | 532 |
| | MR | 303 | 299 | 88 | 88 |
| Maximum value | 1 | 885 | 875 | 761 | 520 |
| | 2 | 1408 | 1603 | 801 | 721 |
| | 3 | 443 | 417 | 836 | 876 |
| | MR | 354 | 357 | 121 | 114 |

The threshold defining the ring as faulty was the maximum value of the signal generated for the model ring. The authors observed that, in the case of the scanning of the external surface of Ring 3, both components of the signal exceeded the border value only in Test 4 (Table 3). The results that were not higher than the border value are presented in bold.

Table 3. Peak-to-peak value of the signal for Ring 3

| | Scanning of the outer surface | | Scanning of the inner surface | |
|---|---|---|---|---|
| Test no | Real [mV] | Imaginary [mV] | Real [mV] | Imaginary [mV] |
| 1 | **312** | 398 | 505 | 729 |
| 2 | 434 | **270** | 541 | 689 |
| 3 | **217** | 417 | 477 | 876 |
| 4 | 267 | 386 | 836 | 868 |
| 5 | 443 | **246** | 777 | 532 |

## 6. Comparison of results

The results of the tests performed on the industrial stand are different from the tests on the laboratory stand. The values of the signal generated by the industrial measurement system are several times higher than are those generated by the laboratory stand. Table 4 shows the quotient of the average values of the results obtained on the laboratory and industrial stand (Equation 1). The problem during the tests on the industrial stand concerned the noise with the value of about 100 mV, which for the test on the laboratory stand is only about 10 mV.

$$K = \frac{U_I}{U_L} \tag{1}$$

Where:

K – Signal comparison coefficient,
$U_I$ – Average value of the signal on the industrial stand,
$U_L$ – Average value of the signal on the laboratory stand.

Table 4. Comparison of results obtained on the laboratory and industrial stands

| K coef. | Scanning of the outer surface | | Scanning of the inner surface | |
|---|---|---|---|---|
| Ring | Real [mV] | Imaginary [mV] | Real [mV] | Imaginary [mV] |
| 1 | 2.68 | 2.84 | 7.74 | 4.34 |
| 2 | 3.96 | 5.47 | 8.21 | 8.24 |
| 3 | 2.15 | 2.53 | 2.8 | 3.4 |
| MR | 2.94 | 3.05 | 5.4 | 6 |

## Conclusions

Despite significant differences in the results of measurements, all rings in which artificial test defects were made were qualified as faulty, both in the case of laboratory and in the case of industrial tests. The factor hampering the execution of tests on the industrial stand were the vibrations of the measurement system at the time of the operation of the device, which increased the measurement noise. At the time of the development of the automatic testing machine, it is necessary to increase the stiffness of the structural elements.

The increase value of the signal observed at the time of tests on the industrial stand stems from the complex movement of the measuring head. At the time of the test on the laboratory stand, the measuring head is immobilised, while on the industrial stand it moves along the surface of the cone (when the track is tested), or the cylindrical surface (at the time of the test of the surface of the bearing seated in the shaft).

Because the values of the signal generated at the time of the test of the model ring are different for the scanning of the inner and outer surface, it is justified to define separate border values categorising the ring as faulty. The tests also indicated that it is necessary to analyse the real and the imaginary components. The results of the tests were used in the configuration of the system for the industrial inspection of the quality of bearing rings.

## References

1. Zbrowski A., Matecki K.: The use of computed tomography to analyse grinding smudges and subsurface defects in roller bearing rings. Strojniški vestnik – Journal of Mechanical Engineering, Vol. 60. 2014, 11, pp. 709–715.
2. Zbrowski A., Matecki K.: Wykrywanie wewnętrznych wad materiałowych w pierścieniach łożysk tocznych. Problemy Eksploatacji. 2012, 2, s. 229–243.

3. Zbrowski A., Matecki K.: Zastosowanie metody prądów wirowych w diagnostyce materiałów i elementów konstrukcyjnych. TTS Technika Transportu Szynowego. 2013, 10, s. 951–962.
4. Xiang P., Ramakrishnan S., Cai X., Ramuhalli P., Polikar R., Udpa S.S., Udpa L.: Automated analysis of rotating probe multi-frequency eddy current data from steam generator tubes. International Journal of Applied Electromagnetics and Mechanics, Vol. 12. 2000, pp. 151–164.
5. Hohmann R., Lomparski D., Krause H.-J., Kreutzbruck M., Becker W.: Aircraft Wheel Testing with Remote Eddy Current Technique using a HTS SQUID Magnetometer. IEEE Transactions on Applied Superconductivity, Vol. 1. 2001, pp. 1279–1282.
6. Schmidt C., Schultz C., Weber P., Denkena B.: Evaluation of eddy current testing for quality assurance and process monitoring of automated fiber placement. Composites: Part B. Vol. 56. 2014, pp. 109–116,
7. Matecki K., Zbrowski A., Matras E.: Metodyka wykrywania wad materiałowych w pierścieniach łożysk tocznych techniką prądów wirowych. Logistyka. 3/2014, 3, pp. 4187–4197.
8. Samborski T., Zbrowski A.: Model stanowiska do wykrywania wewnętrznych wad materiałowych w pierścieniach łożysk tocznych. Energetyka, Problemy Energetyki i Gospodarki Paliwowo-Energetycznej. 8/2012, pp. 447–451.
9. Zbrowski A., Jóźwik W.: Influence of the gap between measuring head and tested object on the results of an eddy current test method. Solid State Phenomena, Vol. 223. 2015, pp. 246–254.
10. Zbrowski A., Jóźwik W.: Rotational speed and transducer frequency as factors affecting possibility to detect defects in axisymmetric elements with a method of eddy currents. XIV International conference Automation 2015. Warsaw 18–20$^{-th}$ March 2015.
11. Zbrowski A., Matecki K.: Wykrywanie wad podpowierzchniowych metodą prądów wirowych. Problemy Eksploatacji. 2012, 1, s. 35–48.
12. Zbrowski A., Jóźwik W.: Detection of the corrosion of axisymmetric elements by means of the eddy current testing method. Solid State Phenomena. Vol. 227-Corrosion and Surface Engineering IV. 2015, pp. 545–548.

*Scientific work executed within the Strategic Programme "Innovative Systems of Technical Support for Sustainable Development of Economy" within Innovative Economy Operational Programme.*

**Porównanie wyników badania obiektów osiowosymetrycznych z wykorzystaniem metody prądów wirowych na stanowisku przemysłowym i laboratoryjnym**

**Słowa kluczowe**

Prąd wirowy, wykrywanie wad, pierścień łożyskowy.

**Streszczenie**

Celem badań było porównanie wyników uzyskanych na stanowisku przeznaczonym do przemysłowej kontroli jakości pierścieni łożyskowych z rezultatami badań przeprowadzonych na stanowisku laboratoryjnym. Badaniu poddano cztery wewnętrzne pierścienie łożyskowe. W trzech pierścieniach wykonano sztuczne wady testowe odwzorowujące defekty, które mogą wystąpić podczas procesu produkcyjnego. Czwarty pierścień pełnił funkcję wzorcową. Skanowano powierzchnię wewnętrzną oraz zewnętrzną. W zależności od orientacji głowicy pomiarowej wady testowe odwzorowywały defekty powierzchniowe lub podpowierzchniowe.

Zaobserwowano, że podczas badań na stanowisku przemysłowym i laboratoryjnym poziom sygnału jest niższy dla badania powierzchni wewnętrznej, co jest skutkiem oddalenia punktu środkowego głowicy pomiarowej od badanej powierzchni.

Wyniki badań były podstawą do określenia wartości granicznych sygnału pomiarowego określających badany pierścień jako wadliwy. Ze względu na różny poziom sygnału dla badania powierzchni zewnętrznej i wewnętrznej zaproponowano określenie osobnych progów dla powierzchni wewnętrznej i zewnętrznej. Uzyskane wyniki badań umożliwiły opracowanie metody kalibracji systemu do automatycznej kontroli jakości pierścieni łożyskowych.

INNOVATIVE ECONOMY
NATIONAL COHESION STRATEGY
INSTITUTE FOR SUSTAINABLE TECHNOLOGIES
NATIONAL RESEARCH INSTITUTE IN RADOM
EUROPEAN UNION
EUROPEAN REGIONAL DEVELOPMENT FUND

Project co-financed by the European Union from the European Regional Development Fund

**Stanisław KOZIOŁ, Tomasz SAMBORSKI**
Institute for Sustainable Technologies – National Research Institute, Radom
stanisław.koziol@itee.radom.pl
tomasz.samborski@itee.radom.pl

# A METHOD AND DEVICE FOR THE INDUSTRIAL MEASUREMENT OF TAPERED BORES

**Key words**

Measurement of tapered bores, industrial measurements, measuring instrumentation, tapered bores.

**Abstract**

Quality inspection constitutes an inseparable element of technological processes. Quality inspection frequently employs measuring instrumentation suitable for measurements taken in an industrial environment. Machining of complicated casts can serve as an example, since, during this process, the required accuracy can only be achieved for a stable positioning of the machined element in a lathe. For that reason, some inspections need to be performed directly on the machine. This hampers the inspection of dimensions using a coordinate-measuring machine (CMM) and makes the application of standard measuring instrumentation too time-consuming and, in some cases, even impossible. An example of such a problem is the necessity to measure the opening angle of the tapered bore between the consecutive stages of the machining process.

This article presents a measuring method employing special measuring instrumentation enabling quick and precise inspection of the opening angle of

a tapered bore in the case when such inspection is possible only from the side of the opening with a smaller diameter. The authors analysed the methods recommended for the measurement of tapered bores and patented devices used for this purpose. Based on the results of their analyses, the authors developed three optional designs of a device in which precise mechanical elements and high-class sensors for linear measurements are used. Application of this equipment enables easy measurement of the opening angle of a tapered bore in any position of the opening, which complies with the requirements of the interoperation measurement in industrial conditions.

## Introduction

A technological process of manufacturing complex machine elements involves operations that change the shape or material properties of a machined detail, between which additional technical inspections are carried out to verify correctness of the executed tasks [1]. In the case of machining, the inspection most frequently consists in the verification of the compliance with the required dimensions of given shapes. The measurements are taken directly on the machine or in a specially equipped metrological laboratory. For that purpose, measuring devices, gauges, and more common measuring machines, and modern systems with measuring probes installed directly on numerically controlled lathes are used. However, there are situations in which the measurement needs to be performed on the detail mounted on the machine, but no dedicated measuring instrumentation is available for that purpose, and the access to the inspected area is restricted.

An example is a multistage process of machining a complex cast on a lathe, borer, or a multi-axis milling machine in which the maintenance of the required precision is possible only in the case when the element is permanently fixed in the grip of the machine. In one such process conducted by the authors of the article, it was necessary to make a tapered bore, wherein the measurement was taken from the side with a smaller diameter. In addition, the front surface, perpendicular to the axis of the bore, was machined. The accuracy of the making of the bore had to be confirmed by the measurement of its opening angle with access from the side with a smaller diameter.

The authors analysed the methods recommended for the measurement of tapered bores and the universal measuring instrumentation available [2, 3]. The analysis showed that the most common method for the measurement of the inner tapered bore is by using two measuring balls with different diameters and a micrometre depth meter. However, in the case of measurements conducted by the authors, the application of this method was impossible due to the hampered access from the side of the bore with a smaller diameter. No universal or specialized measuring instruments were found that would allow the authors to conduct the measurements effectively. The Institute has broad experience in the

design and implementation of the advanced methods of quality inspection and the selection of serial and automated production of roller bearings [4, 5] and piston rings [6, 7]. Dominant are the methods of precise measurement of profiles and contactless optical methods [8, 9, 10]. However, due to the technical conditions in which the technological processes are carried out, these methods cannot be applied. In the case presented in this article, the authors had to develop a dedicated measuring device.

The objective of the tasks carried out by the authors was to design a concept of an instrument that would comply with the requirements of the interoperation measurement conducted in industrial conditions. Three different designs were proposed: two with a central axial sensor for linear displacements, and one with miniature linear sensors.

## 1. Device with measuring balls

The concept of instruments with an axial sensor for linear displacements was based on a simple measuring method presented in Fig. 1.

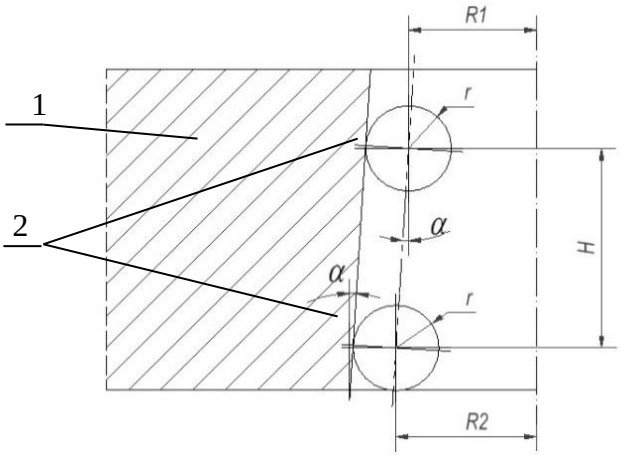


Fig. 1. Principle of measurement of the opening angle of a tapered bore: 1 – detail with a tapered bore (partial semi-section), 2 – measuring balls

The machined element (Fig. 1) contains a tapered bore with opening angle $2\alpha$ whose generatrix is inclined at angle $\alpha$ to the axis. The balls with radius $r$, placed at two different distances $R1$ and $R2$ from the axis of the tapered bore are in contact with the generatrix, which means that the straight line going through their centres is also inclined at angle $\alpha$ to the axis of the bore. Consequently, if distances $H$ of the planes perpendicular to the axis of the tapered bore and passing through the middle of the balls are measured, the value of the angle can be calculated using the formula presented in Fig. 1. Applying this rule to the

measurement of small opening angles of the bore is very accurate due to the strong dependency of value $H$ on angle $\alpha$ [11, 12].

Figure 2 presents the structure and the modus operandi of the device with measuring balls.

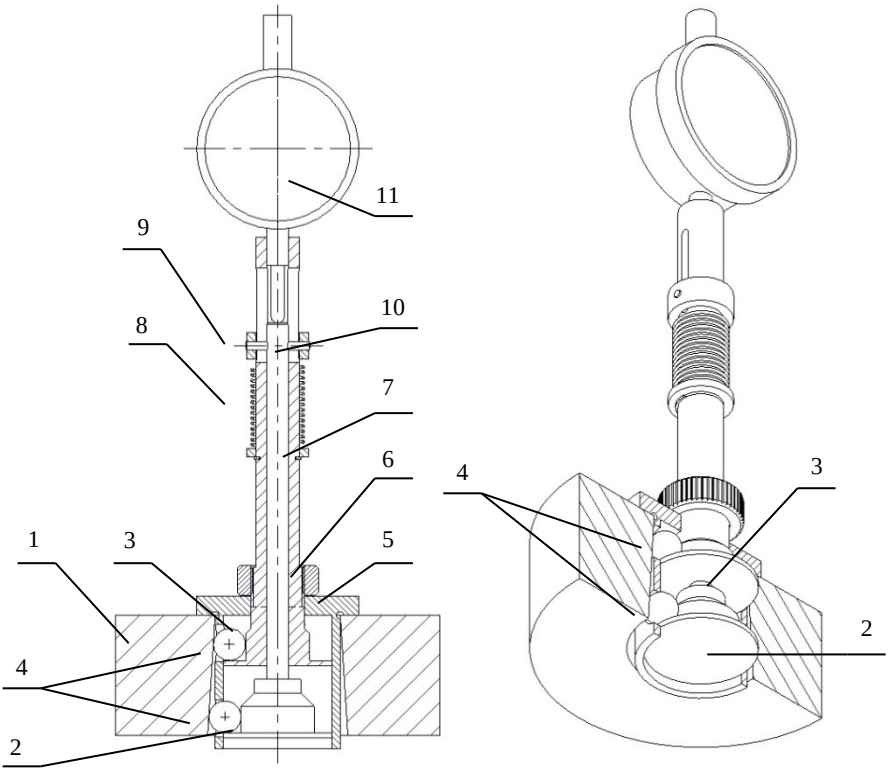


Fig. 2. Structure and modus operandi of the instrument with measuring balls: 1 – detail with a tapered bore, 2 – pivot, 3 – bushing, 4 – measuring balls, 5 – centering bushing, 6 – screw-top, 7 – ring, 8 – spring, 9 – slipping ring, 10 – pin, 11 – precise linear sensor

Inside the opening in the form of a tapered bore made in element 1 (Fig. 2), a pivot and a bushing with cylindrical bottom surfaces with defined diameters and perpendicular flat ring-shaped surfaces were placed. Each of the flat surfaces formed the base on which three measuring balls were evenly placed. The balls remain in contact with the cylindrical and the conical surface of the bore. The centering bushing has an elongated cylindrical body with an opening tapped on a short section of the outer plane. Together with the three measuring balls, the bushing is immobilized in the bore by means of a screw top that presses the bushing to the front surface of the detail. The pivot can slide in the opening of the bushing. This element is connected with the sliding ring by means of a pin passing through the longitudinal channels inside the bushing.

A compression spring between the sliding ring and the ring mounted onto the bushing presses the remaining three measuring balls to the conical plane of the bore. The bushing has six longitudinal openings meant for the positioning of the balls. The openings limit the movement possibilities of the balls and concurrently prevent them from falling out, once the device is removed from the tapered bore. The linear displacement sensor is intended for the measurement of the distance between the pivot and the bushing in an axial direction, which ensures the compliance with the measurement principle presented in Fig. 1.

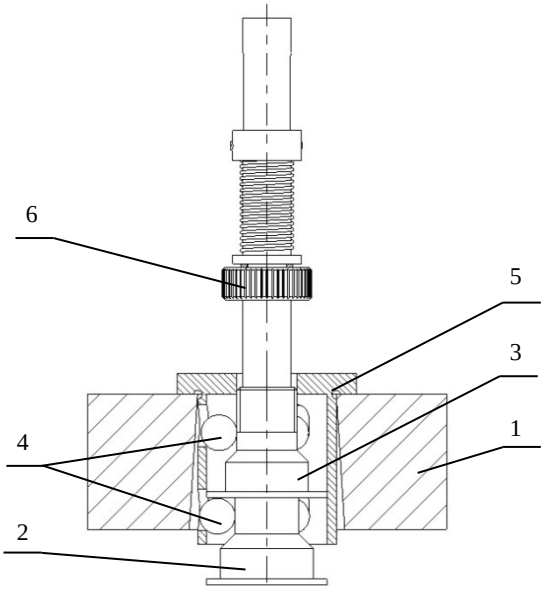


Fig. 3. Position of the device with measuring balls after its placement in the bore: 1 – detail with a bore, 2 – pivot, 3 – bushing, 4 – measuring balls, 5 – centering bushing, 6 – screw-top

The advantage of the device lies in the possibility to place it in the bore from the side with a smaller diameter. Fig. 3 depicts the position of the individual details of the device that enables this task.

When the instrument is placed in or removed from the bore, the screw-top (Fig. 3) needs to be removed from the navigated part of the bushing. Under the influence of the screw, the pivot automatically moves in the opening of the bushing into the extreme position, in which both parts are connected. Under the action of gravity, or as initiated by the user, the pivot and the bushing move along the centering bushing downwardly, which enables the measuring balls to move toward the geometric axis of the instrument. The withdrawal of the balls towards the inner part of the cylinder, marked by the outer plane of the centering bushing, enables the device to be placed in the tapered bore from the side with a smaller diameter.

To start the measurement, once the centering bushing is placed inside the tapered bore (Fig. 3), the bushing moves away from the detail; and after overcoming the resistance of the spring, the balls touch the details of the device and the surface of the tapered bore. Such placement enables the immobilization of the instrument inside the tapered bore by tightening up the screw-top (position in Fig. 2).

## 2. Device with a three-arm probe

The instrument with three-arm probes is based on the same measurement principle as applied in the measurement employing measuring balls. The balls with the elements positioning them in the bore were replaced with probes with three arms with spherical ends. The structure and modus operandi of the device are shown in Fig. 4.

Two three-arm probes were placed in the tapered bore (Fig. 4). The smaller probe has an elongated cylindrical body with an opening tapped on the short section of the outer plane. It is immobilized in the bore by means of a screw top pressing the centering ring to the front surface of the detail and the ball-shaped ends of the arms of the probe to the conical surface of the bore. The bigger probe, on the other hand, has a pivot that can slide in the opening of the body of the smaller probe. The pivot is connected with the sliding ring by means of a pin. The pressing spring between the sliding ring and the ring mounted onto the body of the smaller probe presses the spherical surfaces of the arms of the bigger probe to the conical plane of the bore. The linear displacement sensor is intended for the measurement of the distance between the two probes, which helps one to ensure that the measurement principle presented in Fig. 1 is met.

Figure 5 presents how the three-arm probe is placed in the tapered bore from the side with the smaller diameter. In the resting device and under the influence of the spring, both probes touch. Their small thickness enables them to be placed in the tapered bore from the side with the smaller diameter, once they are positioned at a proper angle with reference to the detail (Fig. 5). After the probes are placed in the tapered bore, the device is positioned in a way that enables the geometrical axes of the device and the bore to overlay and allows the contact with the surface of the cone. In such a position, it is possible to immobilize the probe in the bore by tightening up the screw top.

In both cases, it might be necessary to remove the linear displacement sensor at the time the instrument is being placed in the bore. This is caused by the great changes in the position of the individual elements in relation to each other, whose distance is measured, which can exceed the working stroke of the sensor. Is such a case, it is necessary to use a sensor equipped with an element enabling its unambiguous positioning in the body of the device.

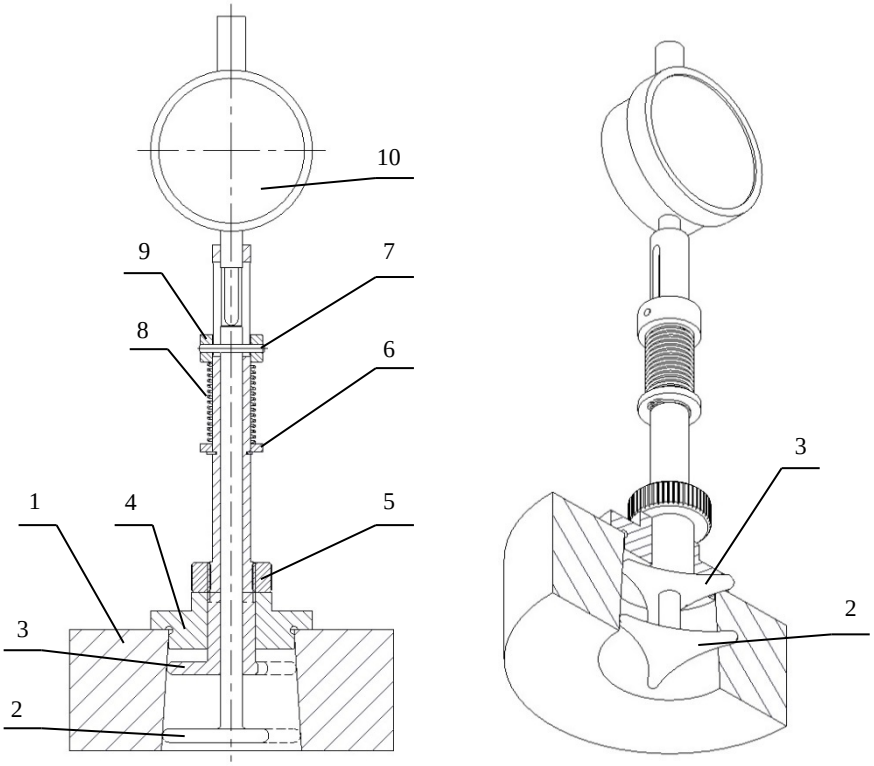


Fig. 4. Structure and modus operandi of the device with three-arm probes: 1 – detail with a tapered bore, 2 – bigger three-arm probe, 3 – smaller three-arm probe, 4 – centering ring, 5 – screw-top, 6 – ring, 7 – pin, 8 – spring, 9 – sliding ring, 10 – precise linear sensor

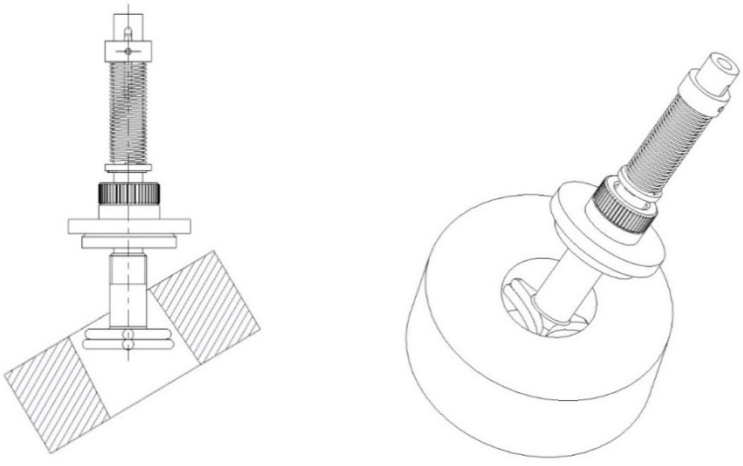

Fig. 5. Means of placing the device with three-arm probes inside the tapered bore from the side with a smaller diameter

### 3. Device with miniature linear sensors

The third concept of the device rejected the usage of a complex mechanical structure and assumed the application of commercially available measuring systems (Fig. 6). The modus operandi of the device requires the flat front surface of the detail, in which the opening is made, to be perpendicular to its geometrical axis, which in practice means that both the plane and the hole are made in the same mounting.

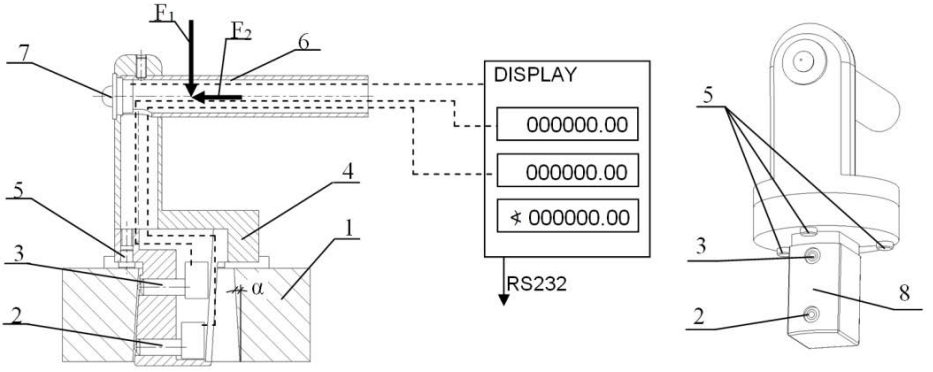


Fig. 6. Structure of the device with miniature linear sensors: 1 – detail with a bore, 2 and 3 – miniature linear sensors, 4 – body, 5 – grip, 6 – handle, 7 – measurement start button, 8 – front surface of the bracket

The body of the device (Fig. 6) is based on a flat surface of the detail by means of three grips. It has a bracket placed in the tapered bore. There are two electronic linear sensors located in the bracket, and their geometrical axes are parallel to the front surface of the detail. The handle is intended for placing the device in the tapered bore and pressing it with forces $F_1$ and $F_2$ to the front and the side of the bore, which ensures the contact of the tips of the measuring sensors with the surface of the cone. The front surface of the bracket (Fig. 7) is shaped in a way that enables one to even the axes of the linear sensors and the axial plane of symmetry of the cone. Each value of the measured angle α corresponds to the readings of the sensors presented on the DISPLAY screen equipped with the angle measurement function. Button 7 helps the user to manually start the measurement.

The measurement consists in the placement of the device in the measured bore, its immobilization through the application of forces $F_1$ and $F_2$, and the initiation of the measurement process is performed by pressing the button. This results in the readings of the linear sensors and their transfer to the PC controlling the measurement process through RS232 in order to select, emit, or archive the report. In the case of any doubts concerning the perpendicularity of

the flat surface of the detail to the axis of the bore, the measurements can be taken in different directions by rotating the device around the geometrical axis of the cone.

Due to the elimination of moving mechanical parts, the instrument with miniature linear sensors is more resistant to the effects the presence of different kinds of contaminants can have on the accuracy of the measurement. A limitation to the application of such a device is the possibility of placing precise linear sensors in the measured bore.

**Summary**

The research described in the paper concerned the design of three concepts of the device for quick, industrial measurement of the opening angle of the cone in the opening in form of a tapered bore. A characteristic feature of the proposed solutions is the possibility to perform the measurements from the side with a smaller diameter, which meets the requirements of the technological process of machining casts with complicated structure developed by the authors of the article.

Due to the specificity of the measurements consisting in the placement of the device in the bore from the side with a smaller diameter, and inducing the contact of the measuring elements on bigger diameters, the three options described are dedicated for the measurement of elements with defined dimensions.

The device with the measuring balls is the most economical due to the availability of precise measuring balls (these can also be roller bearings) and the simple shape of the remaining elements. This instrument is easy to operate because of the automatic centering mechanism. Its disadvantage concerns the number of moving parts and the gaps between them, in which contamination can gather, which impairs precision of the measurements.

The device with three-arm probes requires labour-intensive probes with precise spherical surfaces that must have a high degree of accuracy, smoothness, and surface hardness. The advantages of the solution are the small number of moving parts and the ability of self-centering in the bore.

The device with miniature linear sensors is the most resistant to contamination due to the application of the measuring systems with own sealing. This enables automatically archiving the measurement results and the selection of goods. The disadvantages of this solution concern the high costs of the measuring circuits, low ergonomics of the construction composed of two modules connected through electric cable, and the necessary skills in the handling the device at the time of its positioning in the bore.

All the concepts presented in the article meet the assumed requirements towards measuring devices used in an industrial environment.

Practical application of measuring instruments consistent with the described concepts requires the design of prototypes and the verification of their metrological and performance characteristics in laboratory and industrial environments.

*Scientific work executed within the Strategic Programme "Innovative Systems of Technical Support for Sustainable Development of Economy" within Innovative Economy Operational Programme.*

**References**

1. Feld M.: Technologia budowy maszyn, PWN, Warszawa 2000.
2. Jakubiec W., Malinowski J.: Metrologia wielkości geometrycznych, WNT, Warszawa 2004.
3. Paczyński P.: Metrologia techniczna, Wydawnictwo Politechniki Poznańskiej, Poznań 2001.
4. Zbrowski A., Matecki K.: The use of computed tomography to analyse grinding smudges and subsurface defects in roller bearing rings. Strojniški vestnik – Journal of Mechanical Engineering, Volume 60 (2014) No. 11, pp. 709–715.
5. Zbrowski A., Samborski T.: Bezstykowe metody kontroli jakości w wielkoseryjnej produkcji łożysk samochodowych. Logistyka 3/2014, s. 7071–7080.
6. Giesko T., Zbrowski A.: Metoda i urządzenie do pomiaru profili pierścieni tłokowych. Pomiary Automatyka Kontrola 2009 nr 5, s. 314–317.
7. Giesko T., Wasiak J., Zbrowski A.: Measurements of piston ring profile using contact technique. Problemy Eksploatacji 2005 nr 2, pp. 31–40.
8. Giesko T., Mazurkiewicz A., Zbrowski A., Czajka P.: Optomechatroniczny system do automatycznej kontroli jakości wyrobów w przemyśle. Problemy Eksploatacji 2011 nr 4, s. 103–114.
9. Giesko T., Mazurkiewicz A., Zbrowski A.: Advanced mechatronic system for in-line automated optical inspection of metal parts. International Journal of Simulation: Systems, Science & Technology, (IJSSST), Vol. 11 No 4 September 2010, pp. 36–41.
10. Giesko T., Zbrowski A., Czajka P.: Laser profilometers for surface inspection and profile measurement. Problemy Eksploatacji 2007 nr 1, pp. 97–108.
11. PN-EN ISO 1101:2013-07; Specyfikacje geometrii wyrobów (GPS), Tolerancje geometryczne, Tolerancje kształtu, kierunku, położenia i bicia.

12. Humienny Z., Osanna P.H., Tamre M., Weckenmann A., Jakubiec W.: Specyfikacje geometrii wyrobów. Podręcznik europejski, WNT, Warszawa 2004.

**Metoda i przyrząd do warsztatowych pomiarów stożków wewnętrznych**

**Słowa kluczowe**

Pomiar stożka, pomiary warsztatowe, przyrządy pomiarowe, otwór stożkowy.

**Streszczenie**

Nieodłącznym elementem realizowanych procesów produkcyjnych w przemyśle maszynowym jest kontrola jakości, w której często stosowane są urządzenia do wykonywania pomiarów w warunkach warsztatowych. Przykładem jest obróbka skrawaniem skomplikowanych odlewów, podczas której osiągnięcie wymaganej dokładności jest możliwe jedynie przy stałym, niezmiennym zamocowaniu detalu na obrabiarce. Z tego powodu niektóre operacje kontrolne muszą być wykonywane bezpośrednio na maszynie. Uniemożliwia to kontrolę wymiarów z zastosowaniem maszyny współrzędnościowej, a wykonanie pomiaru za pomocą standardowych narzędzi pomiarowych bywa niemożliwe lub zbyt czasochłonne. Przykładem takiego problemu jest konieczność wykonania pomiaru kąta rozwarcia otworu stożkowego pomiędzy kolejnymi zabiegami obróbczymi.

W artykule zaprezentowano metodę pomiarów z zastosowaniem specjalnego przyrządu pomiarowego pozwalającego na wykonanie szybkiej i precyzyjnej kontroli kąta rozwarcia stożka otworu o kształcie stożka ściętego, w przypadku kiedy jest to możliwe tylko od strony mniejszej średnicy otworu. Przeprowadzono analizę zalecanych metod pomiaru otworów stożkowych, dostępnych narzędzi pomiarowych do pomiarów otworów oraz rozwiązań chronionych prawem patentowym. Opracowano trzy opcjonalne rozwiązania konstrukcyjne przyrządu wykorzystujące precyzyjne elementy mechaniczne i wysokiej klasy czujniki do pomiarów liniowych. Zastosowanie każdego z opracowanych przyrządów pozwala na wykonanie pomiaru kąta stożka w prosty sposób w dowolnej pozycji mierzonego otworu, co spełnia wymagania międzyoperacyjnego lub międzyzabiegowego pomiaru warsztatowego w warunkach produkcyjnych.

INNOVATIVE ECONOMY
NATIONAL COHESION STRATEGY
INSTITUTE FOR SUSTAINABLE TECHNOLOGIES
NATIONAL RESEARCH INSTITUTE IN RADOM
EUROPEAN UNION
EUROPEAN REGIONAL DEVELOPMENT FUND

Project co-financed by the European Union from the European Regional Development Fund

**Krzysztof MATECKI**
Institute for Sustainable Technologies – National Research Institute, Radom
krzysztof.matecki@itee.radom.pl

# STUDY ON SELECTED MECHANICAL PROPERTIES OF SAMPLES OF MATERIAL TAKEN FROM MASS PRODUCED PIPE ELBOWS

**Key words**

Strength tests, mechanical property tests, mechanical properties, static tensle strength.

**Abstract**

The article presents the tests on selected mechanical properties of a material in form of samples taken from mass produced pipe elbows manufactured by means of bending techniques and hydroforming, using high inner pressure, and hydro calibration. The author gives a definition of the parameters and describes the static tensile stress, which according to the PN-EN ISO 6892-:2009 standard is employed for their determination. Additionally, the sampling process is presented and the research instrumentation used is characterised, i.e. the testing machine and its software. Moreover, the author shows how input parameters are set to enable the calculation, edition and acquisition of results. The results of the static tensile stress test are presented in form of graphs and tables delineating the measured values.

## Introduction

A static tensile stress test conducted at the ambient temperature is a basic strength test used to evaluate mechanical properties of metals and their alloys. It enables the comparison and classification of metal materials and the verification of the success of the applied technological processes, particularly as far as thermal and plastic processing are concerned [1]. The currently biding standard on metal tensile stress tests is the PN-EN ISO 6892-:2009 test entitled "Metallic materials – Tensile testing – . Part 1: Method of test at room temperature". According to this standard, the test can be used to determine the mechanical properties of pipes and their elements like elbows, joints, sleeves, etc. which are used in the construction of different installations. Those pipes and elements that are made of stainless steel have been widely applied in many industry branches, e.g. construction, chemical industry, food industry, or energy industry, to name a few, and they prove to be very important in difficult, sometimes even extreme conditions. This is particularly crucial from the point of view of the operational safety of many objects and installations in which practically all elements have to be made of alloyed stainless steel. A specific end user of such devices is the energy sector. Most energy worldwide comes from the combustion of coal, oil, gas or nuclear power stations. The determination of the stainless steel to be used in such systems requires vast knowledge and plenty of experience. In fact, the types of stainless steel most commonly used in this industry sector are high-alloy steels, which due to their mechanical properties are particularly useful in the production of plastically processed elements [2]. However, the requirements the technologies of their processing into commercially available elements need to meet are very high. Due to the growing area of application and the increasing demands, new methods and research instrumentation are developed to enable the monitoring over the material fatigue process employing optical inspection techniques [3, 4, 5] and the high-temperature creep [6].

Currently, it is estimated that building a modern plant for the main industry sectors requires several thousand tons of stainless steel, and a large part of this is in the form of pipes and their elements [7]. These elements are supplied to thousands of users and they are generally assembled in special systems for the transmission of different media in particularly heavy loaded areas that are therefore far more prone to failure. For that reason, mass-produced pipe elbows made of stainless steel and manufactured using the advanced technologies are products that call for a thorough control at each stage of their life. A basic and standardised method for the control of mechanical properties of a material in a final product is the tensile stress test at room temperature, whose methodology is described in detail in the PN-EN ISO 6892-:2009 standard.

The Institute for Sustainable Technologies – National Research Institute conducts investigations on selected mechanical properties of metal samples from

the mass produced pipe elbows. The tests have been commissioned by the international manufacturer of such elements.

## 1. Definitions and determination of selected properties

A static tensile stress test consists in the elongation of samples with the shape defined by the standard until they break. The tests are performed with a predetermined rate of the stress growth. The samples are mounted axially in the grips of the testing machine. At the time of the tests the value of the tensile force and stresses in recorded as a function of sample elongation. The recorded values are transferred onto the coordinate system and they form a "tensile strength chart."

The author gives the definitions of the parameters determined during the test and the values necessary for their determination complying with the PN-EN ISO 6892-:2009 standard, and additionally presents them in the static tensile stress graph, as shown in Fig. 1.

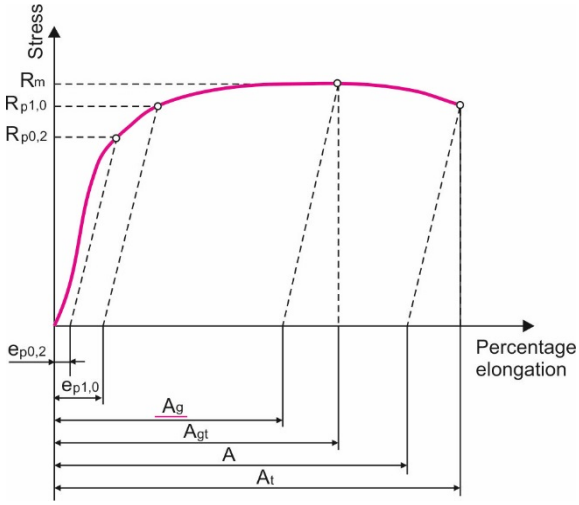


Fig. 1. Static tensile stress graph with no clear yield strength

- The initial thickness of the sample $a_0$;
- The initial width o the sample $b_0$;
- The inner diameter of the elbow opening $D_0$;
- The required % extensometric plastic elongation $e_p$;
- The elongation $\Delta L$ – increase in the initial length $L_0$ after the test (the break) expressed as $\Delta L = L_u - L_0$, where $L_0$ – initial measured length of the sample

before the application of force $L_u$ – measured length after the break of the sample;
- The % elongation – elongation of the initial measured length $L_0$ in %;
- The permanent elongation after the break A – permanent elongation of the measured length after break $L_u - L_0$, expressed in % of the initial measured length $L_0$:

$$A = \frac{L_u - L_0}{L_0} \times 100\% \tag{1}$$

- The total % elongation at the time of the break $A_t$ – total elongation (elastic and plastic elongation) at the time of the break expressed in % of the measured length $L_0$;
- The % elongation for the greatest force ($A_{gr}$) – increase in the measured length of the sample at the greatest force, expressed in % of the initial measured length $L_0$, wherein in this range the following can be observed: the total % elongation at the greatest force $A_{gt}$ and the disproportionate % elongation at the greatest force $A_g$;
- The % contraction Z – the greatest change in the cross-sectional area ($S_0 - S_u$), taking place during the tests, expressed in % of the initial cross-sectional area $S_0$, whereas $S_u$ refers to the smallest cross-sectional area after the break of the sample:

$$Z = \frac{S_0 - S_u}{S_0} \times 100\% \tag{2}$$

- The greatest force $F_m$ – the greatest force in the sample at the time of tests after exceeding the yield strength;
- The tensile strength $R_m$ – the tension corresponding to the greatest force $F_m$;
- The yield strength during the disproportionate increase (a conventional yield strength, yield of elasticity) $R_p$ – tension defined for the required % plastic extensiometric elongation $e_p$ – the value symbol is supplemented with an index determining the conventional % increase in the measured length of the extensometer, e.g. $R_{p0,2}$.

## 2. Test samples

Depending on the type of the tests, the samples need to be properly selected and prepared to guarantee that the results are free from interferences or external influences stemming from the presence of additional unfavourable phenomena [8].

Fig. 2 presents mass produced pipe elbows made of the 1.4571 stainless steel and obtained by means of a bending technique, hydroforming using high inner pressure, or hydro calibration.

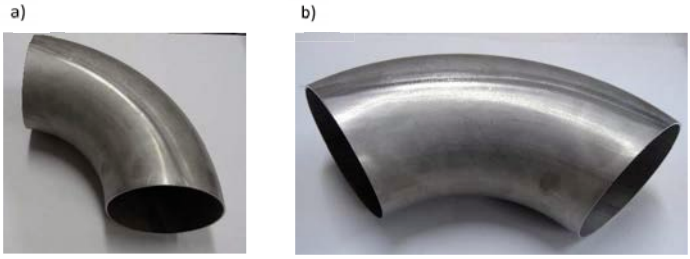


Fig. 2. Elbows made according to the EN 10253 standard: a) elbow type EN 10253-90-3-139,7×2,0-W-1.4571; b) elbow type EN 10253-90-3-169,7×2,0-W-1.4571

The shape and size of the samples, particularly of their measured parts, were selected in compliance with Appendix B containing guidelines on the dimensions (Table B.1 – Dimensions of samples) and the tolerance in the initial width of the measured parts (Table B.2 – Tolerance in the width o the test element).

Due to the shape of the object, the author excluded the possibility of direct tests, e.g. the expanding method [9, 10] or the tests performed in real thermal conditions [11]. It was found that the samples should be paddle-shaped, which would enable the execution of the static tensile strength test in the laboratory environment.

The specimens were sampled from the axial areas of the elbows with the maximum radius, first in the form of 22.5 mm wide patches milled with metal slitting saw from the elbows fixed in a suitable device mounted on the router table. The way the patches were milled is presented in Fig. 3.

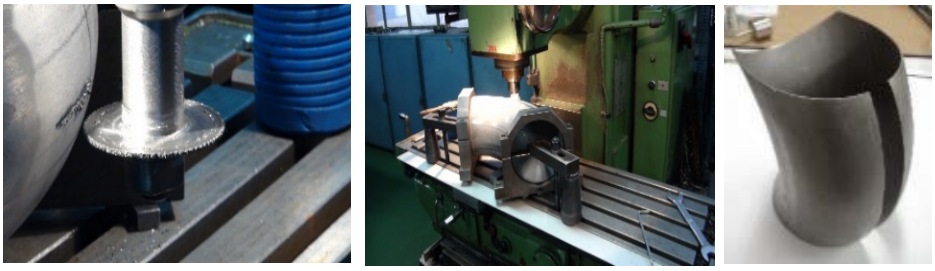

Fig. 3. Sampling of patches from pipe elbows

In the sampled patches fixed in a special grip, the sample measurement areas were also cut using the "half-side milling cutter". The value of the tolerance in the initial width of the sample was maintained at the level advised by the standard. Fig. 4 depicts the way the sample measurement area was obtained from the elbow pipes.

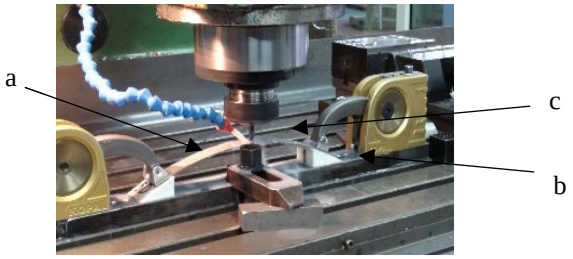


Fig. 4. Preparation of the sample measurement area: a) sample patch; b) grip; c) end mill

In order to determine the permanent elongation after the break A, the measurement lines were drawn on the measurement area (see Fig. 3) that divided the initial measured length $L_0$ into ten even parts. This was performed according to Appendix H to the standard in question [12]. The gripping parts of the samples were flattened, which significantly facilitated their proper assembly in the grips of the testing machine. Fig. 5 presents the samples taken from the elbows on which the measurement lines are drawn and whose ends are flattened into convenient gripping parts.


Fig. 5. Test samples a) after milling, b) after tracking, c) with flattened ends

## 3. Test stand

The static tensile strength test was performed on the Instron 5582 testing machine equipped with the dedicated control software, which is responsible for the setting of the test conditions, as defined by the standard, or in point 10 of the PN-EN ISO 6892-1 standard, and collects and processes data at the time of the

test. The data is then presented as a tensile strength graph and tables with test results. The Bluehill 3® software and its interface and the package of modules for metal tests guarantee total control over the test parameters complying with the requirements of the ISO 6892-1 and other standards concerning tensile stress tests on elements made of steel [13]. The machine is equipped with manual wedge grips with clamping pads for flat samples, and its control room has a sample protection function that monitors the force acting on the sample during mounting, and additionally controls the device in such a way that no excessive force is applied. In conjunction with the force measurement system reset function, the system compensates the influence of the weight of the grips and the force with which the samples are mounted.

## 4. Tests and their results

The test consists in loading the sample mounted in the jaws of the machine and measuring the loading force and the displacement of its crossbar. The tensile stress graph is generated on regular basis from the file with the recorded data and presented on the coordinate system: tensile force – sample elongation. Based on the data file or after the test is finished, values $R_{p02}$, $R_{p1,0}$ and $R_m$ are defined in the characteristic points of the graph. Such values like A and Z are calculated based on the measurements of samples before and after the test, and the provisions of the PN-EN 6892-1 standard are applied. The values of conventional values $R_{p0,2}$ and $R_{p1,0}$ are determined from the tension – increase graph by a straight line parallel to the straight part of the strain-stress curve at a distance corresponding to the % of the disproportionate increase, e.g. 0.2%. The ordinate of the point of intersection of the straight line parallel to the strain-stress curve determines the yield strength at the disproportionate increase.

An important parameter of the test is the speed at which the material is elongated. This value is controlled in the test based on the estimated speed of deformation in the length of the sample's parallel part. The speed is set through the control over the movement of the cross-bar of the machine at the speed equal to the product of the set deformation speed and the length of the parallel measurement area of the sample. For the tested samples the author assumed the following movement velocities of the machine's cross-bar: 0.3 mm/min for $R_{p0,2}$ and $R_{p1,0}$, and 0.5 mm/min for $R_m$, $A_{50}$ and Z.

Before the test, the samples are subjected to a dimensional inspection, during which the initial thickness and width (respectively $a_0$ and $b_0$) are measured. The average values of these quantities, introduced into the test parameters, are used to determine the initial cross-sectional area of samples ($S_0$), and the value of tensions defined as a ratio of the force acting on the sample at any time of the test, to the initial sample cross-sectional area $S_0$.

For each sample, after its break, the material elasticity parameters were determined according to the standard (i.e. $A_{50}$ and Z). The permanent elongation

after the break $A_{50}$ (the index refers to the initial measured length) was determined following the recommendations in point 20.1 of the standard [12] and Appendix H. The measurement of the appropriate quantities was conducted after thorough axial folding of each sample with the accuracy up to 0.1 mm, and the values of these quantities are presented in Table 1.

Table 1. Comparison of sample parameters before and after the break

| Sample number | Initial gauge length of a test piece [mm] | Section of a sample operational part | Number of sections between X i Y | N-n | Value (N-n) odd | | | | | Percentage elongation after fracture $A_{50}=[(XY+YZ`+YZ``-Lo)/Lo]100\%$ | Value (N-n) even | | | Percentage elongation after fracture $A_{50}=[(XY+2XY-Lo)/Lo]x100\%$ |
|---|---|---|---|---|---|---|---|---|---|---|---|---|---|---|
| | | | | | (N-n-1)/2 | (N-n+1)/2 | XY | YZ` | YZ`` | | (N-n)/2 | XY | YZ | |
| | $L_0$ | N | n | | | | | | | $A_{50}$ | | | | $A_{50}$ |
| 169.7/1 | 50.00 | 10 | 9 | 1 | 0 | 1 | 59.55 | 0 | 6.11 | 31.32 | | | | |
| 169.7/2 | 50.00 | 10 | 7 | 3 | 1 | 2 | 47.64 | 5.95 | 11.87 | 30.92 | | | | |
| 169.7/3 | 50.00 | 10 | 5 | 5 | 2 | 3 | 34.95 | 12.23 | 18.46 | 31.28 | | | | |
| 169.7/4 | 50.00 | 10 | 4 | 6 | - | - | - | - | - | - | 3 | 28.51 | 18.06 | 29.26 |
| 139.7/1 | 50.00 | 10 | 7 | 3 | 1 | 2 | 48.04 | 6.17 | 12.26 | 32.94 | | | | |
| 139.7/2 | 50.00 | 10 | 7 | 3 | 1 | 2 | 48.82 | 6.40 | 12.68 | 35.80 | | | | |
| 139.7/3 | 50.00 | 10 | 7 | 3 | 1 | 2 | 48.60 | 6.20 | 12.46 | 34.52 | | | | |

The % contraction Z was determined based on the measured initial parameters of the cross-section of the sample, i.e. the initial thickness $a_{0,}$ the initial width $b_{0,}$ and the parameters of the cross-section after the break, i.e. the thickness of the cross-section $a_u$ and the width $b_u$.

The measurement of these quantities was taken with a workshop microscope and then it was averaged. The values of these quantities and the parameters determined on their basis are presented in Table 2.

Table 2. Comparison of parameters of a sample before and after the break

| Sample number | $a_{0śr}$ [mm] | $b_{0śr}$ [mm] | $S_0 = a_{0śr} \times b_{0śr}$ [$mm^2$] | $a_{uśr}$ [mm] | $b_{uś®}$ [mm] | $S_u = a_{uśr} \times b_{uśr}$ [$mm^2$] | $Z = (\frac{S_0 - S_u}{S_0}) \times 100\%$ |
|---|---|---|---|---|---|---|---|
| 169.7/1 | 1.60 | 12.45 | 19.92 | 0.87 | 9.81 | 8.53 | 57.16 |
| 169.7/2 | 1.65 | 12.45 | 20.54 | 0.76 | 9.55 | 7.26 | 64.67 |
| 169.7/3 | 1.61 | 12.46 | 20.06 | 0.99 | 9.25 | 9.16 | 54.35 |
| 169.7/4 | 1.63 | 12.50 | 20.38 | 0.84 | 9.30 | 7.81 | 61.66 |
| 139.7/1 | 1.55 | 12.48 | 19.34 | 0.65 | 9.28 | 6.03 | 68.82 |
| 139.7/2 | 1.58 | 12.50 | 19.75 | 0.86 | 9.05 | 7.78 | 60.59 |
| 139.7/3 | 1.58 | 12.49 | 19.73 | 0.89 | 9.27 | 8.25 | 58.19 |

As a result of the tests carried out, a summary tensile strength graph and the values $Rp_{02}$, $Rp_{1,0}$ and Rm were obtained. Fig. 6 presents the tensile strength graphs for samples taken from pipe elbows with a diameter of 139.7 mm and 169.7 mm.

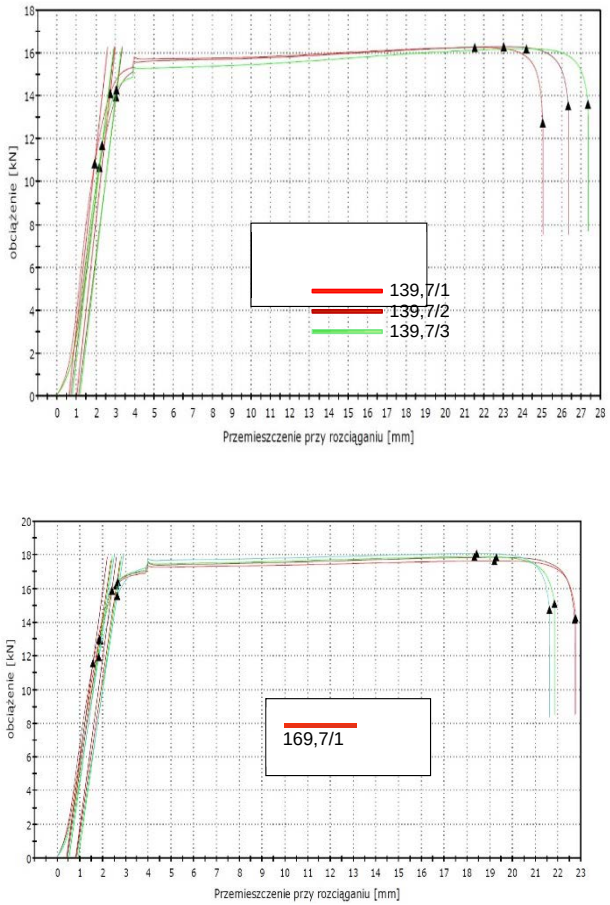


Fig. 6. Graphs of the static tensile strength test for samples taken from pipe elbows

The determined values of mechanical properties $R_{p02}$, $R_{p1,0}$, $R_m$, $A_{50}$ and Z for samples taken from elbows EN 10253-90-3-139,7×2,0-W-1.4571 are presented in Table 3, and the ones determined for samples taken from pipe elbows EN 10253-90-3-169,7×2,0-W-1.4571 are shown in Table 4.

Table 3. Comparison of values $R_{p02}$, $R_{p1,0}$, $R_m$, $A_{50}$ and Z from samples taken from pipe elbows EN 10253-90-3-139,7×2,0-W-1.4571

| | Sample label | $F_{max}$ [kN] | $R_{p0,2}$ [MPa] | $R_{p1}$ [MPa] | Tension at $F_{max}$ $R_m$ [MPa] | % contraction of the cross-section $Z_{50}$ [%] | % elongation after the break A [%] |
|---|---|---|---|---|---|---|---|
| 1 | 139,7/1 | 16,3 | 561,31 | 729,73 | 840,62 | 68,82 | 32,94 |
| 2 | 139,7/2 | 16,3 | 541,27 | 707,32 | 824,91 | 60,59 | 35,80 |
| 3 | 139,7/3 | 16,2 | 562,87 | 723,92 | 820,62 | 58,19 | 34,52 |
| Maximum | | 16,3 | 562,87 | 729,73 | 840,62 | 68,82 | 35,80 |
| Minimum | | 16,2 | 541,27 | 707,32 | 820,62 | 58,19 | 32,94 |
| Average | | 16,2 | 552,07 | 720,32 | 828,72 | 62,53 | 34,42 |
| Standard deflection | | 0,05 | 12,05 | 11,62 | 10,52 | 5,57 | 1,43 |

Table 4. Comparison of values $R_{p02}$, $R_{p1,0}$, $R_m$, $A_{50}$ and Z from samples taken from pipe elbows EN 10253-90-3-169,7×2,0-W-1.4571

| | Sample label | $F_{max}$ [kN] | $R_{p0,2}$ [MPa] | $R_{p1}$ [MPa] | Tension at $F_{max}$ $R_m$ [MPa] | % contraction of the cross-section $Z_{50}$ [%] | % elongation after the break A [%] |
|---|---|---|---|---|---|---|---|
| 1 | 169,7/1 | 17,6 | 520,02 | 647,42 | 705,97 | 57,16 | 31,32 |
| 2 | 169,7/2 | 17,9 | 503,23 | 635,02 | 714,36 | 54,67 | 30,92 |
| 3 | 169,7/3 | 17,9 | 516,98 | 655,85 | 715,52 | 54,35 | 31,28 |
| 4* | 169,7/4 | 18,1 | 586,1 | 764,22 | 887,32 | 61,66 | 29,26 |
| Maximum | | 17,9 | 520,02 | 655,85 | 715,52 | 58,72 | 31,32 |
| Minimum | | 17,6 | 503,23 | 635,02 | 705,97 | 54,35 | 30,92 |
| Average | | 17,8 | 513,41 | 646,09 | 711,95 | 55,39 | 31,17 |
| Standard deflection | | 0,17 | 8,95 | 10,48 | 5,21 | 1,54 | 0,22 |

* sample excluded from tests

Due to the values of the determined parameters that significantly differed from all the other parameters, Sample 4 with the label 169,7/4 taken from elbow 4- EN 10253-90-3-169,7×2,0-W-1.4571 from the patch asymmetric to the axis of the product, was excluded from the tests.

The 1.4571 steel is an austenitic stainless steel which according to different sources [14] is characterised by the following minimum mechanical properties: resistance to elongation $R_m$ = 520 – 670 MPa, conventional yield strength $R_{p0,2}$ = = 220 MPa and $R_{p1,0}$ = 260 MPa and elongation A = 40%.

## Summary

A tensile strength test is a basic and at the same time indispensable strength test in the control over the quality of goods made of stainless steel type 1.4571.

The mechanical properties of this steel, higher than these given by selected sources, e.g. $R_{p0,2}$, $R_{p1,0}$ and $R_m$ result from the manufacture technologies and processes employed, particularly the processes of preliminary bending and hydroforming of their final shapes. As a result of cold plastic processing, the mechanical properties of austenitic stainless steel reach higher values. This is followed by the so-called strengthening through squeeze that reduces the ductility parameters like A and Z.

The asymmetry of areas from which the samples were taken with reference to the axis of the elbows has an influence on the result of the determined properties and limits the possibility to compare the results. The use of a suitable sampling technique, instrumentation, and tools significantly reduces the risk of an error.

The determination of the elongation of the sample with no measurements and calculations vitiated by an error, and its control at the time of the tensile strength test until the sample breaks, should be performed using extensometers with a varied measurement base and automatic grips.

*Scientific work executed within the Strategic Programme "Innovative Systems of Technical Support for Sustainable Development of Economy" within Innovative Economy Operational Programme.*

## References

1. Bochnia J., Matecki K.: Statyczna próba rozciągania w świetle normy PN-EN 10002-2+AC1, Problemy Eksploatacji 2002, Nr 3, s. 127–136.
2. http://www.stalenierdzewne.pl/sites/default/files/FormingPotential_PL.pdf.
3. Zbrowski A., Samborski T., Giesko T., Boroński D.: System pomiarowy do monitorowania pękania połączeń montażowych stosowanych w przemyśle lotniczym. Technologia i Automatyzacja Montażu nr 3/2010, s. 5–11.
4. Zbrowski A., Samborski T., Giesko T., Boroński D.*:* Opto-mechatronic system for fatigue crack monitoring of riveted joint. Problemy Eksploatacji 2010 nr 4, pp. 153–162.

5. Zbrowski A.: Modułowa struktura systemu mechanicznego w mechatronicznej głowicy pomiarowej Systemu Monitorowania Pękania (SMP). Problemy Eksploatacji 2002 nr 4, s. 199–208.
6. Samborski T., Zbrowski A., Kozioł S., Majcher A.: Mechatroniczne stanowisko do badań zmęczeniowych. Energetyka. Problemy Energetyki i Gospodarki Paliwowo-Energetycznej, Zeszyt tematyczny nr XXII, listopad 2011, s. 76–79.
7. Real E., Mirambell E.: Flexural behaviour of stainless steel beams. Original Research Article Engineering Structures, Volume 27, Issue 10, August 2005, pp. 1465–1475.
8. Kozioł S., Zbrowski A.: Technologia przygotowania próbek do badań wytrzymałościowych materiałów stosowanych w konstrukcjach lotniczych – Problemy Eksploatacji 2011 nr 2, s. 251–264.
9. Zbrowski A., Jankowski K.: Badania wytrzymałości tulejowych elementów tłumiących. Autobusy – Technika, Eksploatacja, Systemy Transportowe. 3/2013, s. 339–406.
10. Zbrowski A., Jankowski K.: Test roztłaczania w kontroli jakości tulei polimerowych. Zeszyty Naukowe Politechniki Rzeszowskiej 288, Mechanika 85, t. XXX, z. 85 (1/13), styczeń–marzec 2013, s. 79–88.
11. Samborski T., Zbrowski A., Kozioł S.: Chamber for thermo-mechanical tests of high voltage insulators. Przegląd Elektrotechniczny (Electrical Review) nr 11a/2012, s. 337–339.
12. PN-EN ISO 6892-1; październik 2009. Metale – Próba rozciągania – Część 1: Metoda badania w temperaturze pokojowej.
13. http://www.instron.pl/wa/solutions/ISO-6892-Tensile-Testing-Metallic-Materials.aspx.
14. Afshan S., Rossi B., Gardner L.: Strength enhancements in cold-formed structural sections – Part I: Material testing Journal of Constructional Steel Research, Volume 83, April 2013, pp. 177–188.

**Badania wybranych właściwości wytrzymałościowych próbek materiału pobieranych z produkowanych seryjnie kolan rurowych**

**Słowa kluczowe**

Badania wytrzymałościowe materiałów, badania własności mechanicznych, własności mechaniczne materiałów, statyczna próba rozciągania.

**Streszczenie**

W artykule przedstawiono badania wybranych właściwości wytrzymałościowych materiału w postaci próbek pobranych z produkowanych seryjnie kolan rurowych wytwarzanych z rur techniką gięcia oraz technologiami hydroformowania poprzez formowanie wysokim ciśnieniem wewnętrznym i hydrokalibrowanie. Podano definicje wyznaczanych parametrów oraz opisano statyczną próbę rozciągania służącą w świetle normy PN-EN ISO 6892-:2009 ich wyznaczeniu. Omówiono sposób pobierania próbek z gotowego wyrobu i przygotowania ich do badań. Scharakteryzowano instrumentarium do pomiarów próbek, maszynę wytrzymałościową wraz z oprogramowaniem oraz pokazano wprowadzanie najważniejszych parametrów wejściowych służących obliczeniom oraz edycji i akwizycji wyników. Omówiono i skomentowano wyniki statycznej próby rozciągania przedstawione w postaci wykresów oraz wyznaczanych wielkości podanych w formie tabel.

INNOVATIVE ECONOMY
NATIONAL COHESION STRATEGY
INSTITUTE FOR SUSTAINABLE TECHNOLOGIES
NATIONAL RESEARCH INSTITUTE IN RADOM
EUROPEAN UNION
EUROPEAN REGIONAL DEVELOPMENT FUND

Project co-financed by the European Union from the European Regional Development Fund

**Mirosław NESKA**
Institute for Sustainable Technologies – National Research Institute, Radom
miroslaw.neska@itee.radom.pl

# MEASUREMENT SYSTEM FOR IR ABSORPTION

**Key words**

Infrared radiation, infrared detector, measurement uncertainty.

**Abstract**

Radiation absorption measurement systems are widely used in the evaluation of different types of materials. They require a stable transceiver radiation measuring circuit. The article presents a transceiver infrared radiation system developed by the author, in which, apart from a stabilized power supply of transmitting and receiving subsystems, the dedicated software for temperature correction of output signals was also used. The system has two measuring circuits at wavelengths of 860 nm and 950 nm. The paper presents characteristics and measurement uncertainties of the system, determined by means of the reference material. This type of a system can be used in systems for IR transmission or reflection tests, and it can be of help in radiation absorbance studies.

## Introduction

Infrared radiation (IR) is nowadays widely used in many areas, e.g. physico-chemical investigations, optics and materials engineering [1], as well as industrial applications [2]. In the studies, the infrared radiation is usually used in the form of a beam, which is transmitted through or reflected from a surface of the test object. Measurement systems using IR beam for the transmission through the test objects, employ the phenomenon of the spectral absorption in the infrared radiation of the test object [3], while the measuring systems using a reflected beam of IR, use the phenomenon of the emissivity of the test object [4].

The measurement using the phenomenon of the absorption is becoming more widely used, inter alia, in non-contact and non-destructive materials investigations, such as thin silicone materials research for medical applications [5], or the study on thickness and opacity of plastic specimens [6].

In the infrared absorption measurements transceiver circuits of radiation can be used, wherein, light emitting diodes (LED) are used as radiation sources. When the *p-n* semiconductor junction of the LED is polarised for the conduction, it emits radiation, when the electron loses energy, producing only the photon during the radiative recombination [7, 8]. An important feature of the diodes of this type is their linear characteristic in a wide range of the optical power to the current, which increases the use of the LED, e.g. for the systems of transmission of analogue information. Other advantages of LEDs include their long lifetime, durability, energy efficiency, wide range of colours, easy-dimming, design flexibility, environmental compatibility, and low-voltage power supply [9].

Power and control systems of diodes can be broadly divided into two systems for producing a continuous and a modulated beams of light [10, 11]. The system of modulated beam of light can be achieved by placing a pulse-width-modulated (PWM) function generator in the power supply circuit of the LED. Use of a PWM generator in the power supply circuit of diode, enables the *p-n* junction temperature stability and control of the optical power, radiated by the LED during the radiative recombination [12].

The semiconductor components are also used as photoconductive elements (photodetectors), in which photons cause the electron move from the valence band to the conduction band, due to the low energy of the gap between the bands. This phenomenon causes excitation and increases the conductivity of the semiconductor. Examples of such photoconductive elements can include photoresistors, photodiodes, phototransistors, or photothyristors. The phototransistors as photodetectors allow one to obtain an increased current signal by interaction of photons [13]. The increase in the intensity of light on the light-sensitive surface of a phototransistor causes an almost linear increase in its output current, at the constant voltage polarity of the *p-n* junction.

The article presents a system for the measurement of IR absorption, which uses two basic circuits, i.e. a radiation source and a photodetector circuit. As radiation sources IR LEDs are used, and in the photodetector circuit as photodetectors phototransistors are used. The developed system has two measuring channels in the infrared radiation with a radiation wavelength of 860 nm and 950 nm.

## 1. The power and control system

The developed measurement system for the IR absorption is composed of circuits of IR sources and photodetectors (Fig. 1). The system has two measurements channels, which enable research in the IR wavelengths between 860 nm and 950 nm.

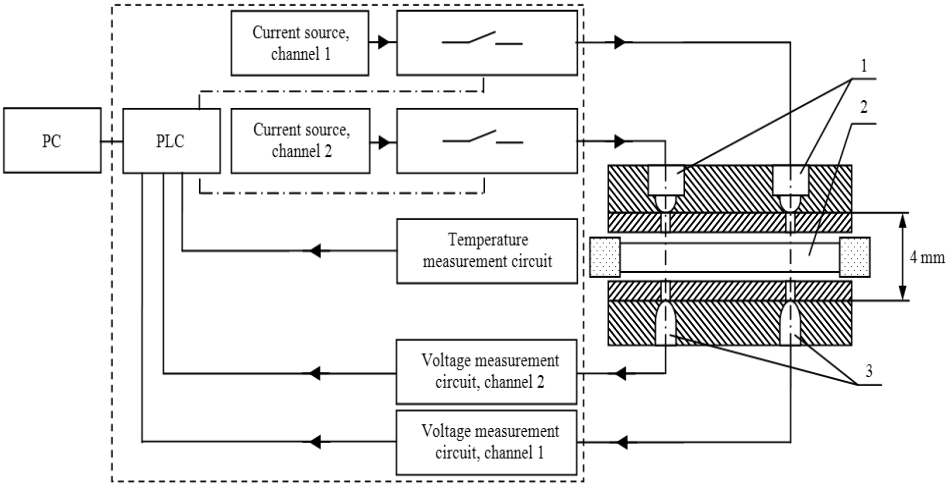


Fig. 1. Scheme of the two channel test stand for IR measurements. 1 – IR sources, 2 – test object, 3 – photodetectors

In each of the measurement channels, in the IR source circuit, the following elements can be found: a current source, an IR LED, a subsystem of transistor and a subsystem of PWM generator. The output signals of the PWM generators are programmable on the platform level of the PLC. The purpose of this circuit is to obtain the modulated IR signals at the optical outputs. The IR LEDs with the emission surfaces from materials such as *GaAlAs* (VSLY3850) and *GaAs* (CQY37N) are used as the IR sources [14]. The IR source circuit developed enables to maintain the desired constant level of radiation intensity source at the nominal level of operating parameters specified by the manufacturer.

The photodetector circuit, on the other hand, is composed of the following subsystems and components: stabilised power sources, voltage sources, phototransistors and voltage measurement subsystems. The task of this circuit is to measure the intensity of infrared radiation, by the current measurement in the phototransistor circuit, with its maximum sensitivity at 900 nm (Fig. 2). The current measurement in the circuit is perform using the indirect method, by voltage measurement across a resistor with a constant and known value of resistance.

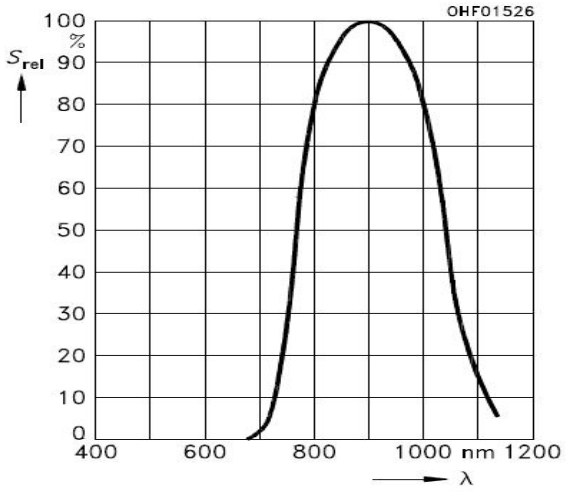


Fig. 2. Relative spectral sensitivity ($S_{rel}$) of a phototransistor type SFH309FA [15]

A measurement signal received from the phototransistor circuit is forwarded to a twelve-bit A/D converter of the PLC, where the signal is processed and analysed. Then measurement data via the Ethernet interface are transmitted and stored in a database of the PC.

## 2. Measurement method

The measurement method developed for IR absorption enables investigations for two parallel measurement channels in the infrared radiation wavelength between 860 nm and 950 nm. During the test, the IR LED sources are supplied by a PWM modulated current with defined parameters of the frequency and the duty cycle by the manufacturer recommended. The generated optical output signals from the IR LEDs have the optical power higher than 5 mW, and the signals are transmitted through a test object onto the photodetectors, which have the maximum sensitivity at the wavelength of 900 nm. Then, in the photodetector circuits, the current values are measured using the indirect method of voltage measurement. The developed measurement

method gives a possibility of implementation to the measuring system of programmed temperature compensation. The temperature is measured concurrently to the current, in the work environment of the elements of the measurement system. The programmed temperature compensation of the current value is accomplished in the PLC, according to the developed algorithm presented in Figure 3.

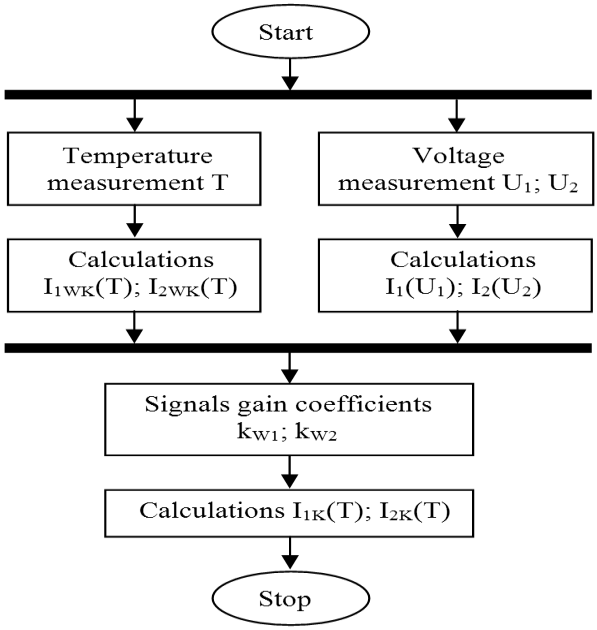


Fig. 3. Algorithm of determining the current value in the two channel circuits of the IR photodetector

The algorithm describes the concurrent measurement and processing of the temperature (T) and the voltages ($U_1$) and ($U_2$), which are measured in the two circuits of phototransistors. The resistance values in each photodetector circuit are known, while the values of voltages ($U_1$) and ($U_2$) are read, and using the Ohm's law the values of currents ($I_1$) and ($I_2$) are calculated. Then, knowing the time characteristics of the currents ($I_1$) and ($I_2$), and temperature (T), characteristics of the currents as functions of the temperature are determined (Fig. 4). After approximation of the measurement data of the $I_1$ and $I_2$ currents, their functions of average values were determined as functions $\bar{I}_1(T)$ and $\bar{I}_2(T)$, and for them the temperature compensation functions $I_{1WK}(T)$ and $I_{2WK}(T)$ were calculated. Variables $I_1$ and $I_2$, and functions $I_{1WK}(T)$ and $I_{2WK}(T)$ implemented to matrix arrays to receive the equation (1) of functions $I_{1K}(T)$ and $I_{2K}(T)$.

$$\begin{bmatrix} I_1 & I_{1WK}(T) & 0 & 0 \\ 0 & 0 & I_2 & I_{2WK}(T) \end{bmatrix} \cdot \begin{bmatrix} k_{W1} \\ k_{W1} \\ k_{W2} \\ k_{W2} \end{bmatrix} = \begin{bmatrix} I_{1K}(T) \\ I_{2K}(T) \end{bmatrix} \tag{1}$$

In the developed method, the equation (1) was defined by the following parameters of: boundary conditions ($T \geq 0$ºC), and amplification coefficients of output signals $k_{W1}$ and $k_{W2}$. The use of the amplification coefficients allows one to shape the output signals of the measurement system using the software of the PLC.

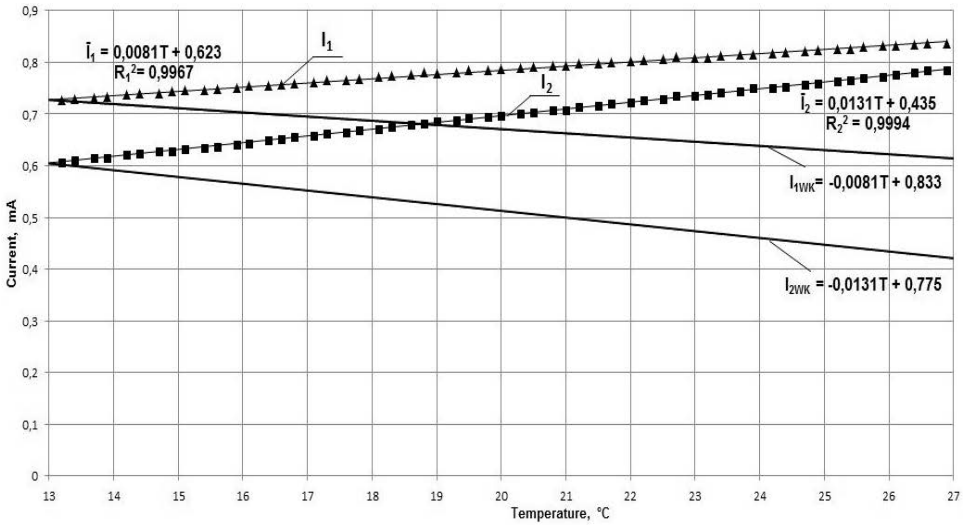


Fig. 4. Characteristics of measurement signals of currents as functions of temperature and their temperature compensation functions. $I_1$, $I_2$ – current values measured on the channels 1 and 2; $I_{1WK}$, $I_{2WK}$ – temperature compensation functions of currents for channels 1 and 2

## 3. Verification of the system

The developed system for the measurement of the IR absorption was installed in the mechanical housing (Fig. 5), to protect the IR transceiver circuit from ambient light radiation.

The system was subjected to long-term investigations under various thermal conditions. As a test object, a certified test material (Densitometric Screen S/N012, Eclipse Laboratories Inc.) was used.

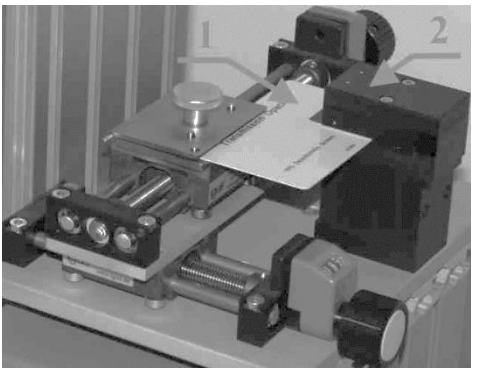


Fig. 5. View of test object (1) and the IR measuring head of the system (2)

Investigation results were obtained in the PC using an original programme, developed in the LabVIEW environment. The received data are presented as a function of time in Figure 6.

The expanded uncertainties of the results of current measurements with the programmed temperature compensation in both measurement channels 1 and 2 were determined for a 99% level of confidence and the coefficient of expansion $k_p = 2.576$, using calculation methods type A and B [16]. The received expanded uncertainties for the two measurement channels $I_{1K}$, and $I_{2K}$ have the same value of 0.036 mA [17].

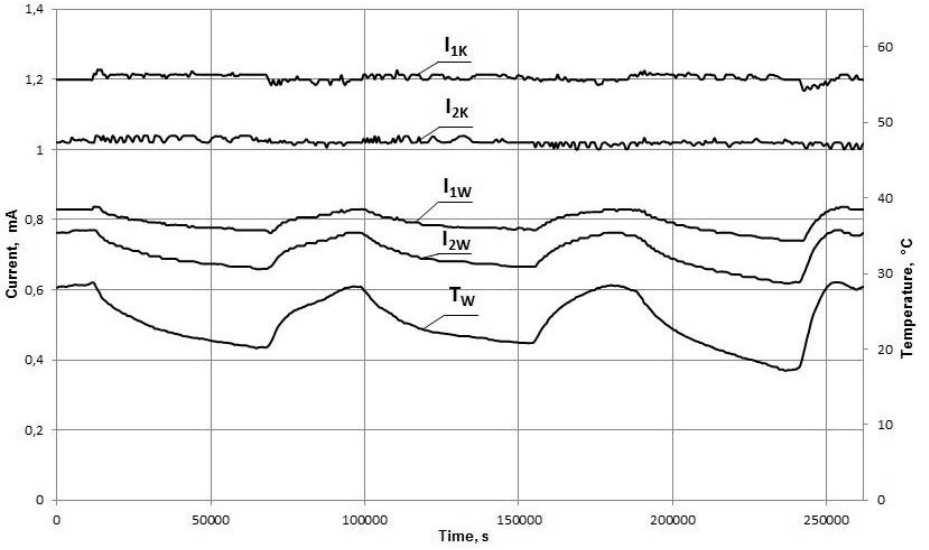


Fig. 6. Examples of characteristics of programmed temperature compensation of measured currents and temperature as functions of time. $I_{1W}$, $I_{2W}$ – measuring current on the channels 1 and 2; $I_{1K}$, $I_{2K}$ – current measurements with programmed temperature compensation on the channels 1 and 2; $T_W$ – temperature measurement

**Summary**

The system for the measurement of IR absorption was developed. The system retains the thermal stability of optical signals. The measurement method of test objects in the infrared radiation in two wavelengths 860 nm and 950 nm was described. A verification of the developed system was conducted, using the certified test material and by subjecting the system to long-term investigations under different temperature conditions. As a result of the performed investigations received the positive evaluation of verification for the measuring channels of the system. For the developed system estimated the expanded uncertainty at a 99% confidence level.

The developed measuring system can operate independently or can be used as a submodule of other systems, such as e.g. network control system (NCS) [18], or systems using mathematical modelling of processes and advanced procedures of control [19].

Other examples of application of the measuring system can include systems for investigation of transmission or reflection of infrared light such as a non-destructive infrared inspection of foils [20], the study on specimens of biological and chemical installations [21, 22], or the identification and detection of objects in industrial applications [23].

*Scientific work executed within the Strategic Programme "Innovative Systems of Technical Support for Sustainable Development of Economy" within Innovative Economy Operational Programme.*

**References**

1. Rydzkowski T.: Metods of research on polymers sturkture. Crystallinity. Teka Kom. Bud. Ekspl. Masz. Elektrotech. Bud. – OL PAN. 2008, pp. 143–148.
2. Seshadri A., Pagilla P. R.: Optimal web guiding. Journal of Dynamic Systems, Measurement, and Control. Vol. 132, no 1/2010, pp. 011006-1––011006-10.
3. Rocha W.R.M., Pilling S.: Determination of optical constants *n* and *k* of thin films from absorbance data using Kramers–Kronig relationship. Spectrochimica Acta Part A: Molecular and Biomolecular Spectroscopy. 123 (2014), pp. 436–446.
4. Herve P., Cedelle J., Negreanu I.: Infrared technique for simultaneous determination of temperature and emissivity. Infrared Physics & Technology. 55 (2012), pp. 1–10.
5. Park I.S., Ha J.S.: Thickness measurement of silicon thin film coated on metal mold by analyzing infrared thermal image. International Communications in Heat and Mass Transfer. 36 (2009), pp. 462–466.

6. Shams Nateri A., Hajipour A.: Measuring thickness of translucent plastic by scanner. Optik. 125 (2014), pp. 452– 456.
7. Scajev P., Karaliunas M., Kuokstis E., Jarasiunas K.: Radiative and nonradiative recombination rates in cubic SiC. Journal of Luminescence. 134 (2013), pp. 588–593.
8. Dodd P., Stellwag T., Melloch M., Lundstrom M.: Surface and perimeter recombination in GaAs diodes: an experimental and theoretical investigation. IEEE Transactions on Electron Devices. 38 (1991),
pp. 1253–1261.
9. Choi J.H., Shin M.W.: Thermal investigation of LED lighting module. Microelectronics Reliability. 52 (2012), pp. 830–835.
10. Żagan W.: Podstawy techniki świetlnej. Wydawnictwo Politechniki Warszawskiej. Warsaw 2005 (in Polish).
11. Czajka P.: The determination of characteristics of highly-efficient LED diodes impulse work. Maintenance Problems. 2 (2008), pp. 33–44 (in Polish).
12. Ohyama S., Iizuka J., Takayama J., Kobayashi A.: Position measurement using an enclosed signal field with pulse-width-modulated function. Sensors and Actuators A. 113 (2004), pp. 54–59.
13. Shih N.F., Pai F.J., Chuang W.J., Hong J.W.: Current gain control of near infrared c-Si phototransistors. Solid-State Electronics. 44 (2000), pp. 1399–1404.
14. Information on http://www.vishay.com.
15. Information on http://www.osram-os.com.
16. Evaluation of measurement data – Guide to the expression of uncertainty in measurement. JCGM 100:2008.
17. Neska M., Majcher A.: Estimation of the uncertainty of measurement in a two-channel system for tests on the intensity of infrared radiation. Maintenance Problems. 3 (2014), pp. 45–55.
18. Majcher A.: Model of the event driver networked control system for the diagnostics use. 10th International Science and Technology Conference: Diagnostics of Processes and Systems. Zamość 2011. Maintenance Problems. 2 (2011), pp. 131–140.
19. Mazurkiewicz A.: Innovative technological solutions for sustainable development. Published by Institute for Sustainable Technologies-National Research Institute, Radom (Poland) – Shanghai (China), 2010, ISBN 978-83-7204-955-1, pp. 29–61.
20. Just P., Ebert L., Echelmeyer T., Roscher M.A.: Infrared particle detection for battery electrode foils. Infrared Physics & Technology. 61 (2013), pp. 254–258.
21. Skowroński J., Bojarska M., Neska M.: The concept of the system for parameterization of functionalized membranes. Solid State Phenomena. Vol. 223 (2015), pp. 3–10.

22. Kato K., Omoto H., Tomioka T., Takamatsu A.: Visible and near infrared light absorbance of Ag thin films deposited on ZnO under layers by magnetron sputtering. Solar Energy Materials & Solar Cells. 95 (2011), pp. 2352–2356.
23. Zbrowski A., Samborski T., Kozioł S.: The model of the system for prototype production of the RFID identifiers. Maintenance Problems. 3 (2011), pp. 251–263 (in Polish).

**Układ pomiaru tłumienia promieniowania podczerwonego**

**Słowa kluczowe**

Promieniowanie podczerwone, detektor podczerwieni, niepewność pomiaru.

**Streszczenie**

Układy pomiaru tłumienia promieniowania znajdują szerokie zastosowanie w ocenie różnych typów materiałów. Wymagają one stabilnego toru nadawczo-odbiorczego promieniowania. W artykule przedstawiono opracowany układ nadawczo-odbiorczy promieniowania podczerwonego, w którym obok stabilizowanych źródeł zasilania podukładów, nadawczego i odbiorczego, zastosowano programową korekcję temperaturową sygnałów wyjściowych. Układ posiada dwa tory pomiarowe o długościach fal 860 i 950 nm. W artykule zaprezentowano charakterystyki i niepewności pomiarowe układu wyznaczone przy wykorzystaniu referencyjnego materiału.

Układ tego typu może być zastosowany w systemach badania przepuszczalności lub odbicia światła podczerwonego, czy badaniach absorbancji promieniowania.

**Sandra ŚMIGIEL, Damian LEDZIŃSKI, Tomasz MARCINIAK, Adam MARCHEWKA**
University of Technology and Life Sciences, Bydgoszcz
sandra.smigiel@utp.edu.pl, damian.ledzinski@utp.edu.pl, tomasz.marciniak@utp.edu.pl, admiar@utp.edu.pl

# BPM DETECTION ALGORITHM IMPLEMENTED ON A MOBILE DEVICE

**Key words**

ECG, algorithm, BPM, mobile device.

**Summary**

Mobile devices are steadily increasing their position in the field of new inventions, such as monitoring the work of the heart. The need for monitoring and control the patients' health, especially the aspects related to normal cardiac function (measurement of rhythm), is one of the main directions in the field of ongoing research. Development direction, determined with the advancement of technology, is to find a way of linking the technique with medicine. In this article, the conducted of analysis covered the various algorithms used in the process to determining the value of BPM, providing the heart rate. The aim of the authors was to determine the possibility of their use in relation to a variety of mobile devices, such as tablets, smartphones, and also processors for embedded devices. This task consisted of the evaluation of the signal processing by each device. In further steps, based on the data collected, the authors analysed the possibility of using the specific devices to evaluate the ECG signal recording in real time. The summary of the study was to identify the effectiveness of the detection of BPM using various algorithms on designated devices.

## Introduction

In many areas of medical diagnosis, measurement and analysis of electrophysiological signals have an important role. They are an invaluable source of information for the methods and the correct functioning of various organs in living organisms. One of aspects measured is mapping the signals of the heart known as electrocardiogram [6].

Electrocardiography is a graphic record of changes in electrical potential, which is registered from the surface of the chest during depolarization and repolarization of cardiac muscle cells. Typical ECG allows specifying the location of the P wave, QRS complex, T wave and U wave. Amplitude, the frequency of occurrence, and the interval between each wave are the parameters used to define a number of abnormalities of the heart. The ability to interpret the ECG wave is a very important element of knowledge, because decisions that are based on it determine further treatment strategy, influencing both the quality and length of the patient's life [5, 6].

Currently available tools in the field of medical science provide many opportunities that can lead to the correct diagnosis of the cause of the patient state. Analysis of the literature in the field of cardiac devices points to deficiencies in mobile use of them. In addition, a more and more common limitation is the lack of functionality associated with simultaneous, automatic, and personalized computer analysis, directed to a user and disease. Given the rapid development of new technology, there are no obstacles to provide this functionality [6].

After analysing of the needs, the authors have developed and tested (on a variety of mobile devices) the algorithms used in the process of determining the value of BPM (Heart Rate) described in this article. The process of determining the value of BPM is based on measuring the distance between two R peaks [4]. There are three modes of heartbeat (used to identify a variety of cardiac dysfunction). Standard duration is 60-80 beats per minute, and anomalies are as follows: bradycardia < 50 beats per minute, and tachycardia > 100 beats per minute. Depending on the length of the RR, there are three modes of operation of the heart, which are used to identify the activity of various disorders. According to the latest research, the heart rate is new therapeutic target in clinical cardiac. Reduction in heart rate is undoubtedly a necessary way to proceed in the treatment of many diseases of the circulatory system [1, 2, 8].

## 1. Material

The shape of the ECG signal recorded by the electrocardiograph depends primarily on the measurement system, which means how to connect the electrodes to the patient. The example of an ECG for the purpose of this article is based on three unipolar limb leads. These leads record the heart's electrical

field changes, which are based on signals from the positive electrode (examiner), located at the measuring electric potential, and the neutral electrode voltage (equal to zero). The absolute value of the potential is measured at the point of the application of the positive electrode. A scheme of electrode placement is as follows: lead aVR – right upper limb, lead aVL – left upper limb, and lead aVF – left lower limb. Indifferent electrodes consisted of a combination of lead aVR with right lower limb and lead aVF also with the right lower limb [6].

## 2. Methods

The study was conducted in three stages. The first stage of the research included registration of the ECG signal, pre-processing, and the design of the algorithms for heart rate detection (BPM).

The pre-processing consists in a set of operations on the magnitude of retrieved signals, and it provides a numerical value to work within the following steps. In general, within these activities two stages are distinguished: normalization and filtering of the resulting signal. Part of the first step is to remove interference – the power network 50 Hz frequency, noises such as breathing movements, and other. Then, the sample was analysed in two ways [1, 8].

The first is the FFT. The popular way of the frequency analysis of the ECG signal has been the Fourier Transform, which is usually performed by the Fast Fourier Transform (FFT) algorithm. Fast Fourier Transform is a fundamental transform in digital signal processing with applications in frequency analysis, signal-processing limitations of high-gain amplification, and signal filtering [7].

The second is the WT. Wavelets Transform, which is a method to analyse a signal in time and frequency. It allows the representation of the signal in the range of time scale by means of "wavelet coefficients" that reflect the degree of correlation between the signal and wavelet. The most commonly used is Discrete Wavelet Transform (DWT). DWT gives the decomposition of a signal. To implement DWT, the iterative algorithm Mallata is used, i.e. a simple and fast algorithm for the decomposition of the analysed signal [3]. In the output of scaling function, it is the input of next level of decomposition. In the context of this article, the study was based on the characteristics of the Daubechies Wavelet, which has a shape similar to the morphology of the components sought, i.e. symmetric Gaussian wavelet [1, 4, 9]. The study used the 4 and 6 types of this wavelet (db4, db6).

### 2.1. Heart Rate detection algorithms

- Difference Algorithm (Diff BPM Algorithm):

It analyses the derivatives ECG waves, which are defined based on the difference in values of the two adjacent samples.

The value of the R-peaks is computed according the following equation:

$$s_i^{'} = s_{i+1} - s_i \tag{1}$$

where

$s_x^{'}$ – the value of new sample x,

$s_x$ – the value of sample x.

- Threshold Algorithm:

This algorithm determines the threshold above which further steps are indicated and the positions of R-peaks are counted. The threshold value is determined for a certain portion (sliding window) or for all of the ECG wave (Fig. 1).

The value of threshold is indicated at the point as follows:

$$t_i = \left(\max_w - avg_w\right) * R + avg_w \tag{2}$$

where

$t_x$ – the threshold value at the point x,

$\max_w$ – the maximum value for the area w,

$avg_w$ – the arithmetic mean of the area w,

$R$ – constant value of 0.6.

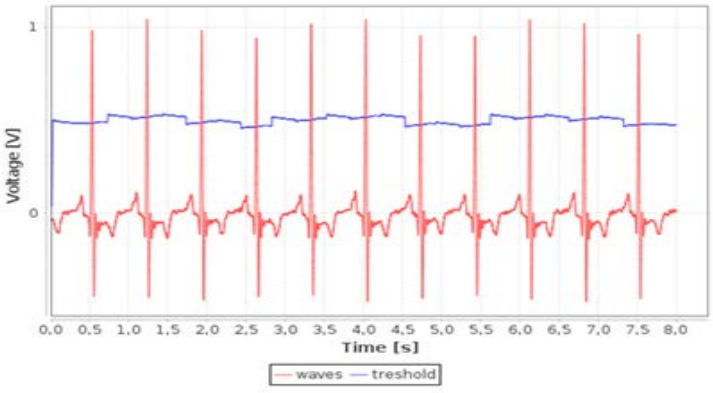


Fig. 1. The sample of ECG wave with the threshold

- Counting Algorithm:

The algorithm counts the position of R-peaks that are above the threshold. After that, it divides the number of occurrences by the time in which they occur, thereby obtaining the value of BPM.

The second stage of the study included the statistical analysis of the data, which was performed using the tools of Statistica software 10 Site License. Statistical inference is started by identifying the characteristics of the variables. Determining the distribution of the variables was based on the Shapiro-Wilk test. In view of the obtained results' non-parametric distribution of the variables was confirmed (score $p < 0.05$), and further analysis was based on non-parametric tests. Hereafter, based on descriptive statistics, the following were determined: the mean, standard deviation, median, quartiles, and percentiles. The obtained data scatter was confirmed by statistical tests Grups (score $p < 0.05$). Correlation analysis, due to non-parametric distribution, was performed by Spearman rank tests.

The third stage of the study focused on tests of the algorithms performance. For this purpose, the authors described algorithms implemented on a few different devices with different processors and memory size. All devices had processors with ARM architecture. The best of them was a quad-core ARM Cortex-A15 clocked at 2500 MHz, having a total capacity of 35.000 DMIPS. The worst of them are single-core ARM11 700 MHz clocked at 900 DMIPS, having 900 DMIPS. In any case, all of the algorithms were employed in real time. The results presented algorithm execution times for the worst case.

## 3. Results

In this paper, the analysis of the data was performed using the following abbreviations:

Fast Fourier Transform – F, Wavelet Transform DB4 – W44 (4-level), Wavelet Transform DB6 – W64 (4-level), Wavelet Transform DB4 – W45 (5-level), Wavelet Transform DB6 – W65 (5-level), 1, 2 - 1s, 2s width of the window, N – the entire signal of ECG, D – Diff BMP Algorithm.

- Evaluation of algorithms in statistical terms:

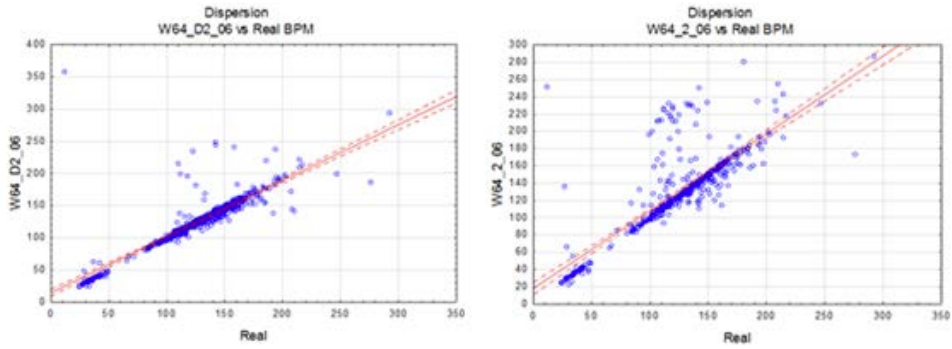


Fig. 2. The best algorithms for Wavelet Transform

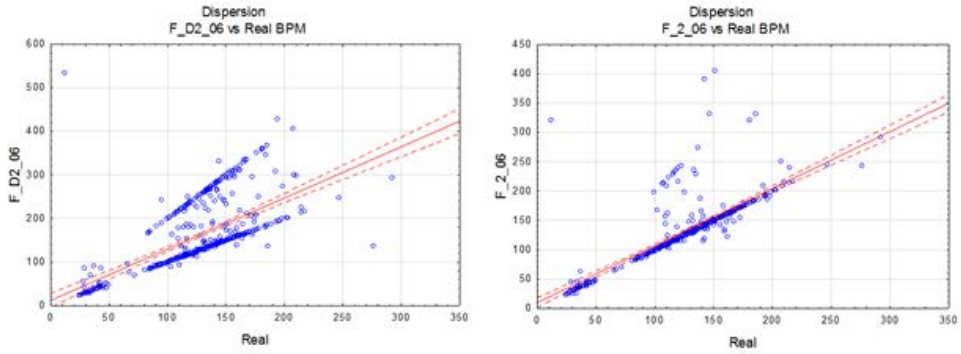


Fig. 3. The best algorithms for Fourier Transform

The obtained results demonstrate the statistical significance. Correlation analysis performed by Spearman rank tests demonstrated for W64_D2_06 that the best score for Wavelet Transform was r = 0.94, and for W64_2_06 the value r = 0.83 (Fig. 2). Correlation analysis performed by Spearman rank tests demonstrated value r = 0.71 for F_D2_06, and for F_2_06 the best score for Fast Fourier Transform was r = 0.89 (Fig. 3).

- Evaluation of algorithms in terms of performance: Tests were conducted to determine if signal processing is possible in real time on a variety of devices.

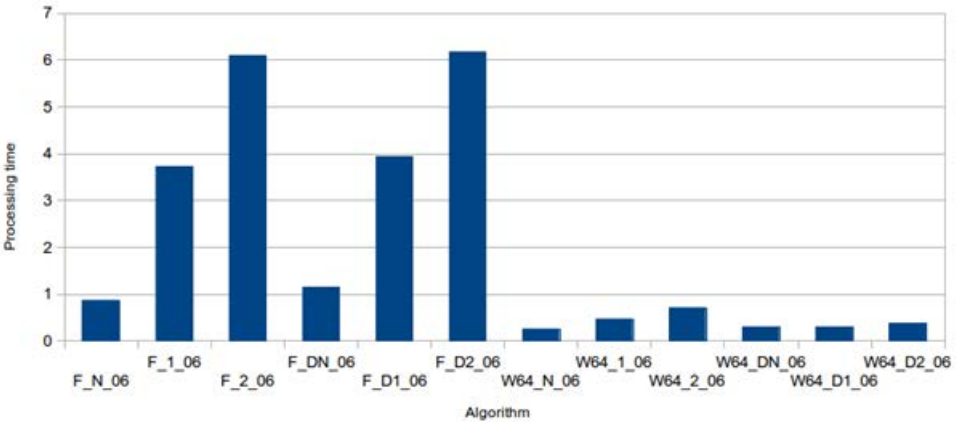


Fig. 4. Processing time of algorithms

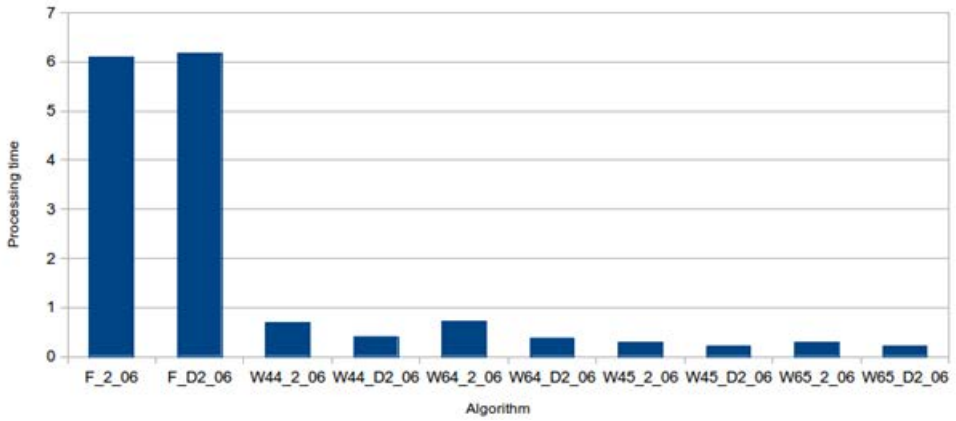


Fig. 5. Processing time of algorithms

## Conclusion

The paper presents the possibility of using Fourier Transform and Wavelet Transform to detect BPM on the example of recorded ECG waves. The range of capabilities of mobile devices in terms of processing algorithms for the detection of BPM was also indicated. The performed analysis, both in statistical and performance terms of the mobile devices, is the first of this type. Analysis of literature indicates that other researchers focused solely on determining the value of BPM. Two ways of examining the recorded ECG waves, in terms of their effectiveness in detecting value of BPM, provided the opportunity to compare and demonstrate the effectiveness of these transforms.

The significance of the application of the reported methods for the detection of BPM confirms the obtained results. Their analysis suggests that the best application in the detection of BPM for the assumed boundary data was obtained by Wavelet Transform. The effectiveness of its application confirms the time calculations, efficiency and quality of their implementation, as well as the obtained effect. In contrast to the Wavelet Transform, the Fast Fourier Transform presents much poorer results. The proposed wavelet shape with similar morphology to the ECG provides the best accuracy in determining the location of R peaks, and thus the value of BPM. This fact is confirmed by the tests carried out. The best results were obtained for Daubechies Wavelet 6 (db6). A little worse results were in terms of db5 and db4. Analysis of possible levels of decomposition based on the select wavelet presents the best for level 4. Both higher and lower levels of decomposition obtained much worse results. Analysis of algorithms developed in terms of the detection of R peaks showed that the highest efficiency for the Diff BMP Algorithm was obtained the ECG waves after Wavelet Transform. In both cases, analysis of ECG waves were the best for 2s slider window.

Any of the described algorithms can be executed in real time, at least on a mobile device with a 700 MHz ARM11 processor. This is due to the characteristics of the device and the analysed transform (DWT). Each level of decomposition in Wavelet Transform causes that the signal has half as many samples. Therefore, algorithms using 5-level Wavelet Transform executes faster than the algorithms using 4-level Wavelet Transform.

Both methods allow one to determine the location of R peaks, and thus the value of BPM. However, the greatest accuracy, in the correct interpretation of the electrocardiogram, which allows recognizing the value of BPM, is provided by the Wavelet Transform.

Analysis of the results confirms the importance of their use in the cardiological diagnosis.

**References**

1. Dingfei G.: Study of ECG Feature Extraction for Automatic Classification Based on Wavelet Transform, The 7th International Conference on Computer Science & Education (ICCSE 2012), pp. 500–503.
2. Hillbom S., Lindberg R., Lindberg E.: Realtime BPM and Beat Detection using ADSP-21262 SHARC DSP, Algorithms in Signal Processors, ETIN80 2014.
3. Marciniak B., Maszewski M., Zabłudowski Ł., Ledziński D.: Innovative optical system for the inspection of manufacturing processes using the wavelet approach, Solid State Phenomena 2015, vol. 223, pp. 291–298.
4. Nouira I., Abdallah A.B., Bedoui M.H., Dogui M.: A Robust R Peak Detection Algorithm Using Wavelet Transform for Heart Rate Variability Studies, International Journal on Electrical Engineering and Informatics 2013, vol. 5, no. 3, pp. 270–283.
5. Pathoumvanh S., Hamamoto K., Indahak P.: Arrhythmias Detection and Classification base on Single Beat ECG Analysis, The 4th Joint International Conference on Information and Communication Technology, Electronic and Electrical Engineering 2014.
6. Piotrowski Z., Różanowski K.: Robust Algorithm for Heart Rate (HR) Detection and Heart Rate Variability (HRV) Estimation, Acoustic and Biomedical Engineering, vol. 118, no. 1, 2010.
7. Ranjeet K., Kumar A., Pandey R.K.: ECG Signal Compression Using Different Techniques,Springer-Verlag Berlin Heidelberg 2011 (ICAC3), pp. 231–241.
8. Seena V.: A review on feature extraction and denoising of ecg signal using wavelet transform, 2nd International Conference on Devices, Circuits and Systems (ICDCS 2014), pp. 1–6.
9. Yun-fu T., Lei D.: Study on Wavelet Transform in the Processing for ECG Signals, World Congress on Software Engineering 2009, pp. 515–518.

**Algorytmy wykrywania BPM realizowane w oparciu o urządzenia mobilne**

**Słowa kluczowe**

ECG, algorytm, BPM, urządzenia mobilne.

**Streszczenie**

Mobilne urządzenia stale zwiększają swoją pozycję w zakresie tworzenia nowych wynalazków, m.in. do monitorowania pracy serca. Potrzeba monitorowania i kontroli stanu zdrowia pacjenta, a zwłaszcza aspektów związanych z prawidłową pracą serca (pomiarem jego rytmu) jest jednym z podstawowych kierunków w zakresie prowadzonych prac badawczych. Kierunkiem rozwoju wyznaczanym wraz z postępem technologii jest znalezienie drogi łączącej technikę z medycyną. Analizując te potrzeby, w ramach niniejszego artykułu poddano analizie różne typy algorytmów wykorzystywane w procesie wyznaczania wartości HR, świadczące o częstotliwości pracy serca. Celem autorów było określenie możliwości ich wykorzystania w odniesieniu do różnorodnych urządzeń mobilnych typu: tablet, smartfon, a także w procesorach urządzeń wbudowanych. Realizacja tego zadania polegała na ocenie czasu przetwarzania sygnału przez poszczególne urządzenia. Na dalszych etapach, w oparciu o zgromadzone dane, analizie poddano możliwość wykorzystania wybranych urządzeń w ocenie zapisu sygnału EKG w czasie rzeczywistym. Podsumowaniem przeprowadzonych badań było wskazanie skuteczności wykrywania HR, poprzez zastosowanie wybranych algorytmów, na wyznaczonych urządzeniach.

INNOVATIVE ECONOMY
NATIONAL COHESION STRATEGY
INSTITUTE FOR SUSTAINABLE TECHNOLOGIES
NATIONAL RESEARCH INSTITUTE IN RADOM
EUROPEAN UNION
EUROPEAN REGIONAL DEVELOPMENT FUND

Project co-financed by the European Union from the European Regional Development Fund

**Szymon ZACHARSKI, Tomasz SAMBORSKI**
Institute for Sustainable Technologies – National Research Institute, Radom
szymon.zacharski@itee.radom.pl, tomasz.samborski@itee.radom.pl

# ROBOTISED AND RECONFIGURABLE SYSTEM TO SUPPORT THE PRODUCTION PROCESS IN THE MACHINING INDUSTRY

**Key words**

Industrial robot, manipulator, automation, production.

**Abstract**

The paper presents a developed reconfigurable system that allows automation of processes running in parallel, carried out on the production line for rolling bearings. In the first process, the washing of tapered roller bearing assemblies of different sizes is performed. The second process involves one hundred percent inspection of the quality of produced bearing rings for the presence of internal defects in materials. In both processes, the role of the system is to transport the blanks into successive processing slots.

An integral element of the developed system is the tool magazine to manipulate objects with different geometries. The control system determines the allocation of the manipulative tasks, depending on the input and output status of supported processing stations. The used hardware and software solutions allow for the elimination of human labour in hazardous conditions and will improve the quality of bearings.

## Introduction

The current global economic conditions lead to an increase in demand for flexible and reconfigurable manufacturing systems. This is due to frequent changes in the product range, small batch production, and strong competition. To ensure the company's competitiveness and flexibility of manufacturing the systems for reconfiguration of the production, facilities should be developed.

Flexible production systems and, frequently used in this area, industrial robots with systems for quick and easy tool switching lead to increased productivity. This is due to the need to lower costs and improve the quality of manufactured products. The increase in the quality of the engineering industry is often achieved through a hundred percent inspection of the elements produced during the manufacturing process. Automatic optical inspection systems are most often used for this purpose. The production line of tapered roller bearings and bearing rollers, inter alia, are subject to automatic optical inspection [1, 2] and assembly of the finished bearing assembly [3–6].

Other types of inspection for bearing manufacturing processes are methods using eddy currents, e.g., to test the rings of rolling bearings [7, 8]. These quality control methods require proper cleanliness of the test piece. For this purpose, the inspection systems are equipped with cleaning modules [9, 10] or, in a process lines, are preceded with washing systems.

Paper [11] describes the concept of the use of an industrial robot to handle bearing assembly washers before the assembly inspection stand. An important aspect of the robotisation of the washer is to eliminate the manual operation in hazardous conditions [12, 13] caused by the presence of hazardous technological liquids.

Robotisation and automation of production processes carried out in the hazardous conditions (dust, noxious fumes, high temperature, heavy elements to be moved) for employees of operations, such as paint shops, grinding facilities, and the chemical industry, are a requirement regulated by environmental regulations and health and safety at work regulations and by [14].

At the Institute for Sustainable Technologies – NRI, a robotic, reconfigurable system was developed for the automation of a tapered roller bearing washer and the stand for on-line inspection of the rolling rings produced in parallel production lines.

The washer for rolling bearings is operated by a worker engaged in monotonous work in hazardous conditions through contact with hazardous substances [15]. The washing process involves placing the assembly in the washing socket of a revolving conveyor moving at a constant speed. The rotary motion of assembly is accomplished by using spindles that lock bearings in

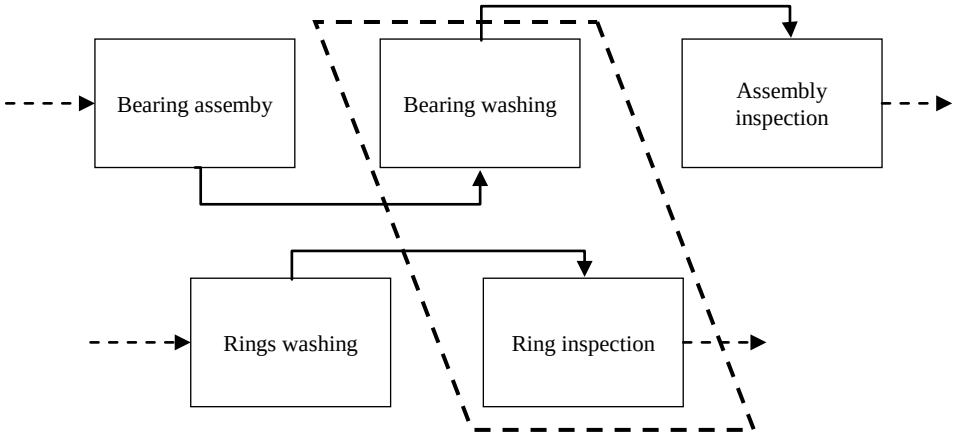


Fig. 1. Diagram of automation regions of production line for bearings and roller rings

washing sockets. After washing, the worker removes the bearing from the socket and places it on the conveyor, where the bearing is transported into a drying device, then into automatic optical inspection module. The washing socket in which a bearing is placed is equipped with an insert adapted to the geometry of the bearing. Figure 2 shows a general view of the cleaning stand. The task of the manipulator is to move the bearings from the positioning module on the belt conveyor and to the drying unit.

a) b)

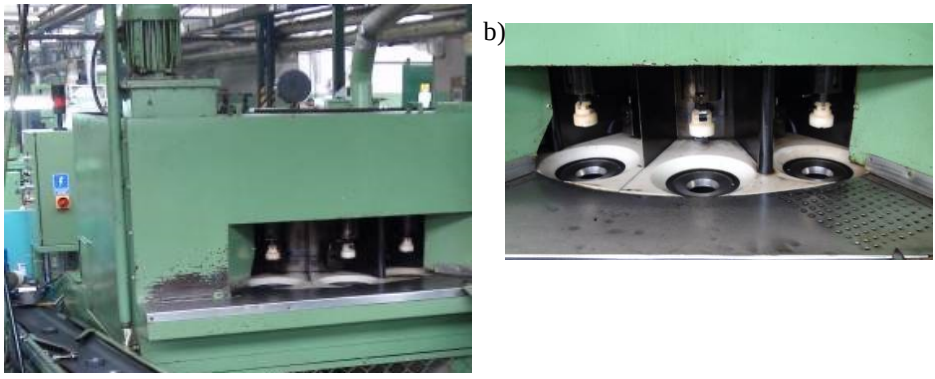

Fig. 2. Technical stand for cleaning the rolling bearings: a) general view, b) view of the cleaning sockets

The second technical slot operated by the reconfigurable system is a stand for the detection of material defects in the rings of rolling bearing [16]. The stand consists of three modules:

– An input module responsible for correct positioning of the tested ring,
– A detection module responsible for the scanning and detection of the material defects, and
– An output module responsible for selection of the rings for good products and faulty products.

The task for the manipulator is to move and properly position the bearing rings fed into the inspection stand.

## 1. The structure of the reconfigurable system

The most important element of the system is a six-axis industrial manipulator with a capacity of 5 kg and a working range of approx. 900 mm that ensures adequate space handling and load capacity required for manufactured items. There is a head for automatic tool change system installed to the wrist of the manipulator, and this is equipped with pneumatic feedthroughs providing the ability to control the tools that use compressed air.

Fig. 3. Test stand

The tools used by an industrial robot were designed and manufactured with regard to the particular kinematics of the two work slots and based on the analysis of the available space. Figure 4 shows tool #1, which is a bearing gripper, and tool #2, which is a ring gripper, mounted in the magazine. The modular design of the tool magazine allows the adaptation of the system to the range of products. Depending on the size and geometry of the transported elements, tools are selected to implement the functions of gripping and manipulation. Checking the presence of tools in the magazine is performed using inductive sensors.

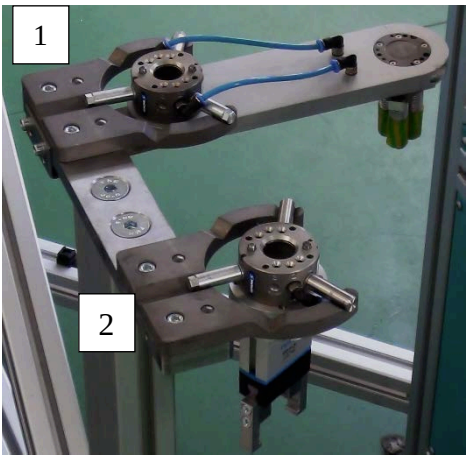


Fig. 4. Tool magazine for the system for automated tool change

Each tool is equipped with an adapter for automated tool exchange. It enables the supply of compressed air for pneumatic tools without having to manually reconnect the wires. In addition, the adapter allows the transmission of electrical signals to the tools, using, e.g., a power supply or position sensors.

Figure 5 shows an example of the elements carried by the industrial manipulator. The bearing (Fig. 5b) is gripped by a cylindrical inner surface with a three-finger, centric pneumatic gripper. In contrast, the bearing ring is gripped by the front and back surface by a pneumatic parallel gripper.

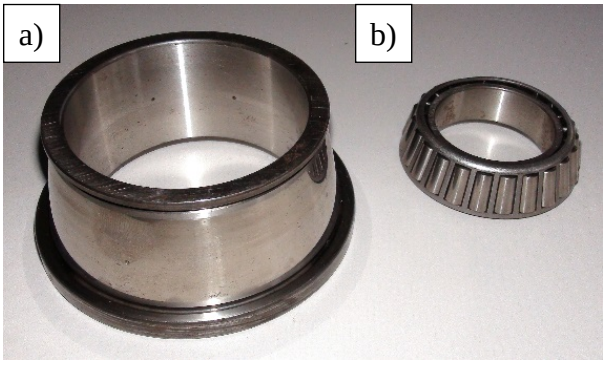


Fig. 5. Elements manipulated by an industrial manipulator: a) inner ring of bearing, b) tapered roller bearing

## 2. System operation

Using the test stand shown in Fig. 3, the robot controller was programmed to handle the washer and the inspection stand of the bearing rings. The control

system determines the allocation of the manipulative tasks, depending on the status of handled input and output processing stations.

Figure 6 presents images of specific points of the trajectory of the movement of the manipulator:

a) assembly of the tool to manipulate the bearing rings,
b) picking the ring from the feeding ramp, and
c) releasing the ring into the input module of the stand for detection of inner defects.

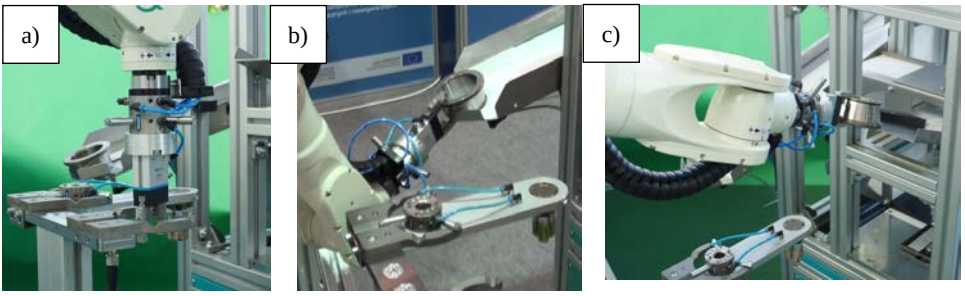


Fig. 6. The work cycle of a manipulator handling the stand for detection of inner defects of bearing rings

Figure 7 presents images of the work cycle of the manipulator handling the model-washing device:

a) assembly of the gripper,
b) picking the clean bearing from the conveyor socket,
c) releasing the bearing onto the transporter, and
d) picking the bearing intended for cleaning from the bearing positioning module on the conveyor.

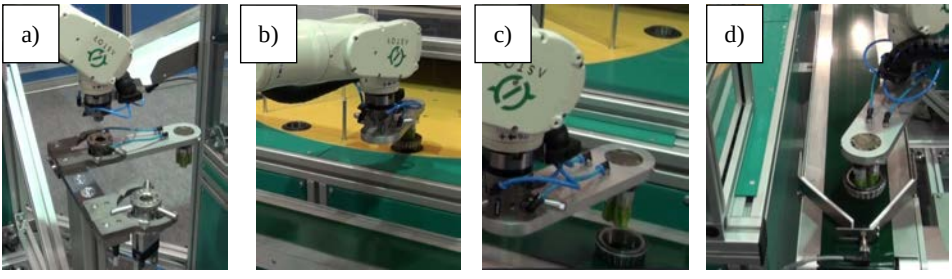


Fig. 7. The work cycle of a manipulator handling the stand for washing the tapered roller bearings

System verification tests carried out on the production line showed the need to modernise the main drive of the washer to provide the necessary synchronization with the manipulator. Figure 8 shows the image of the manipulator operating on the production line.

Fig. 8. Installation of the system on the tapered roller bearings' production line

**Summary**

The introduction of a reconfigurable robotic system for the production line will ensure the high quality of the bearings. The essence of the developed system is the flexible allocation of the manipulative tasks, depending on the input and output status of supported processing stations. The used hardware and software solutions eliminate human work in hazardous conditions. Improving the quality of work and reduction of the negative impact of human tasks on the production process will help to increase the competitiveness of companies in the market. The model system built in the form of a test stand will minimise the time of detention and reduce associated costs to implement the system on a production line of rolling bearings.

*Scientific work executed within the Strategic Programme "Innovative Systems of Technical Support for Sustainable Development of Economy" within Innovative Economy Operational Programme.*

**References**

1. Zbrowski A., Giesko T.: Automatyzacja kontroli jakości wyrobów w linii technologicznej wytwarzania wałeczków łożysk tocznych. Technologia I Automatyzacja Montażu 2008 nr 2, s. 36–40.
2. Giesko T., Mazurkiewicz A., Zbrowski A.: Advanced mechatronic system for in-line automated optical inspection of metal parts. International Journal of Simulation: Systems, Science & Technology, (IJSSST), Vol. 11, No 4 September 2010, pp. 36–41.

3. Wójcicki T., Czajka P., Giesko T.: Automatyczna inspekcja montażu uszczelek łożysk tocznych z wykorzystaniem komputerowych metod przetwarzania i analizy obrazów. Zeszyty Naukowe Politechniki Rzeszowskiej Nr 273 Mechanika, z. 79, 2010, s. 27–36.
4. Zbrowski A., Samborski T.: Bezstykowe metody kontroli jakości w wielkoseryjnej produkcji łożysk samochodowych, Logistyka 2014, nr 3, s. 7071–7080.
5. Czajka P., Giesko T., Matecki K., Zbrowski A.: Metoda i system laserowej inspekcji montażu uszczelek w łożyskach tocznych. Technologia i Automatyzacja Montażu 2010 nr 2, s. 22–28.
6. Czajka P., Garbacz P.: Metoda optycznej inspekcji w procesie montażu łożysk tocznych, Problemy Eksploatacji, 4/2011, s. 65–78.
7. Matecki K., Zbrowski A., Matras E.: Metodyka wykrywania wad materiałowych w pierścieniach łożysk tocznych techniką prądów wirowych, Logistyka 2014 nr 3, s. 4188–4197.
8. Zbrowski A., Matecki K.: Wykrywanie wewnętrznych wad materiałowych w pierścieniach łożysk tocznych. Problemy Eksploatacji, 2/2012, s. 229–243.
9. Zbrowski A.: Cleaning system for automated optical inspection of heads of bearing rollers. Solid State Phenomena. Vol. 198, Mechatronic Systems and Materials IV (2013), pp. 289–294.
10. Zbrowski A.: Metoda przygotowania powierzchni wałeczków łożyskowych do procesu automatycznej optycznej inspekcji. Problemy Eksploatacji 2009 nr 1, s. 209–215.
11. Zbrowski A., Samborski T., Zacharski S.: Proces adaptacji manualnego gniazda technologicznego do pracy w cyklu zautomatyzowanym. TTS Technika Transportu Szynowego 10/2013, art. nr 95, s. 975–985.
12. Stamirowski J.: Elastyczność systemów produkcyjnych w kontekście dynamiki produkcji Postępy Nauki i Techniki Nr 9, 2011, s. 38–51.
13. Tolio T.: Design of Flexible Production Systems, Springer-Verlag, Berlin Heidelberg, 2009.
14. Rogoś E., Zbrowski A.: Perspektywy rozwoju systemów zwiększających bezpieczeństwo ekologiczne. Bezpieczeństwo i Technika Pożarnicza. Safety & Fire Technique. Nr 20/4/10 Józefów, December 2010, s. 47–58.
15. Zbrowski A., Samborski T., Zacharski S.: Koncepcja robotyzacji gniazda technologicznego mycia złożeń łożyskowych w procesie produkcyjnym. TTS Technika Transportu Szynowego 9/2012, art. nr 60, s. 609–618.
16. Samborski T., Zbrowski A.: Model stanowiska do wykrywania wewnętrznych wad materiałowych w pierścieniach łożysk tocznych. Energetyka, 2012, s. 447–451.

**Zrobotyzowany i rekonfigurowany system wspomagający wytwarzanie w przemyśle maszynowym**

**Słowa kluczowe**

Robot przemysłowy, manipulator, automatyzacja, wytwarzanie.

**Streszczenie**

W artykule zaprezentowano opracowany rekonfigurowalny system umożliwiający zautomatyzowanie biegnących równolegle procesów technologicznych realizowanych na linii produkcyjnej łożysk tocznych. W ramach pierwszego procesu realizowane jest mycie złożeń stożkowych łożysk tocznych o różnej wielkości. Drugi proces obejmuje stuprocentową kontrolę jakości produkowanych pierścieni łożyskowych pod kątem występowania wewnętrznych wad materiałowych. W obydwu procesach rolą systemu jest transport półwyrobów do kolejnych gniazd technologicznych.

Integralnym elementem opracowanego systemu jest magazyn narzędzi umożliwiający manipulowanie obiektami o różnej geometrii. System sterowania decyduje o przydziale zadań układu manipulacyjnego w zależności od stanów wejściowych i wyjściowych obsługiwanych stanowisk technologicznych. Zastosowane rozwiązania sprzętowe i programowe pozwalają na wyeliminowanie pracy człowieka w szkodliwych warunkach oraz przyczynią się do poprawy jakości produkowanych łożysk.

INNOVATIVE ECONOMY
NATIONAL COHESION STRATEGY
INSTITUTE FOR SUSTAINABLE TECHNOLOGIES
NATIONAL RESEARCH INSTITUTE IN RADOM
EUROPEAN UNION
EUROPEAN REGIONAL DEVELOPMENT FUND

Project co-financed by the European Union from the European Regional Development Fund

**Jordan MĘŻYK**
Institute for Sustainable Technologies – National Research Institute, Radom
jordan.mezyk@itee.radom.pl

# A SYSTEM OF INDUSTRIAL MANIPULATOR EQUIPPED WITH FUNCTIONS FOR ADAPTATION AND RECONFIGURATION

**Key words**

Industrial manipulator, reconfiguration, adaptation, modular robotics.

**Abstract**

The article presents a system for an industrial manipulator equipped with advanced functions for reconfiguration and adaptation. Currently standard industrial manipulator systems perform their function in an invariable, planned in advance manner; however, in near future, it is certain that there will be high demand in the market for systems that allow adaptation of their configuration to the variable situation in the production line. The use of mechatronic systems and devices that are capable of reconfiguration and adaptation to changing tasks in the technical process allows an increase in the flexibility and effectiveness of industrial plants.

Presented solution assumes the fitting of a standard industrial manipulator with additional systems to allow its reconfiguration, monitoring its environment, and adaptation of its parameters according to current needs. The described system of reconfiguration and adaptation functions for the industrial manipulator allows the introduction of the robotic technology into the areas where, so far, it was not possible or unprofitable, that is for the production line with a short series of product production.

## Introduction

Robotic systems have become very popular on large production plants. Once programmed can perform their operation continuously without making mistakes or fatigue. However, the cost of robotisation is high, so smaller facilities still need to rely on human labour. There is a clear tendency to produce machinery capable of operating on different variants of the same product. Additionally, there are machining centres to perform multiple operations on one product. Using such equipment requires extended changeover times, so quick change of the assortment is not possible [1].

A solution for that problem would be application of a reconfigurable system [2]. Such a system of a modular structure should allow quick changeover of components, thus adapting the system to a new series of products. Automation of changeover processed with independent decision-making and automated adaptation of machine parameters constitutes a flexible and efficient production system.

The system presented in this article is a system with functions of reconfiguration and adaptation based on an industrial robotic arm. It is intended for use in small production facilities with variable production assortment. The concept of the system consists in using a typical industrial manipulator and retrofitting it with additional modules for flexible tool switching and for monitoring the environment of the robot and the production line. In addition, the system includes a software expert system to store the information about the production process and available tools and for making the decisions on subsequent actions.

## 1. Modular robotics

Robotics is a research area that is currently under rapid development. It has been noticed that the extension of robot capabilities is strictly related to its modularisation. Manipulators built from modules can be optimised in their functionality and costs.

There exist several examples of modular robots developed in laboratories. Such an example might be a Hydrabot – The Modular Electro-Hydraulic Robot Arm (Fig. 1) designed by Abed Alnaif from University of Waterloo [3]. Hydrabot is constructed of several identical links, each of them utilising one degree of freedom.

A similar concept is presented by William J. Schonlau [4, 5]. His Modular Robot (Fig. 2) is built of series of 1 DOF modules, but there exist four types of modules: rotary joint, linear joint, elbow link, and straight link – two of them active and two passive.

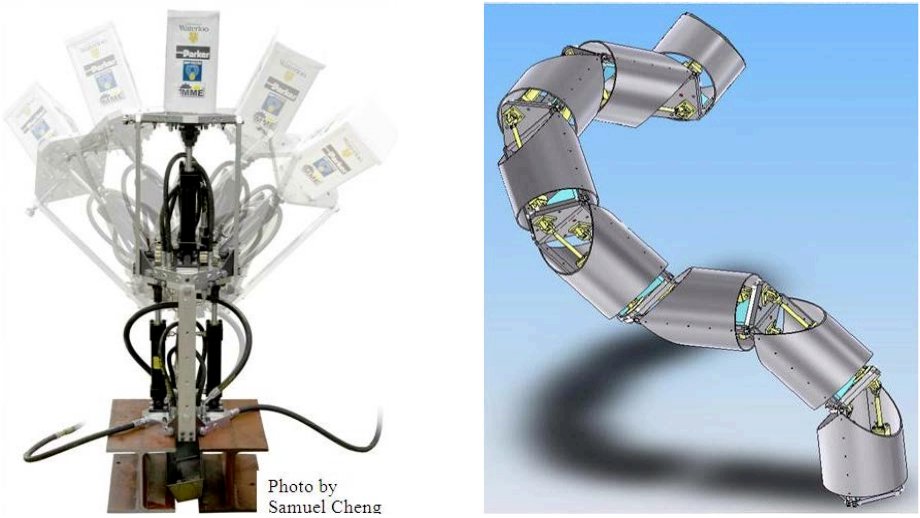


Fig. 1. Hydrabot – The Modular Electro-Hydraulic Robot Arm [3]

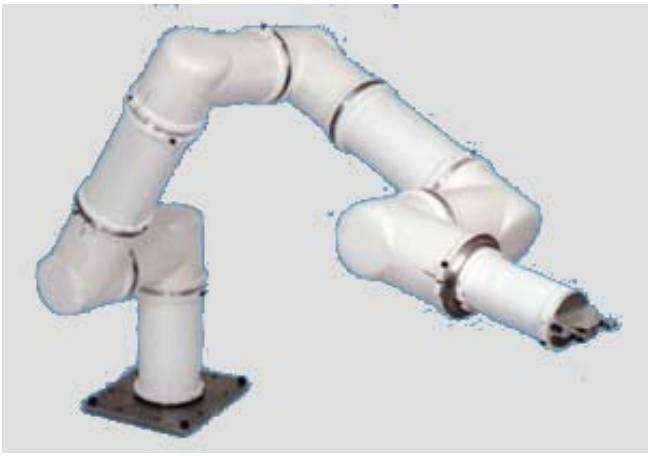

Fig. 2. The Modular Robot [4, 5]

A slightly different concept is presented by Schunk [6]. Their modular robot, called Powerball (Fig. 3), is constructed from 2 DOF modules with integrated drive control. The modules differ in size but are the same in functionality.

The above concepts referred to standard manipulators and their modular variations. However, the term modular robotic is understood as a system that consists of multiple identical modules joined in various configurations to create robots of totally different structure and performed task. Such a system

was presented by Graham Ryland and Harry Cheng from University of California [7, 8]. Their iMobot (Fig. 4) is built from small modules that link together like a chain to form larger robotic modules. The modules have two joints at the centre that can rotate 180 degrees. The robots have four degrees of freedom, so they can stand themselves up, roll end over end, stack themselves, and inch along like a caterpillar.

Fig. 3. Powerball modular robot [6]

Fig. 4. iMobot [7, 8]

## 2. The manipulator system

The system of industrial manipulator equipped with functions for adaptation and reconfiguration was developed at the Institute for Sustainable Technologies – National Research Institute (ITeE – PIB) in Radom. It is built on the industrial, available commercially, robotic arm and retrofitted with additional modules and

systems that allow dynamic reconfiguration of the manipulator and its slot (surrounding), depending on the tasks currently planned on the production line. This modification is to allow the robotic system to be used in operations where it was not beneficial or impossible.

The whole system consists of several mechatronic modules, which are the robotic arm, coupler module, tool modules, and tools – finger gripper, pneumatic gripper, smart camera module, laser scanner module, and milling module. The coupler module is a mechatronic module that allows the connection of tool modules. The tool modules are mechanically fixed to the gripper with use of a pneumatic actuator, so the switching of the tool does not require the operator's participation. The coupler module allows the supply of the tool modules with media, such as compressed air, electrical current, and communication with tool modules with use of Ethernet lines. The construction of the tool modules is based on the tool plate equipped with electronic circuits that standardise the communication protocol for different types of tools and allow storage of the tool data. Therefore, it is possible to add new tools to the system, those that were not defined in the system beforehand.

The tool modules are built on universal tool plates with the use of standard, commercially available, components, such as grippers, measurement devices, and motors. The software of the manipulator allows adaptation of its movement parameters depending on the type of the tool and the performed task. The functionality of the coupler module allows building measurement tools that required large data transfers, such as cameras and laser scanners, and controlling the movement and behaviour of the system based on the data acquired from the measurement devices in real time. An extra module was added to the system, which is a tool magazine that allows communication with and testing of the tools.

The system was integrated and tested in the Laboratory of Mechatronics of ITeE-PIB. The system operates in a model work cycle in a simulated industrial environment, which proved the functionality of all elements of the system, such as tool switching with use of coupler module, with full operation of all tools. Verification tests were performed for each module and for each task, such as milling, laser scanning, gripping, and manipulation of elements.

To complete the system of the manipulator, it was equipped with a belt conveyor that allows simulation of a production line. The manipulator with a tool magazine and belt conveyor consist a complete model of an operational slot for a robot.

## 3. System modules

As the base of the system, a large industrial robotic arm was selected. It is a Kawasaki FS30N (Fig. 5) robot with a gripping range of 1676 mm and load capacity of 30 kg [9].


Fig. 5. Kawasaki FS30N robot [9]

The basic parameters of the robot are gathered in Table 1.

Table 1. Selected parameters of Kawasaki FS30N robot [9]

| Parameter | Value |
|---|---|
| Degrees of freedom | 6 |
| Payload | 30 kg |
| Maximum linear speed | 8900 mm/s |
| Maximum reach | 1676 mm |

The reason for selecting such a heavy robot is that the application of any additional equipment on the robot's wrist enlarges the forces acting on the wrist. There is no problem if the equipment hangs straight downward from the wrist, then the forces act longitudinally to the axis of the wrist. The problem becomes critical when the equipment is positioned away from the vertical axis. The maximum moments of inertia need to be addressed. The producer of the robotic arm provides the chart of wrist load capacity (Fig. 6), which allows the determination of the maximal weight of the equipment and the distance of its mass centre from the centre of the wrist [9].

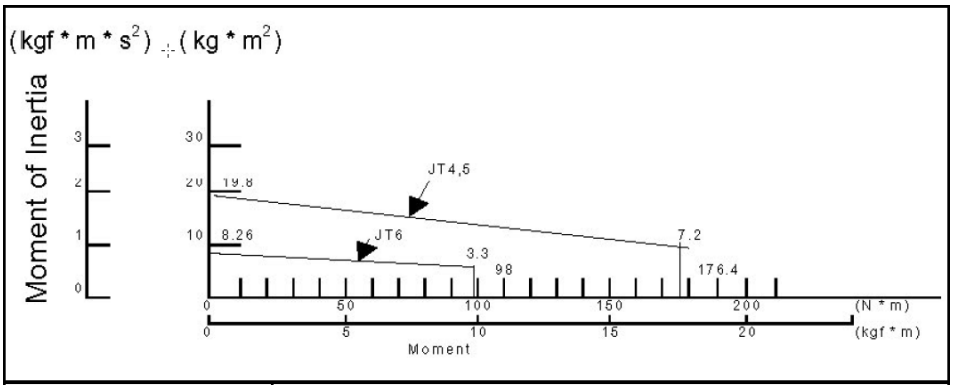


Fig. 6. The wrist load capacity of Kawasaki FS30N robot [9]

The effector modules (tools) are intended for typical tasks: manipulation tasks, technological tasks, and measurement tasks. Below, the tools developed with the system are presented.

The finger gripper module (Fig. 7) was developed in two versions: two finger gripper and three-finger gripper. Its construction is based on a standard pneumatic gripper driver from Festo [10].

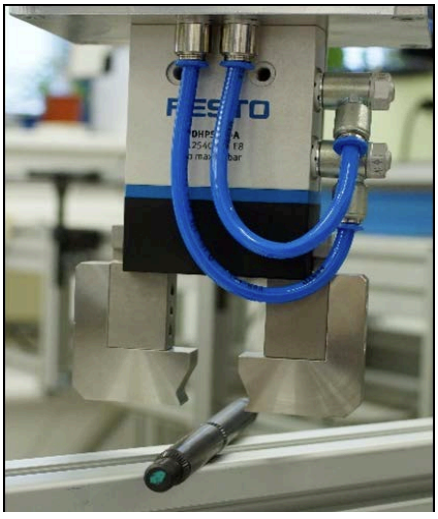

Basic parameters:

Supply: pneumatic

Load capacity: 10 kg

Maximum diameter of manipulated elements:

12–14 mm

Exchangeable gripper jaws

Fig. 7. Finger gripper – two finger version and its parameters [10]

The magnetic gripper module is constructed with the use of a standard electromagnet from Stephnson Gobin [11]. It allows manipulation of steel elements of regular and irregular shapes weighing up to 20 kg. In addition, the

pneumatic gripper was developed. It uses a standard Festo gripper [12] and allows manipulation of objects with smooth surfaces weighing up to 30 kg.

As mentioned above, the system of the manipulator is capable of performing measurements that require large data transfers, such optical inspection, and laser scanning. Two modules to perform such measurements were developed.

The vision system module (Fig. 8) uses a smart-camera from Cognex [13]. The camera uses GigE Vision interface based on standard Ethernet protocol. The use of the smart-camera allows the image analysis and inspection process to be performed on the camera with the transfer of only analysis results to the supervisory system. The module allows product inspection and the measurement of the tested object to adapt the operation parameters of the manipulator.

Basic parameters:
Sensor: 1/1.8'' CMOS
Resolution: 800x600 px
Sampling: up to 102 fps

Fig. 8. The vision system module and its basic parameters [13]

The developed laser scanner module (Fig. 9) uses a 3D laser scanner from LMI [14]. The measurement range is 210 mm and the resolution is below 40 μm. This allows precise measurement of the geometry of the tested object. The results of measurements are used to inspect the object and to adapt the parameters of manipulator operations.

Basic parameters:
Measurement range: 210 mm
Resolution: < 40 μm
Field of view: 96–194 mm
Sampling: up to 5000 Hz

Fig. 9. Laser scanner module and its basic parameters [14]

For the machining process simulation, a simple spindle module was developed. It is based on a small DC motor of 230 W and a nominal rotary speed of 11 000 rpm. The module allows simple machining in soft materials.

## Conclusion

The developed system of an industrial manipulator equipped with functions for adaptation and reconfiguration constitutes a complete system for an industrial production slot. Retrofitting the robotic arm with additional modules allows easy accommodation of the standard machinery to variable production conditions.

Typical applications of the system can be found in any production branch. However, it is the sector of small and medium enterprises that will mostly benefit from the application of the system, which allows using only one robotic system for different products and tasks on the production line. Therefore, smaller companies will be able to robotise their production lines without sacrificing large amounts of financial resources for investment. In addition, the robots already owned by the enterprise can be retrofitted to allow the reconfiguration and adaptation of the machinery.

*Scientific work executed within the Strategic Programme "Innovative Systems of Technical Support for Sustainable Development of Economy" within Innovative Economy Operational Programme.*

## References

1. Nazarian E., Ko J., Wang H., Design of multi-product manufacturing lines with the consideration of product change dependent inter-task times, reduced changeover and machine flexibility, Journal of Manufacturing Systems, vol. 29, 2010, pp. 35–46.
2. Bi Z.M., Lang S.Y.T., Verner M., Orban P., Development of reconfigurable machines, International Journal of Advanced Manufacturing Technology, vol. 39, 2008, pp. 1227–1251.
3. Alnaif A., Hydrabot – The Modular Electro-Hydraulic Robot Arm, 2009, Website article: http://www.eng.uwaterloo.ca/~aalnaif/.
4. Schonlau W., MMS, a Modular Robotic System and Model-Based Control Architecture, SPIE Sensor Fusion and Decentralized Control in Robotic Systems, Boston Massachusettes, September 1999.
5. Schonlau W., MMS, a Modular Robotic System, 2009. Website: http://www.oocities.org/~schonlau/.
6. Powerball Lightweight Arm LWA 4.6: Manoeuvrable, powerful and high-precision. Schunk Company website: http://www.pl.schunk.com/schunk/

schunk_websites/news/news_detail.html?article_id=19960&country=POL&lngCode=PL&lngCode2=EN.
7. iMobot – an intelligent reconfigurable modular robot, Integration Engineering Laboratory website: http://iel.ucdavis.edu/projects/imobot/.
8. Ryland G.G., Cheng H.H., Design of iMobot, an Intelligent Reconfigurable Mobile Robot with Novel Locomotion, Proc. of 2010 IEEE International Conference on Robotics and Automation, Anchorage, Alaska, May 3–8, 2010.
9. Kawasaki FS30N Product Specification. Kawasaki Robotics (USA) Inc., Website: http://www.kawasakirobotics.com/.
10. Parallel gripper DHPS. Instruction Manual. Festo. Website: http://festo.com/.
11. Type 58 Magnet Technical Information, Stephenson Gobin, 2004.
12. Vacuum suction grippers ESG, Product Catalogue, Festo, 2014.
13. In-Sight 7020 Specifications. Cognex. Website: http://cognex.com/.

**System manipulatora przemysłowego z funkcjami adaptacji i rekonfiguracji**

**Słowa kluczowe**

Manipulator przemysłowy, rekonfiguracja, adaptacja, robotyka modułowa.

**Streszczenie**

Artykuł przedstawia system manipulatora przemysłowego wyposażonego w zaawansowane funkcje rekonfiguracji i adaptacji. Standardowe systemy manipulatorów przemysłowych wykonują swoje funkcje w sposób stały, z góry zdefiniowany, jednak w przyszłości wzrośnie zapotrzebowanie na systemy, które umożliwiają dostosowanie swojej konfiguracji do bieżącej sytuacji na linii produkcyjnej. Wykorzystanie urządzeń i systemów mechatronicznych charakteryzujących się zdolnością do rekonfiguracji i przystosowania do zmienianych zadań w procesach technologicznych umożliwia zwiększenie elastyczności i efektywności systemów przemysłowych. Przedstawione rozwiązanie zakłada wyposażenie standardowego manipulatora przemysłowego w dodatkowe systemy umożliwiające zmianę konfiguracji systemu, monitorowanie jego otoczenia oraz zmianę parametrów według potrzeb.

Prezentowany system manipulatora wyposażonego w funkcje adaptacji i rekonfiguracji umożliwienia wprowadzenie techniki robotowej do zadań, w których do tej pory było to nieopłacalne lub niemożliwe, tj. na liniach o krótkich seriach produkcyjnych.

**Ryszard WOCIANIEC, Sławomir BUJNOWSKI, Zbigniew LUTOWSKI, Łukasz ZABŁUDOWSKI**
University of Technology and Life Sciences, Bydgoszcz
ryw@utp.edu.pl; slaw@utp.edu.pl; zbigniew.lutowski@utp.edu.pl; lukasz.zabludowski@utp.edu.pl

# PACKAGING GLUING MACHINE

**Key words**

Packaging, type of construction, machine technology.

**Summary**

The food industry needs to attract consumers with attractive packaging. An example might be a package opening to the form a three-dimensional figure. Manufacture of such packages involves the creation of a typical box that is glued after the placement of the product placement. Then, an extra cover, forming interesting spatial model, is glued to the box. The fusing machine described in the article was designed for a company where the extra covers had been manually glued with double-sided adhesive tape. The device takes the box from the store at a speed matched to the cycles of its work. Subsequent cycles of operation of the devise are box transport to the gluing position, cover loading from a tray, cover lubrication with adhesive, and pressing the cover to the box for a specified time interval. The finished product is directed to a flat table to the next packaging step.

## Introduction

Packaging prepared in the printing consists of two parts: a proper package, containing the product, and an additional decorative lid. The lid is supplied in

the form of flat fused elements that must be assembled and glued to the product. Then the whole package is wrapped in shrink-film. During intuitively unpacking, the customer opens the additional cover that creates a spatial form. In the presented case, a "safari" animal is produced (Fig. 1). Only then the customer can access the chocolates placed inside the carton. Such an attractive form of packaging is addressed to children, who are the main target for this product [2, 3].


Fig. 1. Final form of the package

So far, the packaging manufacturing practice was primitive and inefficient, because it was based on gluing two elements with an additional cardboard lid (Fig. 2). Each step was performed manually and the result is shown in Fig. 3. Experience has shown that the hot bonding technique with a limited lifetime glue cannot be used due to the need for precise and reproducible (serial) application of an additional lid on the box [1]. Mechanical application of the adhesive requires fast assembly of related parts. In practice, components are glued with double-sided tape. The effectiveness of this process was not sufficient. In order to increase the efficiency of the process and improve the obtained effect with a limited number of errors occurring in the production, the development team decided to build a machine with an automatic bonding cycle [4].

Fig. 2. Glued elements: lid of the packing and carton

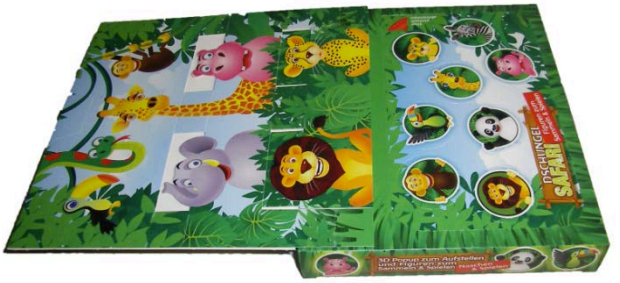


Fig. 3. Glued pieces

## 1. Construction and operation

Fusing (Fig. 4) comprises a body (1), the storage boxes chain conveyor (2), the displacement mechanism for the lids with head gripping and manipulating the lids (3), the reservoir of adhesive and the glue feed mechanism (4) with the magazine of lids (5).

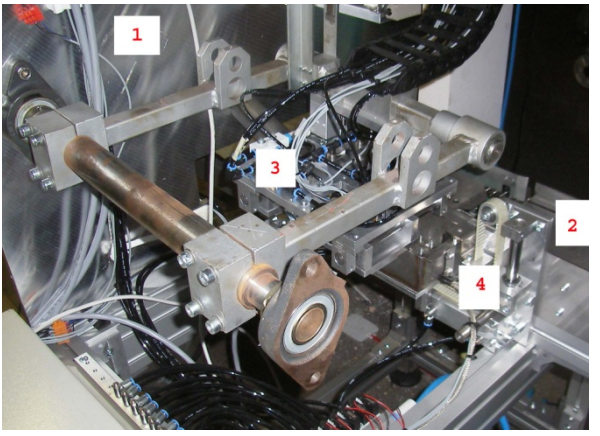


Fig. 4. Machine during the installation process

Construction materials are aluminium alloy AL5083 12 mm thick, 1.4301 and 1.4305 steel. Aluminium alloy Al5083 parts were machined with proprietary group milling technology of multiple items from one plate in two operations on the milling centre.

The body is made of aluminium AL5083 plates seated on a frame of aluminium profiles. The chain conveyor is mounted to the frame, as well as the container for boxes. At the input location, the fusing machine receives cartons with the proper contents and lids, which are packed in packages. For proper operation of the whole process, adhesive is supplied periodically. A glued package appears at the output (Fig. 3). The form of the box container is determined by the shape and size of the rectangular boxes. Boxes are delivered in packets for the vertical tray where they are taken by chain conveyor hooks. The periodically moving chain conveyor supplies the boxes to the box-gluing zone. Due to inaccuracies in the positioning of the chain conveyor connected with its tension, scale errors, and errors of the operation of positioning the chain, a conveyor with an optical sensor and the mechanical referencing system (Fig. 5) was built.


Fig. 5. Principle of the box positioning on the chain conveyor

The chain conveyor (Fig. 5) stops the box (1) before reaching the predetermined position. Then, the actuator acting as a fixed base is extended (3). The swivel clamp of CLR FESTO type (3) pushes the box to a fixed base. Determination of the position in a direction perpendicular to the motion direction is provided by a contoured side, pressing the box to the fixed side. In the absence of a box, the conveyor continues the periodic movement, until a box on the gluing position is detected.

The magazine is a typical, well-known solution with skewed guides and pneumatically adjustable pressure. It is seated on three adjustable supports, which allows lid adjustment in relation to the carton located on the chain conveyor. Three-point support allows movement of the magazine in the horizontal plane. This movement is a combination of linear and rotary motion.

Delivery of the adhesive was initially carried out using a typical pump. However, because of the low price of the device requirement, it was decided to build a mechanical glue delivery module. The choice of this solution was influenced by the shape of the box, which significantly deviates from the flat surface. In addition, it was decided to apply multipoint glue application, with clearly marked drops of glue. A locally thicker layer of glue properly fused the box to the lid.

The glue delivery system (Fig. 6) consists of a heated glue tank (1) with a retractable frame (2) with evenly spaced screws (3) immersed in the adhesive. The mechanism (4) driven by pneumatic actuator via a toothed belt moves the frame and glue from the screws (3) to the lid, and the adhesive is applied.


Fig. 6. Glue delivery system

The purpose of the lid movement mechanism are to get the lids from the tray, signal an empty magazine if needed, provide the cover over the glue applicator module, move the lid to be adhered on the box located on the conveyor, let down the lid to contact with the box, wait a few seconds, and return to the starting position. After that, the finished box is moved to the exit of the machine.

## 2. Control unit

A block diagram of the control system is shown in Figure 7. The PLC controller controls the gluing system. The controller is equipped with an HMI panel, inverter, 16 digital inputs to handle PT100, digital outputs, and outputs that can support PWM.

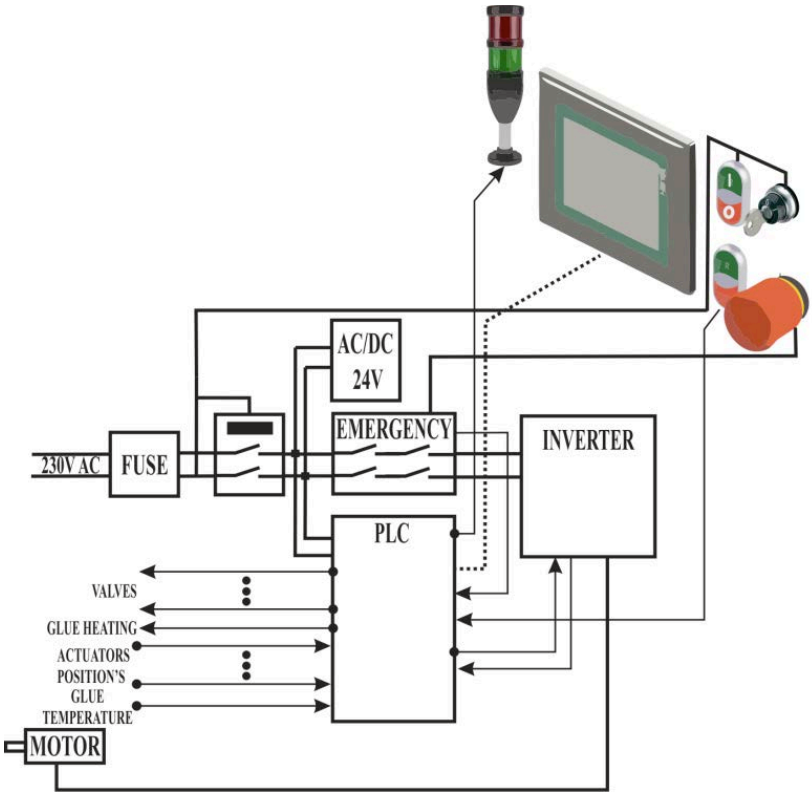


Fig. 7. Block diagram of the control system

The system is equipped with a safety relay with an emergency pushbutton stop and power supply cut off in case of an emergency. The safety relay cuts off the power supply to the inverter, heaters, and the valve island. All actuators are equipped with position sensors for both extreme positions. The system does not have a pressure sensor that allows monitoring the pneumatic system, but a timeout system was implemented in the software to supervise the movement of individual elements of the system. In case of an emergency, an adequate message appears on the HMI desktop, with the possibility to resume system operation. It was necessary to carefully select the sensors working near the glue tank. The temperature reaches 170°C. A capacitive sensor recognizing the presence of a cover was particularly sensitive to temperature.

## Conclusion

The machine reached the assumed yield of 7 pcs/min. The mechanical box positioning method and the covers position adjustment in the tray was a good solution. The concept of the application of the glue with the use of a specially designed module was also convenient. The main advantage of this solution is

simple replacement of the frame with glue placing screws. This allows for glue application points position adjustment according to the client's requirements. The use of a tank, which has to be heated, is a disadvantage of this solution, because it generates a long device start-up period. However, the advantage is the fact that the supplementation of the glue in the tank is possible without interrupting the working cycle of the machine.

## References

1. Korin Ch, Lestelius M., Tryding J., Hallback N.: 4 Y-peel characterization of adhesively-bonded carton board: an objective method, Journal of Adhesion Science and Technology 2007, vol. 21, no. 2, pp. 197–210.
2. Marsh K., Bugusu B.: Food Packaging – Roles, Materials, and Environmental Issues, Journal of Food Science 2007, vol. 72, no. 3, pp. 39–55.
3. Robertson G.L.: Food packaging. Principles and Practice, CRC Press Taylor & Francis Group 2013.
4. Strormer A., Franz R.: IGRESIVES: a research project on migration from adhesives in food-packaging materials in support of European legislation and standardization, Taylor & Francis 2009, vol. 26, no. 12, pp. 1581–1591.

## Maszyna do klejenia opakowań

### Słowa kluczowe

Opakowania, postać konstrukcyjna, maszyna technologiczna.

### Streszczenie

Przemysł spożywczy musi przyciągnąć konsumentów atrakcyjnym opakowaniem. Przykładem może być otwierane pudełko do postaci trójwymiarowego obrazu. Produkcja takich rozwiązań polega na tworzeniu typowego klejonego po wyprodukowaniu opakowania. Po tym etapie dodawana jest pokrywa, tworząc dodatkowy interesujący model przestrzenny przyklejany do pudełka. W firmie, dla której zaprojektowano maszynę opisaną w artykule, dodatkowe pokrywy były przyklejane ręcznie za pomocą taśmy dwustronnie klejącej. Urządzenie pobiera opakowanie z magazynu z prędkością dopasowaną do cyklu jego pracy. Kolejne cykle pracy urządzenia to: transport opakowań do miejsca klejenia, załadunek pokrywy z podajnika, pokrycie pokrywy klejem, dociśnięcie pokrywy do pudełka i utrzymanie tego stanu przez określony czas. Gotowy produkt jest skierowany na stół do następnego etapu pakowania.

**Joanna ROGALA-ROJEK, Mariusz LATOS**
KOMAG Institute of Mining Technology, Gliwice
jrogala@komag.eu

# MANAGEMENT OF ENTERPRISE ASSETS WITH THE USE OF THE iRIS SYSTEM

**Key words**

Mining industry, IT systems, RFID technology.

**Abstract**

The KOMAG Institute of Mining Technology, in collaboration with ELSTA Group, had worked on IT systems supporting the management of assets in the mining industry for many years. Experience gained from the implementation of developed solutions using RFID technology results in the necessity to extend these systems with the registration of component functionality as well as adapting the solutions to the current user's needs. The increase of interest in the present solutions forced KOMAG to undertake work on a complex, modular identification system – iRIS. The system enables the identification of the main subsystems of mining machines, underground and on the surface, capital assets, equipment of offices, as well as forms of transport, by marking them with RFID transponders or barcodes. The main assumptions of the iRIS system and possibilities of its use are presented.

## Introduction

Studies on the implementation of the RFID (Radio Frequency Identification) technology in the mining industry were initiated at the KOMAG Institute of Mining Technology in 2004. A system for electronic identification

of powered roof support components has been developed as a result of collaboration between KOMAG, Silesian University of Technology, and the ELSTA Group. The system has been implemented, commercially or on a testing level, in nearly 30 hard coal mines in Poland as well as in companies manufacturing the powered roof supports. Valuable feedback information, including suggestions of functionality changes or improvements, has been obtained from the users during research work. The advantages of the implementation of an RFID-based system resulted in increased interest from manufacturers and users of the mining machines and equipment. Therefore, a project aimed at a development and commercial implementation of a complex hardware and software solution for identification of machines, equipment, fixed assets, and transportation means has been started.

## 1. Electronic system for the identification of powered roof support components

The longwall system, in which powered roof supports play the main role in protecting mining personnel, dominate in the Polish hard coal mining industry.

Safe operation of the powered roof support depends on proper technical maintenance realized according to the work schedule as well as on the periodical assessment of its technical conditions. The periodical assessment requires collection and processing of a lot of data, e.g. processing information about a date and scope of last repair, the intensity of the operation, as well as conditions in which the support had operated. These factors have a direct influence on the scope of servicing activities as well as on the range of technical assessment. To manage of such a huge amount of information, it is required to use a computer database [1], [2], [3], [4].

In the process of the allocation, the roof supports have to be frequently disassembled and reassembled. As a result, the replacement of components in each of the roof supports occurs. It creates a need for the identification of the main components of the powered roof support, according to the EN-1804 harmonized standard [3].

The marking methods used in the collieries for identification of powered roof supports in a form of data plates have been based on welding identification codes or paint marks (Fig. 1). It does not properly secure the marking in tough operational conditions that occur in the mines. This makes accurate technical assessment and inspections difficult [3], [6].

The first system for the electronic identification of powered roof support components has been implemented, commercially or on a test level, in nearly thirty hard coal mines in Poland as well as in companies manufacturing the powered roof supports [3, 4].

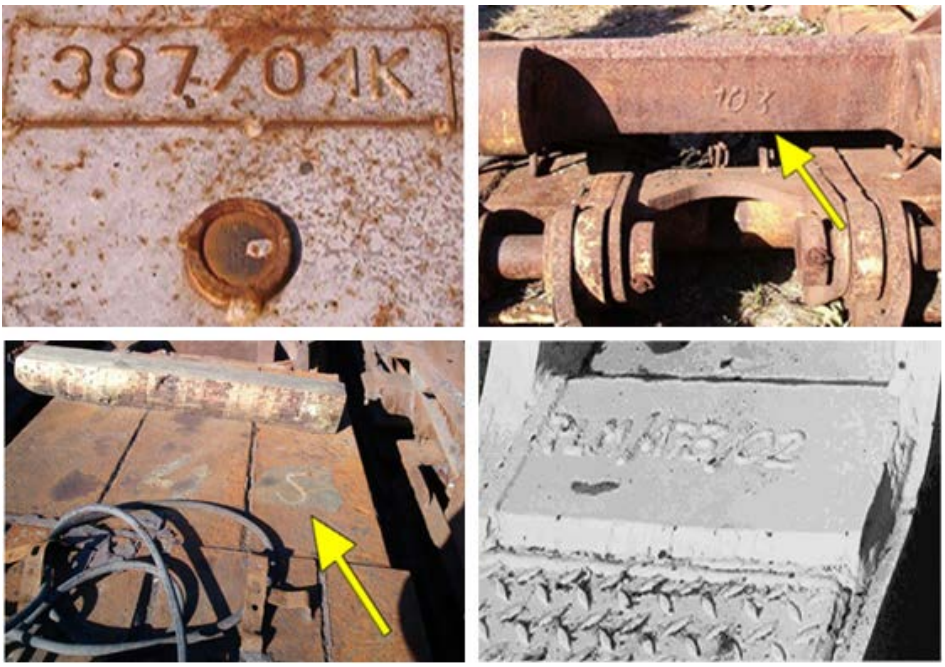


Fig. 1. Examples of marking methods used in the collieries [3, 4]

A consortium consisting of KOMAG Institute of Mining Technology, Silesian University of Technology, and the ELSTA Group have started to work on a successor system for the identification of powered roof support components, with the recording of time and conditions of their use, based on RFID (Radio Frequency Identification) technology [1, 2].

Fig. 2. Examples of installation of TRID-01 transponders on the support components [3, 4]

The basic components of a powered roof support were identified explicitly, with the use of RFID transponders, in the developed system. The introduction of

logic relations between the transponder identification number and a series of support attributes allowed automating logistic processes associated with repair or replacement of selected components. It enabled rational management of the capital assets [4].

The first KOMAG identification system consisted of the following [4]:

- Passive, electronic transponders TRID-01, which were permanently fixed on the roof support components (Fig. 2);
- RFID reader (TRMC-01 microcomputer (Fig. 3), TRH-01/* reading lance (Fig. 4) and a docking station (Fig. 5)); and,
- Gather software, which enabled the management of the database with information about the roof supports and their components.

Fig. 3. TRMC-01 microcomputer manufactured by ELSTA Group [4], [10], [11]

Fig. 4. Reading headers manufactured by ELSTA Group [4], [10], [11]


Fig. 5. Docking station type SDR-01 manufactured by ELSTA Group [4], [10], [11]

## 2. iRIS – system for identification of machines, equipment, fixed assets, and forms of transportation

The increase of interest in the modern systems, which are resistant to environmental conditions, for identification of machines, equipment, fixed assets, and forms of transportation, which are used in hard coal mines, was the reason to start collaboration between the ELSTA Group and the KOMAG Institute of Mining Technology. It aimed at the development of comprehensive, modular system, based on RFID technology [5], [7], [8].

Based on the experience of the ELSTA Group, research on a prototype of intrinsically safe mobile terminal and new applications dedicated for portable devices were conducted. The work aiming at a development of the iRIS IT software (intelligent Rapid Identification System), compatible with the previous hardware solutions and aimed at comprehensive identification and control of fixed assets was carried out in KOMAG. The iRIS system consists of the following platforms [5], [7], [8], [9]:

- PECM (for machines, equipment and components used underground),
- PEUBP (for explosion-proof machines and equipment),
- PEŚT (for transport forms),
- PEMP (for machines, equipment and components designed for use on the surface), and
- PEŚTB (for office equipment).

R&D work on the first system for electronic identification of powered roof support components was the basis for a development of new, integrated hardware and software iRIS solutions.

A new model of the system has a layered structure (Fig. 6). The applications of the iRIS system were qualified to the master management layer. This model provides full functional flexibility, and the product, based on it, satisfies most of declared customers' needs [5], [7], [8].

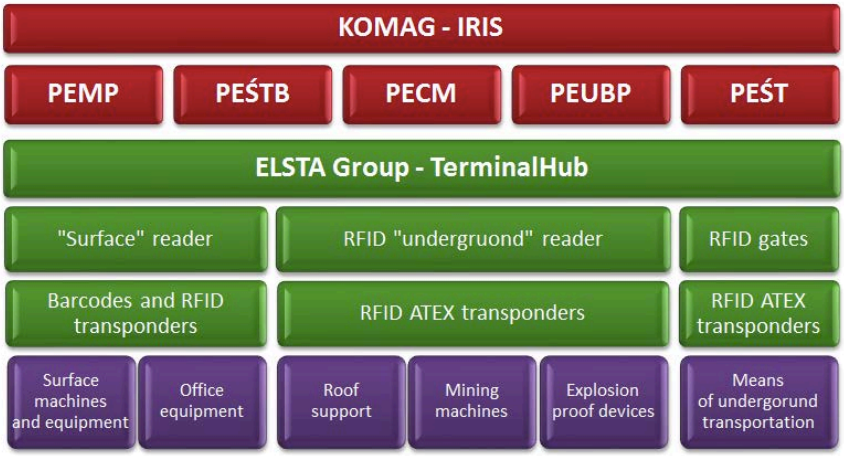


Fig. 6. System structure [7]

A new generation of devices manufactured by the ELSTA Group cooperate with the iRIS software system. For this purpose, new communication modules have been developed (Fig. 7–8) [10], [11]. Due to the large number of devices based on the RFID technology, the new IT system can cooperate both of the available hardware platforms: TRMC-01 as well as new portable terminals.


Fig. 7. Mobile terminal manufactured by ELSTA Group [11]

Fig. 8. Wireless reading header manufactured by ELSTA Group [11]

The following assumptions for the development of a new version of the system have been formulated [5], [7], [9]:

- A backward compatibility with the TRMC-01 terminals,
- A possibility to use mobile terminals with access via TCP/IP network (wired, wireless),
- A possibility of simultaneous communication with many terminals (old and new ones),
- A possibility to support different hardware platforms functionalities, a possibility to record all the processed parameters values and types of actions performed by the mobile terminals during their synchronization,
- A possibility to record data files sent by the terminals and storing them in the internal files' structure (clients should have access to the data on demand everywhere, if the network is available),
- A possibility of work with a specified terminal and session,
- The separation of data transmission directions, and
- Data files should be stored on a server and available through the web services.

"TerminalHub" application, providing an interface for management of the terminals, has been developed by the ELSTA Group (Fig. 7), while KOMAG has implemented the modules that are responsible for communication with this application [5], [11].


Fig. 9. TerminalHub software – web interface [5], [7], [11]

"TrmcGateway" application, which is used as a gateway for TRMC-01 terminals, has been developed to enable communication between the iRIS and the old generation terminals. This auxiliary application is available to the user who has a PC computer connected to the SDR-01 docking station. When connection is detected, the user is informed and data synchronization procedure starts, similar to a mobile terminal [5], [7], [11].

The works on the new mounting methods of the RFID transponders, involving riveting and gluing, have been started as a result of the needs to mark the explosion proof devices (Fig. 10–11).

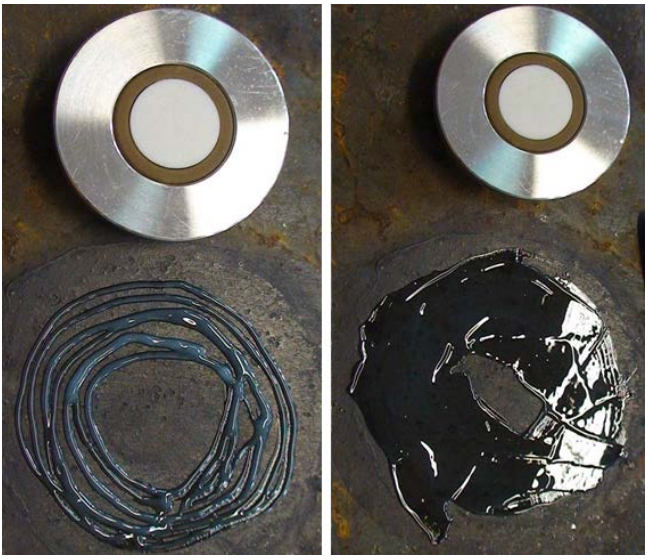

Fig. 10. Alternative methods of TRID-01 transponders assembly [9]

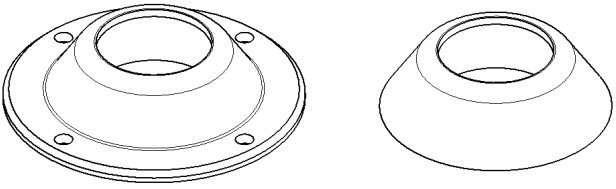

Fig. 11. The elements supporting TRID-01 transponder new mountings methods [9]

## Summary

The system for electronic identification of powered roof support components, developed by KOMAG, Silesian University of Technology and ELSTA Group, consisting of the iRIS system, are successively implemented in

mining facilities. The system is continuously updated and extended with new functionality to provide professional maintenance support for the users. A continuous development of new technologies indicates the need for the adaptation of solutions to the current users' requirements.

The idea of the system is quick identification of basic components of mining machines, fixed assets, office equipment, and forms of transportation, underground and on the surface, by marking them with RFID transponders or barcodes.

The hardware and software solutions presented in this paper simplify the work and provide a reliable source of information about the technical condition of individual components, machines, and equipment. Intrinsic safety, remote reading, and ergonomics issues have been taken into account during designing of the system.

## References

1. Fitowski K., Jankowski H., Jaszczuk M., Jenczmyk D., Krzak Ł., Pieczora E., Stankiewicz J., Szczurkowski M., Rogala J., Warzecha M., Worek C.: RFID nowa metoda identyfikacji elementów w podziemiach kopalń (in Polish). Napędy i Sterowanie No. 2: s. 82–88, 2006.
2. Fitowski K., Jankowski H., Jaszczuk M., Jenczmyk D., Krzak Ł., Pieczora E., Stankiewicz J., Szczurkowski M., Rogala J., Warzecha M., Worek C.: Nowoczesny sposób identyfikacji elementów sekcji obudowy ścianowej za pomocą technologii RFID (in Polish). Conference proceedings: „Nowe trendy w budowie maszyn górniczych 2006", Konferencja Naukowo--Techniczna, Wysowa, 27–28 February 2006, s. 37–39.
3. Jaszczuk M., Piecha A., Pieczora E., Rogala-Rojek J., Fitowski K., Szczurkowski M.: Wykorzystanie technologii RFID oraz nowoczesnych systemów bazodanowych do zarządzania bezpieczeństwem użytkowania sekcji ścianowej obudowy zmechanizowanej (in Polish). Conference proceedings: EMTECH, Ossa k. Rawy Mazowicekiej, May 2009.
4 . Jaszczuk M.,Jenczmyk D., Pieczora E., Rogala J.: Use of RFID technology to increase operational safety of powered roof supports. Conference proceedings: "High Performance Mining", RWTH Aachen, June 3rd and 4th, 2009, pp. 91–102.
5. Mikuła S., Warzecha M., Rogala-Rojek J., Latos M.: Zarządzanie flotą wielozadaniowych terminali mobilnych jako niezbędny element efektywnej strategii zarządzania majątkiem trwałym w zakładzie górniczym (in Polish). KOMTECH 2012 Monograph – Innovative technics and technologies for mining industry. KOMAG Institute of Mining Technology, Gliwice 2012, s. 555–568.

6. PN-EN 1804-1+A1:2011 Maszyny dla górnictwa podziemnego – Wymagania bezpieczeństwa dla obudowy zmechanizowanej – Część 1: Sekcje obudowy i wymagania ogólne (in Polish).
7. Rogala-Rojek J., Latos M., Piecha A., Mikuła S., Warzecha M.: Gospodarka majątkiem przedsiębiorstwa z wykorzystaniem systemu iRIS (in Polish). KOMTECH 2012 Monograph – Innovative technics and technologies for mining industry. KOMAG Institute of Mining Technology, Gliwice 2012, s. 541–554.
8. Stankiewicz K., Jasiulek D., Rogala-Rojek J., Woszczyński M., Jendrysik S.: Control and identyfication systems in the mining industry. Conference proceedings: 22nd World Mining Congress & Expo, vol. II, Istanbul, 11–16 September 2011, pp. 243–250.
9. Warzecha M., Stankiewicz K., Jasiulek D., Rogala-Rojek J., Piech A.: iRIS – system elektronicznej ewidencji środków trwałych w zakładach górniczych (in Polish). Maszyny Górnicze 2011 Nr 3, s. 92–96.
10. http://www.elsta.pl, last access 12/2014.
11. http://www.elektronika.elsta.pl, last access 12/2014.

**Zarządzanie środkami trwałymi przedsiębiorstwa z wykorzystaniem systemu iRIS**

**Słowa kluczowe**

Górnictwo, systemy informatyczne, technologia RFID.

**Streszczenie**

ITG KOMAG, przy współpracy z firmą ELSTA Sp. z o.o. i ELSTA ELEKTRONIKA Sp. z o.o. SKA, od lat prowadzi prace nad systemami informatycznymi wspomagającymi zarządzanie majątkiem w zakładach górniczych. Doświadczenia z wdrażania opracowanych rozwiązań z użyciem technologii RFID skłaniają do doskonalenia autorskich systemów ewidencji elementów maszyn górniczych, jak również dostosowania rozwiązań do bieżących potrzeb użytkowników. Wzrost zainteresowania dotychczasowymi rozwiązaniami skłoniły do podjęcia prac nad kompleksowym, modułowym systemem identyfikacji – iRIS. System umożliwia identyfikowanie podstawowych podzespołów maszyn górniczych w warunkach dołowych oraz powierzchniowych, środków trwałych i wyposażenia biur oraz transportu poprzez oznakowanie ich transponderami RFID lub kodami kreskowymi. W artykule przedstawiono główne założenia systemu iRIS i jego możliwości zastosowań.